Investigating the Relationship Between Subsurface Geology and Land Loss Near Golden Meadow, Louisiana By Utilizing 3-D Seismic and Well Log Data

A Thesis

Presented to

The Graduate Faculty of the

University of Louisiana at Lafayette

In Partial Fulfillment of the

Requirements for the Degree

Master of Science

Amanda Johnston

Spring 2019

Investigating the Relationship Between Subsurface Geology and Land Loss Near Golden Meadow, Louisiana By Utilizing 3-D Seismic and Well Log Data

Amanda Johnston

APPROVED:

Rui Zhang, Chair
Assistant Professor of Geology

Raphael Gottardi
Assistant Professor of Geology

Gary Kinsland
Professor of Geology

Nancye Dawers
Associate Professor of Earth and Environmental Sciences
Tulane University

Mary Farmer-Kaiser
Dean of the Graduate School

Johnston, Amanda. Bachelor of Science, Stephen F. Austin State University, Spring 2015;
Master of Science, University of Louisiana at Lafayette, May 2019.
Major: Geology
Title of Thesis: Investigating the Relationship Between Subsurface Geology and Land Loss Near Golden Meadow, Louisiana By Utilizing 3-D Seismic and Well Log Data
Thesis Advisor: Dr. Rui Zhang
Pages in Thesis: 94; Words in Abstract: 255

Abstract

Wetland loss is one of the most significant environmental and economic threats in the deltaic plain of the Louisiana Gulf Coast. Controls on subsidence include sedimentation from the Mississippi River delta complex, movement along faults, salt tectonics, and compaction. This study focuses on the impact of fault movement on subsidence and wetland loss near Golden Meadow and Leeville, Louisiana. It is hypothesized that this area is affected by active faulting. To test this, I mapped faults over segments of the Golden Meadow Fault Zone (GMFZ), including the Golden Meadow fault and the Lake Enfermer fault, and the Leeville salt dome utilizing industry 3D seismic data, paleontological data, and well log data. Subsurface faults, mapped from a depth of 4000 feet to approximately 1500 feet, are then projected to the surface to compare with areas of measured wetland loss, some of which form marsh breaks and lakes. Results highlight a graben south of the main segment of the Golden Meadow fault. The location of this graben spatially correlates with a portion of Catfish Lake and partially overlies salt adjacent to the main fault surface. The path of Bayou Lafourche, the main distributary channel of the Lafourche lobe of the Mississippi River delta complex, is shown to be fault controlled as it flows over the Leeville Salt Dome. Bayou Lafourche changes orientation and flows on the downthrown side of two radial faults associated with the dome. These results indicate that there is a relationship between surface geomorphology and subsurface structures that, at least in part, exert control on wetland loss in southern Louisiana.

Acknowledgments

This project was funded by The Water Institute of the Gulf under project award number CPRA-2015-COE-JE. The project was paid for [in part] with federal funding from the U.S. Department of the Treasury under the Resources and Ecosystems Sustainability, Tourist Opportunities, and Revived Economies of the Gulf Coast States Act of 2012 (RESTORE Act). The statements, findings, conclusions, and recommendations are those of the author(s) and do not necessarily reflect the views of the U.S. Department of the Treasury, CPRA or The Water Institute of the Gulf.

I want to thank Christopher McLindon with the New Orleans Geological Society for facilitating access to these data for this project. I also thank Stephen Lubanko and the geologists at Castex Energy for providing me with industry 3D seismic data and the knowledge and tools to interpret this data. Big thanks also go out to Seismic Exchange, Inc. (SEI), IHS Kingdom (IHS), and Paleo Data (PD) for allowing seismic data to be included in this thesis. Lastly, I would like to thank my thesis committee, Dr. Rui Zhang, Dr. Raphael Gottardi, Dr. Gary Kinsland, and Dr. Nancye Dawers.

Table of Contents

List of Figures

List of Abbreviations

GMFZ	Golden Meadow Fault Zone
CPRA	Coastal Protection and Restoration Authority
SEI	Seismic Exchange, Inc.
IHS	IHS Kingdom
PD	Paleo Data
GMF	Golden Meadow fault
LEF	Lake Enfermer fault
BC	Bully Camp salt dome
LS	Leeville salt dome
USGS	United States Geological Survey
NGOM	Northern Gulf of Mexico
TSS	Terrebonne Salt Sheet
STSS	South Timbalier Salt Sheet
GR	Gamma-Ray log
SP	Spontaneous Potential log
Big A	Bigenerina A
Big B	Bigenerina B
myo	million years old
E.I.	Expansion Index
TWT	Two-Way Travel time
ya	years ago
kya	thousand years ago

Introduction

A study based on 3D seismic data interpretation and well log analysis investigates the relationship between subsurface geology, geomorphology, and wetland loss near Golden Meadow, Louisiana. How the subsurface geology and surface geomorphology have influenced localized subsidence, and in consequence wetland loss, in regions of the Louisiana gulf coast is poorly understood. Wetland loss occurs when the rate of sea level rise exceeds the rate of vertical marsh growth. The rate of vertical marsh growth must increase by the amount of localized subsidence, or wetland land loss can occur. Localized areas of subsidence are due to natural occurrences like compaction and faulting, or man-made influences such as groundwater and other fluid withdrawal. Areas of wetland loss caused by faulting need to be identified to better understand the effects that subsurface geology exerts on wetland loss in and around the Golden Meadow and Leeville area of Lafourche Parish.

Previous studies have identified the relative age of the Golden Meadow fault (GMF) (Kolvoord et al., 2008), abandoned channels of the Mississippi River delta complex (Gould, 1970 and Chamberlain et al., 2018), and chronology of the regressive and transgressive Miocene delta complexes in the subsurface (Curtis, 1970). On the surface, faults have been identified over southern Louisiana (Lopez et al., 1997, Dokka, 2011, Yeager et al., 2012, Roberts et al., 2008, Kuecher et al., 2001 and Martin, 2006). Explicit offset of the surface along roads and bridges, as well as observations from shallow high-resolution seismic data and LIDAR data, have identified the surface location of the faults (Roberts et al., 2008, Dokka et al., 2011 and Shen et al., 2016). As there are no explicit offsets along LA Highway 1, the major highway extending through the study area, no shallow seismic has been

acquired, and there is too much water over the surface area of the study area to identify faults utilizing LIDAR data. In this study, 3D seismic data and other observed surface indicators are compared to determine the location of surface fault. A marsh break, the line separating healthy marsh from brown marsh, is an example of a surface feature that may indicate faulting, and several of these have been identified within the study area (Gagliano et al., 2003). However, these breaks in the marsh have yet to be well imaged within the study area. Here I use industry 3D seismic and well log data are used to better understand the growth history of faults and their impact on geomorphology and wetland loss. The goal of this study is to compare mapped surface fault projections to wetland loss data to determine whether surface fault locations cause marsh breaks within the study area.

The area of interest lies on a passive margin 40 miles south-southwest of New Orleans, in the deltaic plain of coastal Louisiana. Within the deltaic plain are the drainage basins of the Mississippi and Atchafalaya Rivers; today's deposition occurs predominantly at the coast and offshore Louisiana. The study area is along the Golden Meadow Fault Zone (GMFZ) (Figure 1). The GMFZ is a distributed zone of normal faults, downthrown to the south (Figure 1) (Gagliano et al., 2003). The GMFZ is the northern margin of the Terrebonne salt withdrawal basin. This is a major structural feature in southern Louisiana that formed from salt evacuation (McBride, 1998). Normal faults bound this structure on both sides creating a graben. The southern margin of this trough is a salt ridge with assorted counter-regional faults (Schuster, 1995, McBride, 1998 and Gagliano et al., 2003). Surface projections of fault other segments of the GMFZ have been made in areas surrounding the city of Golden Meadow (Kuecher et al., 2001 and Martin, 2006), except for the Golden Meadow

South Louisiana Fault Zones

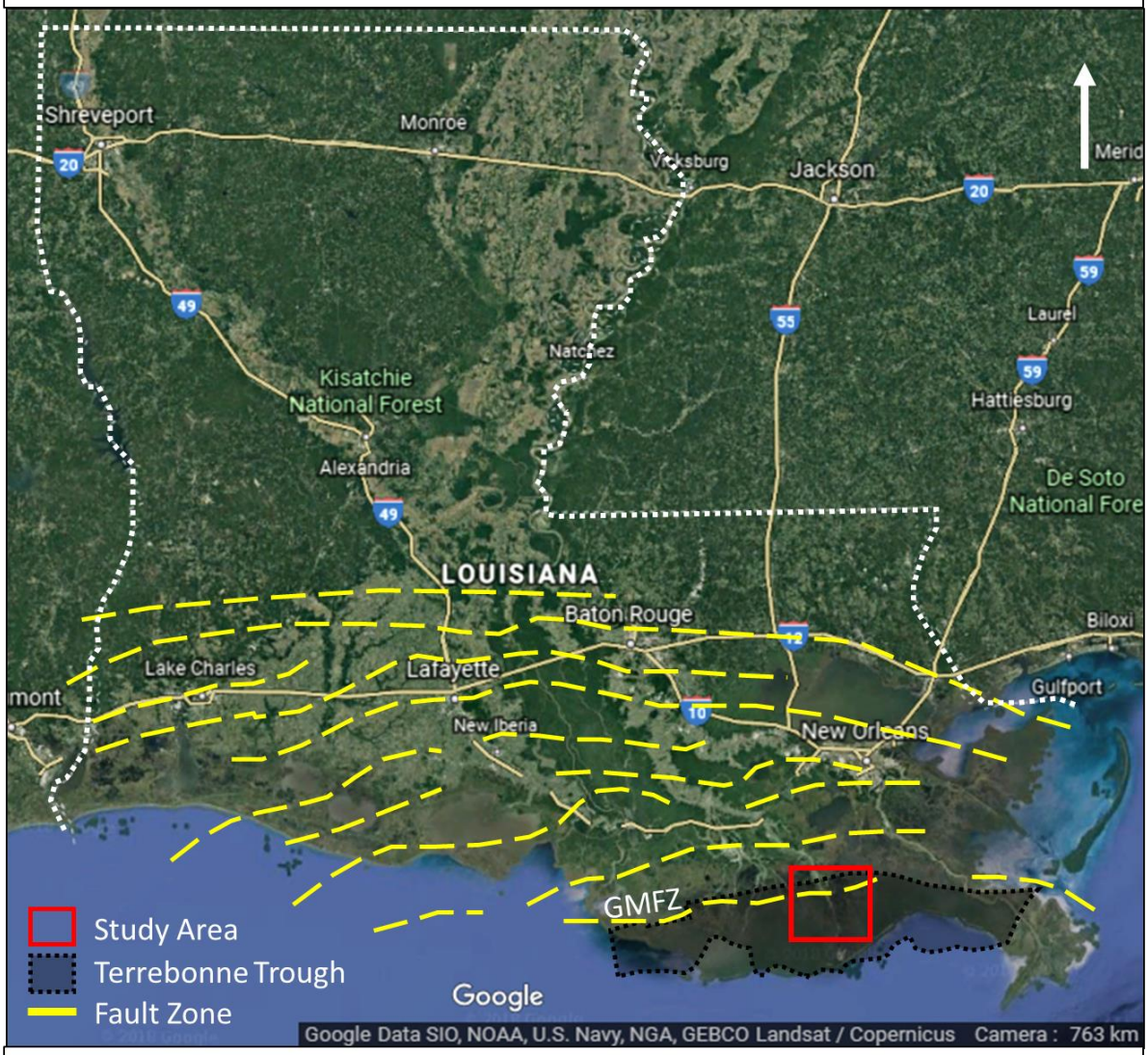

Figure 1. Modified from Gagliano et al., 2003 and McCulloh, 2001. Base map of simplified Cenozoic faults in southern Louisiana in relation to the Golden Meadow Fault Zone (GMFZ), the Terrebonne Trough, and the study area, which is outlined in red. Yellow dashed lines are simplified fault traces in southern Louisiana. The GMFZ to the south, is the northern fault zone that outlines the Terrebonne Trough salt withdrawal basin to the south.

fault (GMF) and Lake Enfermer fault (LEF) have yet to be mapped.

The study area is a part of the Lafourche Delta complex, an historical channel of the Mississippi River that was deposited approximately 750-1500 years ago (Chamberlain et al., 2018). A salt marsh comprises the distal area of the Lafourche Delta complex; the salinity declines towards the northern portion of the study area (Adams, 1976 and Couvillion et al., 2017). There are eight hydrologic basins in southern Louisiana and the study area lies between two of them - the Terrebonne and Barataria basins with a total area of approximately 425mi^2 (1100 km^2) (Figure 2) (Couvillion et al., 2017). Wetland loss data measured by Gagliano (1994) and the USGS (Couvillion et al., 2011) show that these two hydrologic basins have the most significant rates of wetland loss in Louisiana. The GMF and LEF are located within the Barataria Basin. Bathymetry, cores and 2-D seismic data support the hypothesis that faults along the GMFZ may extend to the surface inside and outside of the study area (Keucher et al., 2001, Gagliano et al., 2003, and Martin, 2006). The GMF and the Lake Enfermer fault (LEF), two fault surfaces within the GMFZ, as well as the radial faults surrounding the Bully Camp salt dome (BC) and Leeville salt dome (LS), are described, mapped and projected to the surface utilizing 3D seismic data. Well log data interpretations help constrain the timing of fault movement, along with the amount of stratigraphic growth, or increased thickness of sediments on the downthrown fault block in comparison to the upthrown fault block. These results are outlined in conjunction with wetland loss data from the United States Geological Survey (USGS) to investigate the relationship between subsurface geology and wetland loss.

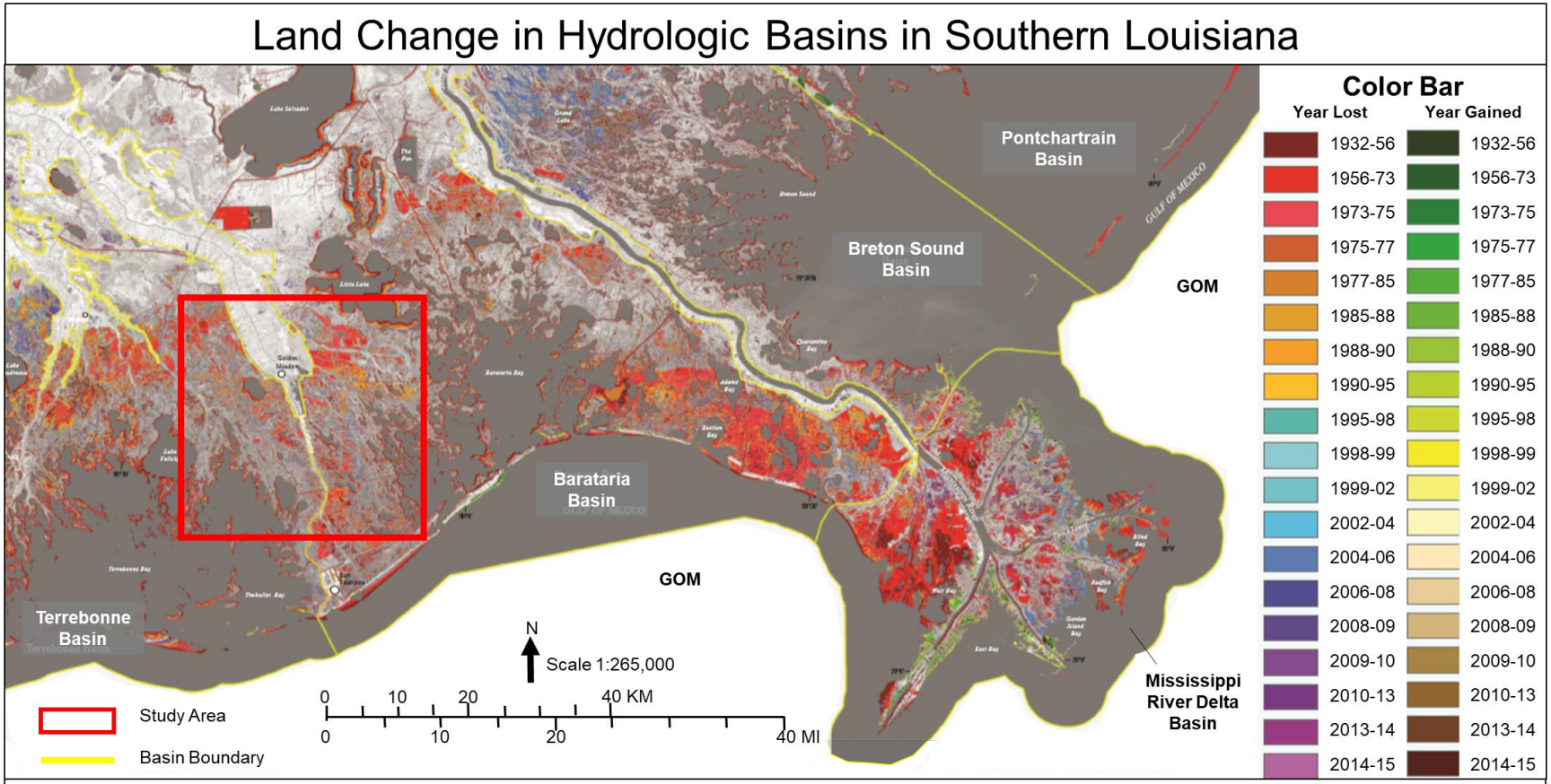

Figure 2. Modified from Couvillion et al., 2017. This figure illustrates land change in southern Louisiana as defined by hydrologic basins. The hydrologic basins are outlined in yellow and the study area is outlined in red. The Terrebonne, Barataria, Breton Sound, Pontchartrain, and Mississippi River Delta Basins are included in this base map. The study area lies between the Terrebonne and Barataria basins. The predominant land change is negative and occurring in the 1970's. The color bar denotes the time period in which land changed occurred.

Geological Setting

In the late Mesozoic, thermal subsidence and crustal attenuation dominated the structural regime of the Northern Gulf of Mexico (NGOM) due to previous rifting (McBride, 1998, Stover et al. 2001 and Yuill et al., 2009). Large amounts of Louann salt were precipitated and deposited in the NGOM in the Late Jurassic (Figure 3). Gradients in the cooling of the transitional and oceanic crust caused the modern basinward tilt, leading to lateral flow of Louann salt towards the basin (McBride, 1998 and Stover et al., 2001). Due to sedimentary loading during the Paleocene and Eocene initiated the movement of the allochthonous Terrebonne Salt Sheet (TSS), and the salt sustained flow into the late Eocene to Oligocene (Winker, 1982, McBride, 1998 and Stover et al., 2001). The TSS continued to flow basinward throughout the Miocene because of further sediment loading (Stover et al., 2001). Miocene deltas deposited this sediment through multiple regressions and transgressions from the Early to Late Miocene (Curtis, 1970) (Figure 3). An additional allochthonous salt sheet, the South Timbalier Salt Sheet (STSS), formed from the Louann salt; this sheet flowed into present-day south-central Louisiana while the TSS was being evacuated into the NGOM (Foote et al., 1992, McBride, 1998, Stover et al., 2001 and Winker, 1982). The final stage of salt evacuation occurred in the Late Miocene (McBride, 1998), and from this a stepped counter-regional fault system formed what is now called the Terrebonne Trough (McBride, 1998, Stover et al., 2001 and Rowan and Inman, 2005). Adjacent to this stepped counter-regional fault system, a salt ridge formed to the south including the Bay Marchand salt dome (McBride, 1998 and Schuster, 1995 and Rowan and Inman, 2005). The STSS continued to flow south and was fed by salt stalks/domes during this time (McBride, 1998). During the middle to late Miocene, a regional acceleration occurred due to either slowed

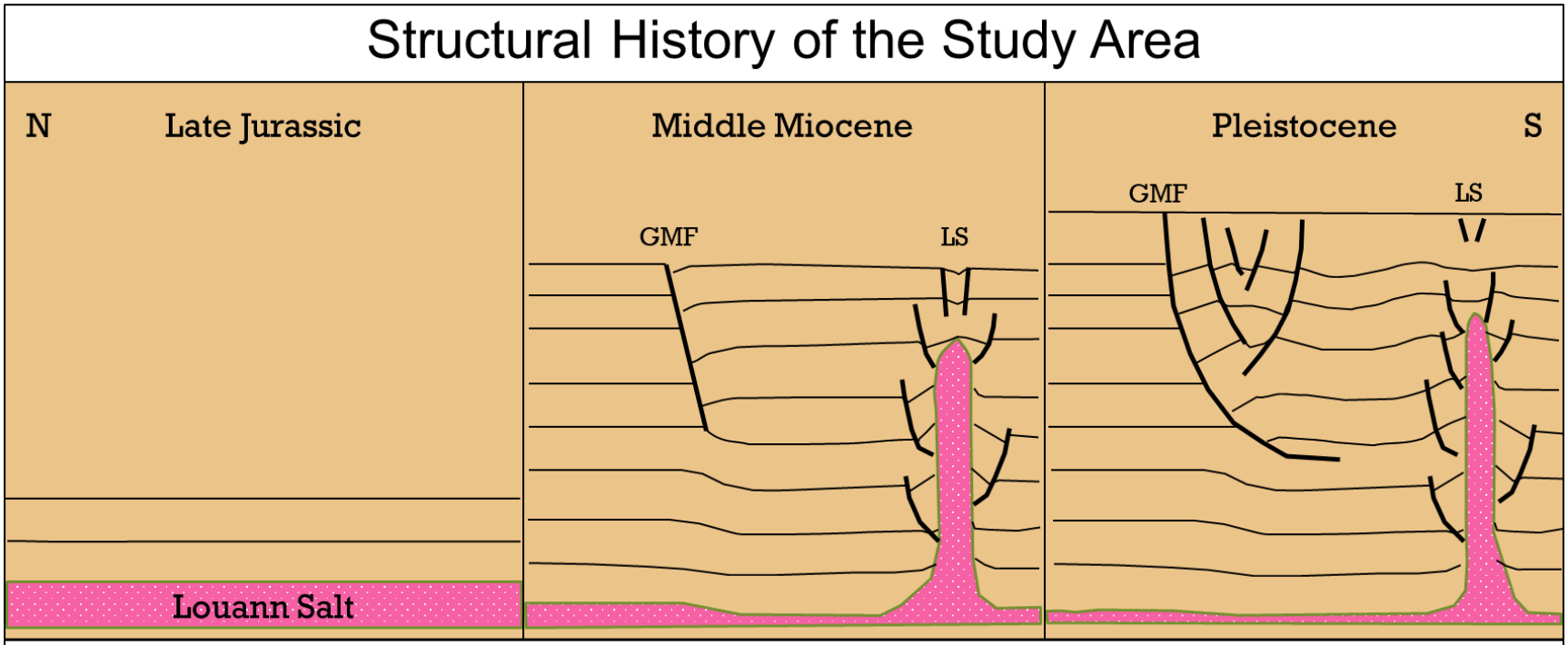

Figure 3. This figure is an over simplified schematic of the structural history and timing of activity of the Golden Meadow fault and Leeville salt dome. The Louann Salt was deposited in the Late Jurassic. With continued deposition the Louann Salt became allochthonous, forming structures like the Leeville salt dome (LS). During the Middle Miocene, the Golden Meadow Fault (GMF) became active (Kolvord et al., 2008). During the Pleistocene, a roll-over anticline has formed on the footwall of the GMF.

deposition or up-dip differential loading of autochthonous salt (McBride, 1998). Listric growth faults like the GMF and LEF, formed during the continued evacuation of the STSS and progradation of deltas from the Middle Miocene through the Late Miocene (Curtis, 1970, McBride, 1998 and Kolvoord et al., 2008) (Figure 3).

During the Pliocene, the modern-day shelf-slope break was the major depocenter of the NGOM (Winker, 1982; Stover et al., 2001, and McBride, 1998). The progradation of the marine depocenter caused mini-basins to form from allochthonous salt movement (Stover et al., 2001). Moreover, with continuing deposition over the study area, the GMF and LEF continued their activity which vertically offset sediments (Figure 3).

Later throughout the Pleistocene and Holocene, ~20-12 kya, sea level lowered which allowed for valleys to form by downcutting (Blum et al., 2008). Sea level rise in the Holocene, along with the construction of deltas, filled these valleys of the lower Mississippi River Valley (Blum et al., 2008). Cyclical sequences of coarse sediments topped by fine-grained top-strata were deposited in the Pleistocene, and Holocene epochs before sea level stabilized approximately 7500 ya (Ayrer, 2013). Sea-level rose to its present level nearly 3-4 kya (Gould, 1970). With sea level stabilization came the formation of the Mississippi River deltaic complex, which is composed of six separate deltas, one of those being the Lafourche delta (Gould, 1970) (Figure 4). Bayou Lafourche, which is a part of the Lafourche delta complex, is an integral part of the study area. Until the artificial closure of Bayou Lafourche ca.1903-1904, it sustained flow as a distributary of the Mississippi River as it continued shifting eastward (Ayrer, 2013).

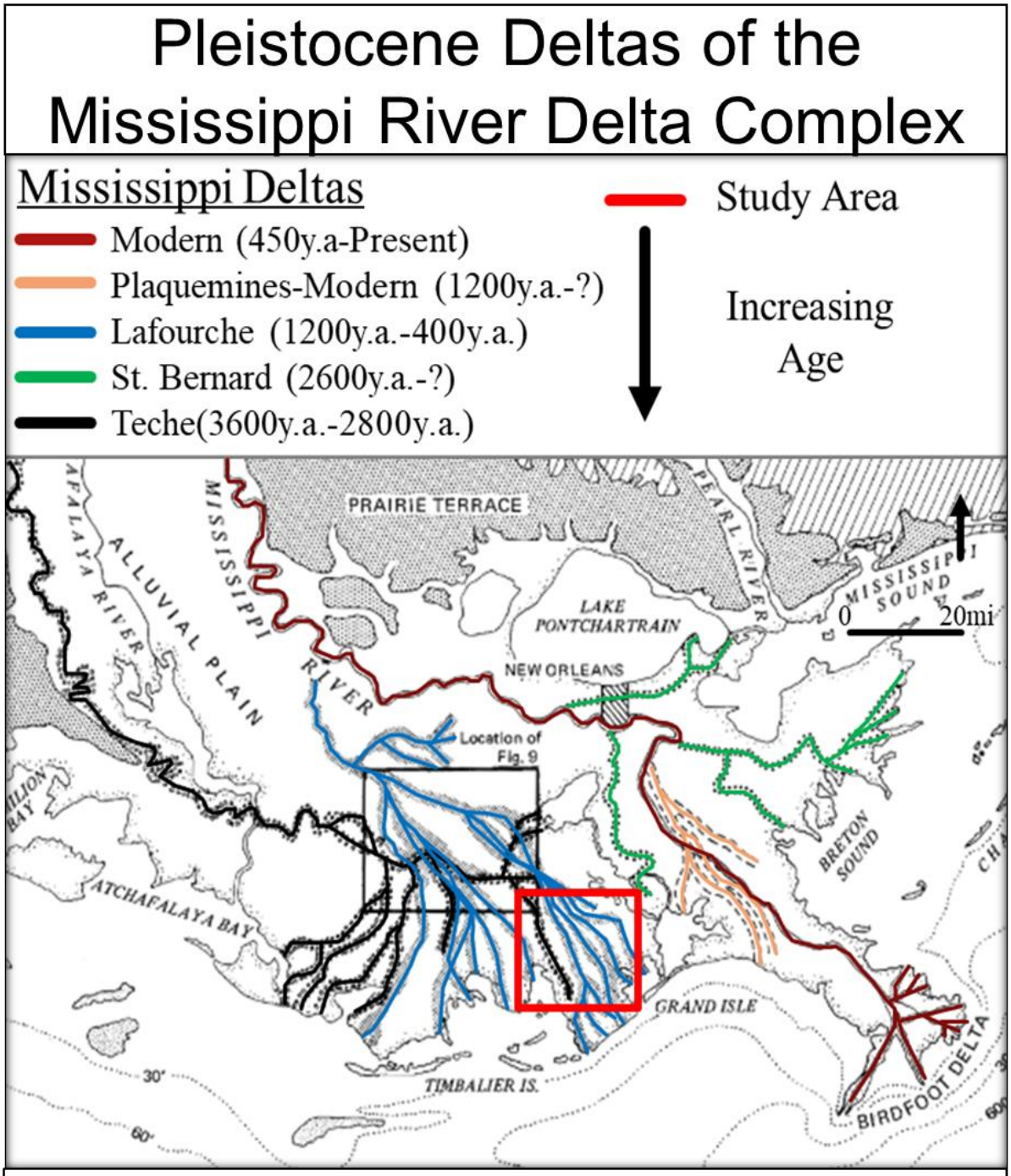

Figure 4. Modified from Gould, 1970. Illustrates depositional patterns of the Mississippi River Delta Complex over southern Louisiana. The red box outlines the study area, and different colored lines indicate specific historical deltas. The Lafourche delta complex is outlined in blue while the Modern delta complex is outlined in brown.

Structural Geology of the Study Area

Faults with a significant increase in both displacement with depth and thickness of correlative sediments from upthrown to downthrown fault blocks are growth or depositional normal faults (Ocamb, 1961). The increased thickness on the downthrown block is due to the contemporaneous displacement occurring with deposition (Kuecher et al., 2001 and Ocamb, 1961). Some of these faults conform to the shape of local depocenters, or isopach patterns (Ocamb, 1961 and Kolvoord et al., 2008). There are two major growth faults located within the study area. Throughout the area the growth faults became active in the Middle to Late Miocene (Ocamb, 1961, Bader Jr. and McWilliams, 1983, McBride, 1998, Stover et al., 2001, and Kolvoord et al., 2008). One of these growth faults is the Lake Enfermer Fault or the LEF. The LEF is a segment of the greater GMFZ and has a suspected surface offset based on observed 'salt marsh dieback' exhibited at the surface, similar to that seen on Empire and Bastian Bay fault segments (Gagliano et al., 2003 and Martin, 2006). This fault has been named for its location in Lake Enfermer and its proximity to the oil and gas field (Lake Enfermer Field). In 1981 the LEF scarp became evident, and according to the National Wetlands Research Center of the USGS, there was fault activity during 1990 – 2000 (Gagliano et al., 2003). The LEF is a large east-west striking normal fault that is at least 5000 ft long and downthrown to the south-southeast (Bader Jr. and McWilliams, 1983) (Figure 5). The second major fault is the Golden Meadow Fault or the GMF. This fault is located along an east-west trending roll-over anticline on the downthrown fault block suggesting a shelf edge failure in the Middle to Late Miocene (Kolvoord et al., 2008 and Little, 2003). The GMF is named for its proximity to the city of Golden Meadow and the Golden Meadow oil and gas field.

Fault Map of the Study Area

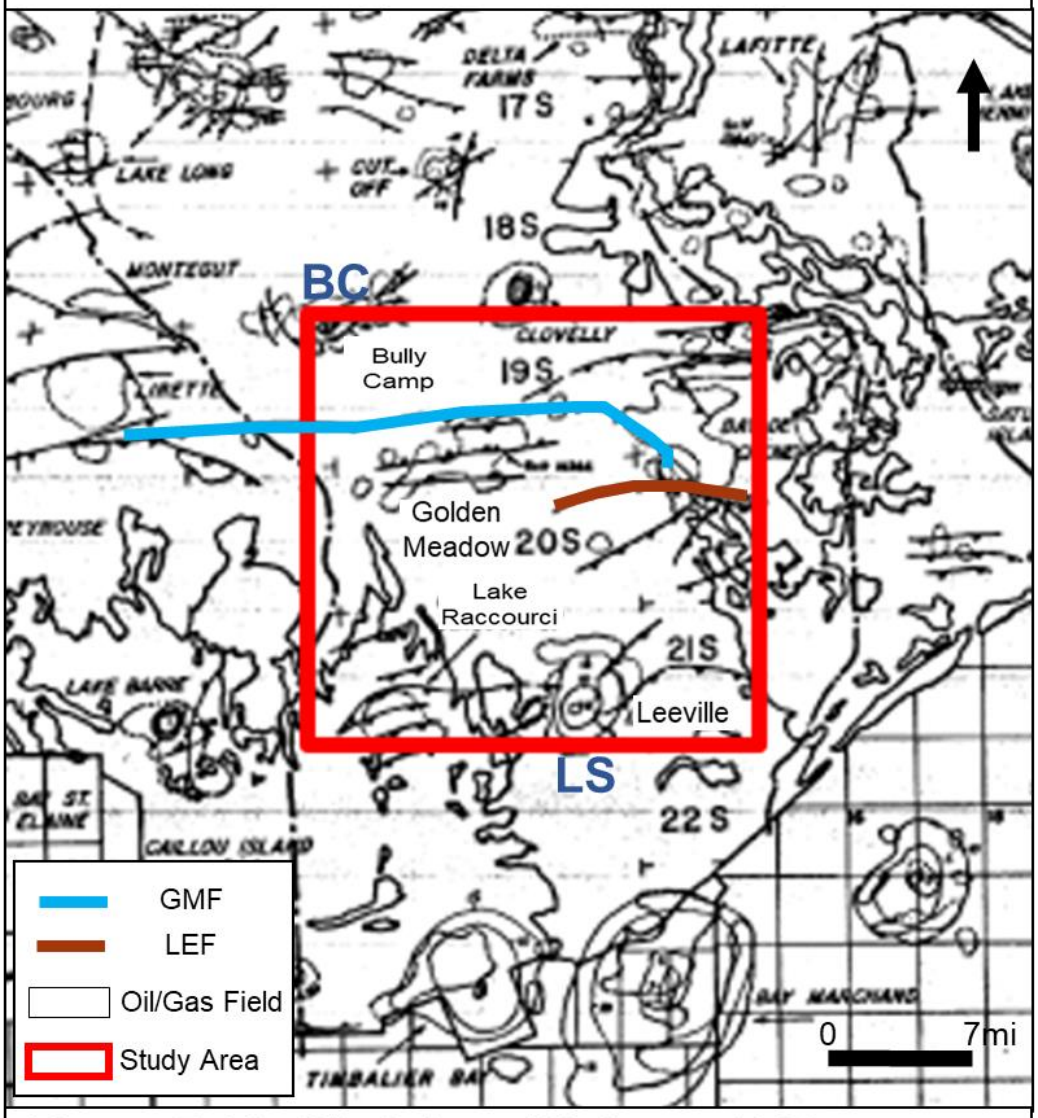

Figure 5. Modified from Wallace, 1962. Illustrates faults, oil and gas fields, and salt domes around the study area. The area within the red box includes the study area. Two growth faults within the area of interest are studied, the Golden Meadow fault (GMF) and Lake Enfermer Fault (LEF). Two salt domes are studied, the Leeville salt dome (LS) and Bully Camp salt dome (BC).

This fault has been interpreted as penetrating the surface for many years. Geophysicists with LSU shot a high-resolution seismic profile along the Bayou Lafourche corridor to attempt to identify the GMF in the near surface (Gagliano et al., 2003). While the fault was missed during the acquisition, it is still thought that the GMF and other segments of the GMFZ are present at the surface due to the geometry of marsh break up during the latter half of the 20th century (Gagliano et al., 2003). Elevation profiles, or cross-sections illustrating the relief of the landscape, also show a graben that may be fault influenced near the city of Golden Meadow (Morton et al., 2002 and Gagliano et al., 2003). Within the present study area, the GMF may have influenced distributary channels by creating bends and branching patterns (Gagliano et al., 2003). These channels may be another indicator of recent fault activity. At depth the GMF is listric and the fault surface partially conforms to a salt body, the Golden Meadow salt dome, near the base of the fault (Figure 6). The depth to the top of the allochthonous Louann Salt is about 15,344 ft (Beckman and Williams, 1990). With the continued sedimentation across the GMF, synthetic and antithetic faults developed on the downthrown side of the fault creating a graben (Kolvoord et al., 2008). The graben is on the down-thrown block of the GMF to the south and the upthrown block of the LEF to the east (Figure 6). The synthetic and antithetic faults of the graben are more planar with depth compared to the listric geometry of both GMF and LEF.

There are three salt domes within the study area, two of which will be studied, the Leeville salt dome (LS) in the south and the Bully Camp salt dome (BC) in the northwest (Figure 5). Salt domes are diapirs of intrusive salt that travel up and pierce through denser overlying sediments because of the salt's lower density and ability to flow plastically at low pressure

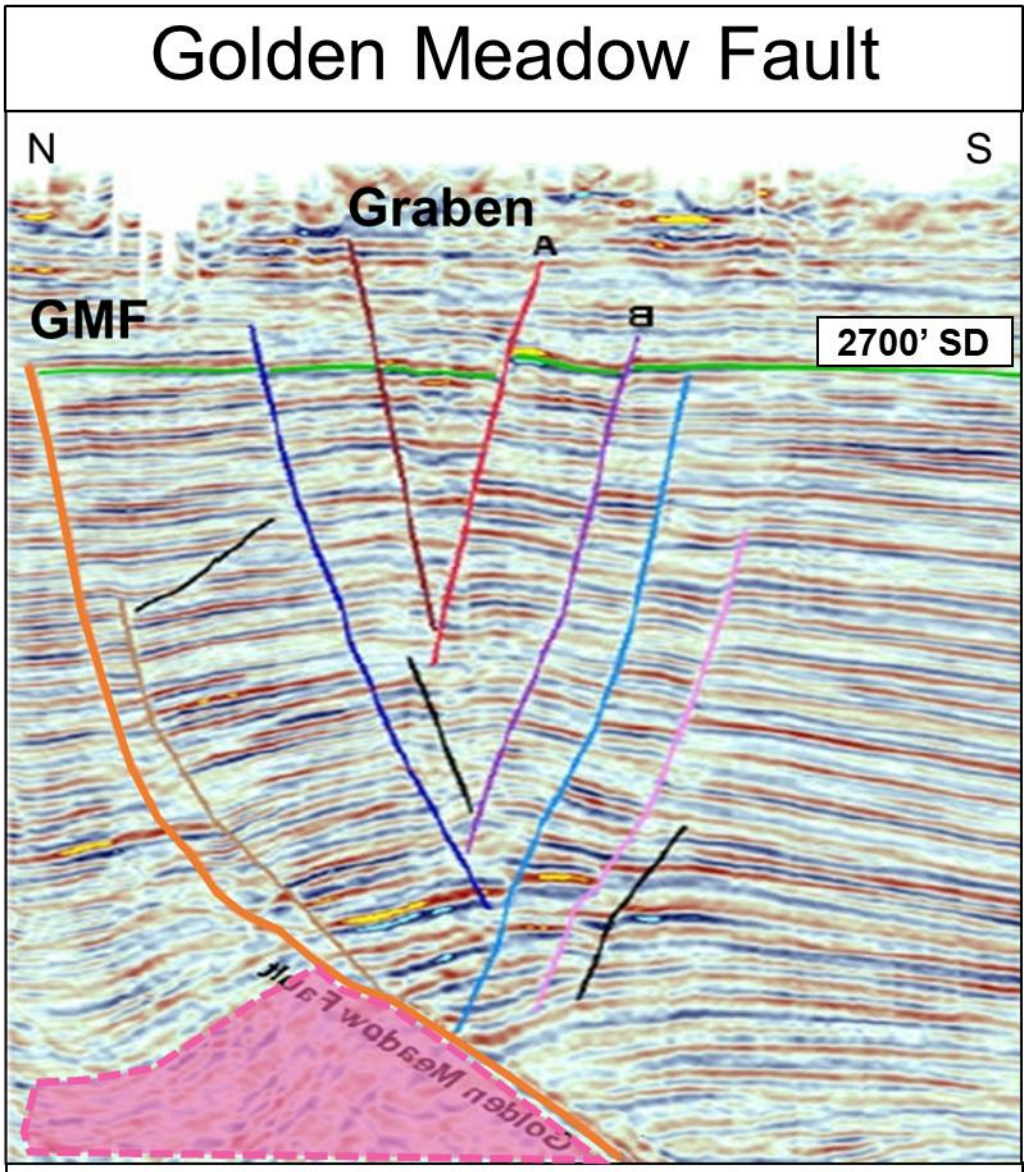

Figure 6. Modified from Kolvoord et al., 2008. Interpretation that of Kolvoord et al., 2008. Illustrates the Golden Meadow fault (GMF) in orange and graben on the downthrown fault block to the south. The GMF is listric with depth and the shape of the fault plane conforms to a salt body. The synthetic and antithetic faults are more linear.

and temperatures (Barton, 1933 and Atwater et al., 1959). There are two ways that a salt dome can form (Barton, 1933). The first is through a tangential compressive force and the second requires a pressure gradient laterally on a slope created from overburden onto the original bedded salt (Barton, 1933). A common characteristic of salt domes is the formation of radial faults around the dome. Most radial faults form at steep dips (> 60 degrees) strikes that are perpendicular to the dome, and displacement that decreases away from the salt-sediment interface (Ocamb, 1961).

The LS is the southernmost structural feature within the study area and is located under the community of Leeville, Louisiana (Figure 5). The LS is thought to have started to form in the Early Miocene (McBride, 1998 and Stover et al., 2001). Radial faults encircle the dome within the overlying sediments. The top of the caprock is -3789 ft subsea, and the top of salt is about -3899 ft (Beckman and Williams, 1990 and NOGS, 1983). The deepest depth of salt encountered within the LS in 1979 was -13,944 ft. This dome was discovered in 1928 by a seismic refraction survey (NOGS, 1983). The second salt dome, the BC, similar to the LS, is also thought to have started to form in the Early Miocene (McBride, 1998 and Stover et al., 2001). Figure 5 depicts the BC located in the northwest corner of the study area, to the west of Galliano, Louisiana. The approximate top of the caprock is -1256 ft and the top of salt is -1296 ft (Beckman and Williams, 1990 and The Diggings, 2019).

Data

3D Seismic Data

I interpreted industry 3D seismic data to map the subsurface structure within the study area.

The seismic survey, the Leeville 3D Merge, was donated by Castex Energy and is owned or controlled by Seismic Exchange, Inc. (SEI) (Figure 7). These seismic data have a dominant frequency of about 12 Hz or 13 Hz, and a bin spacing of 110 feet (Figure 8a-b). Within the shallow seismic data, data quality decreases towards the Earth's surface due to thick Holocene locally. This makes it difficult to interpret fault surfaces to 0 s. Another factor that makes it more challenging to interpret fault surfaces includes no data zones. No data zones are areas where data have been cut, filtered, or not been shot deliberately, for multiple reasons including permitting issues (Figure 9). A time v. depth chart was also donated by Castex Energy that was used to convert fault surfaces in time to depth.

Well Log Data

I also utilized well log raster data totaling 320 logs. The surface locations of the wells are identified in Figure 10. Four types of logs were available for this study: the gamma-ray (GR), spontaneous potential (SP), resistivity, and conductivity. Within the study area, well locations are denoted by black dots (Figure 10). Well log correlations were interpreted in the Pleistocene (about 1800 ft) through the Late Miocene (about 8000-9000 ft).

Micropaleontological Data

Micropaleontological (paleo) data from the Late Miocene were donated by Paleo Data: *Bigenerina A* (Big A) which is 6.76 million years old (myo), and *Bigenerina B* (Big B) which is 9.22 myo.

3D Seismic Survey Outline

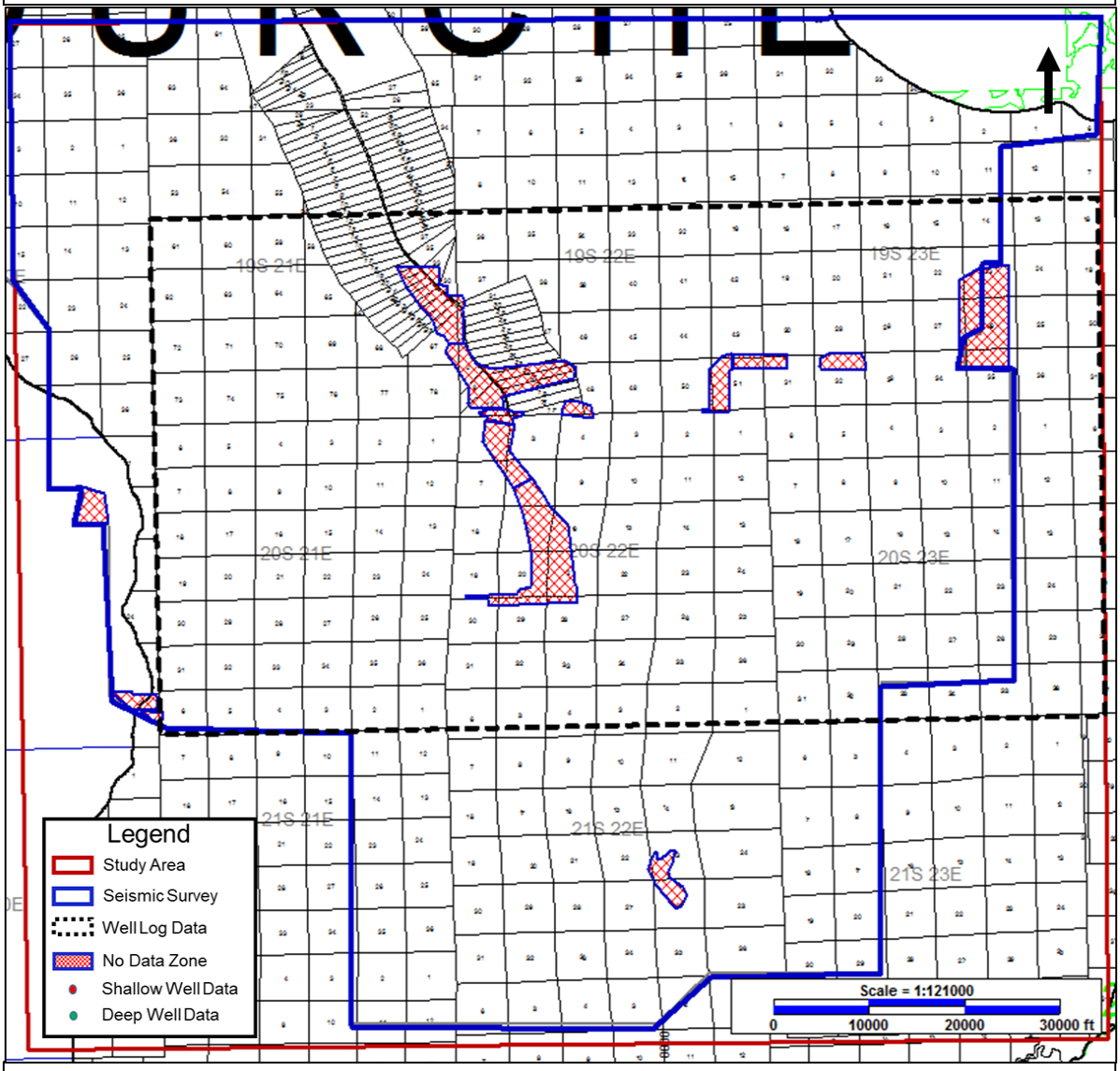

Figure 7. Illustrates the extent of the seismic survey within the study area in blue. The red box outlines the extent of the study, the black-dotted box outlines the well log data coverage centered around the town of Golden Meadow, and the blue outlined polygons with red hachures indicates a no data zone within the seismic survey.

3-D Seismic Data Details

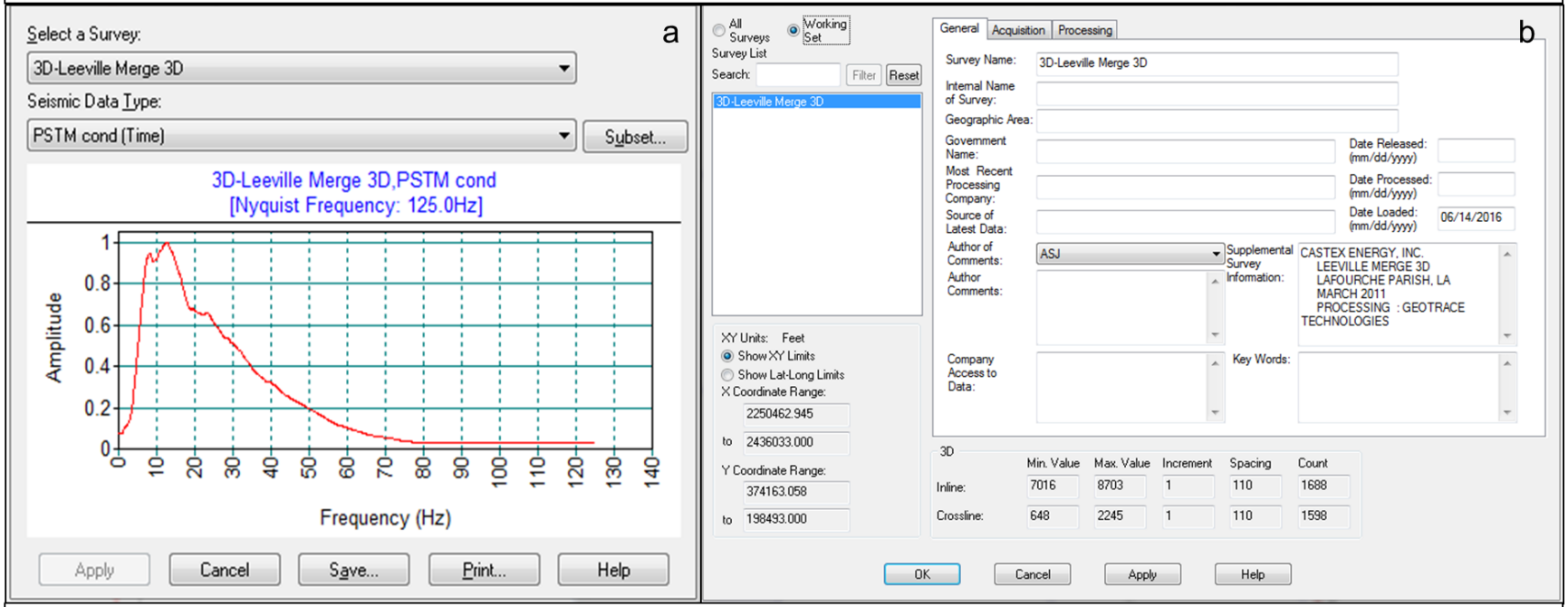

Figure 8. 8a illustrates the frequency (Hz) of the seismic data against amplitude in the seismic spectrum. The dominant frequency of the seismic data is between 12 and 13 Hz. 8b shows the general survey details of the Leeville 3D Merge. This shows that the inline and crossline bin spacing is 110 ft.

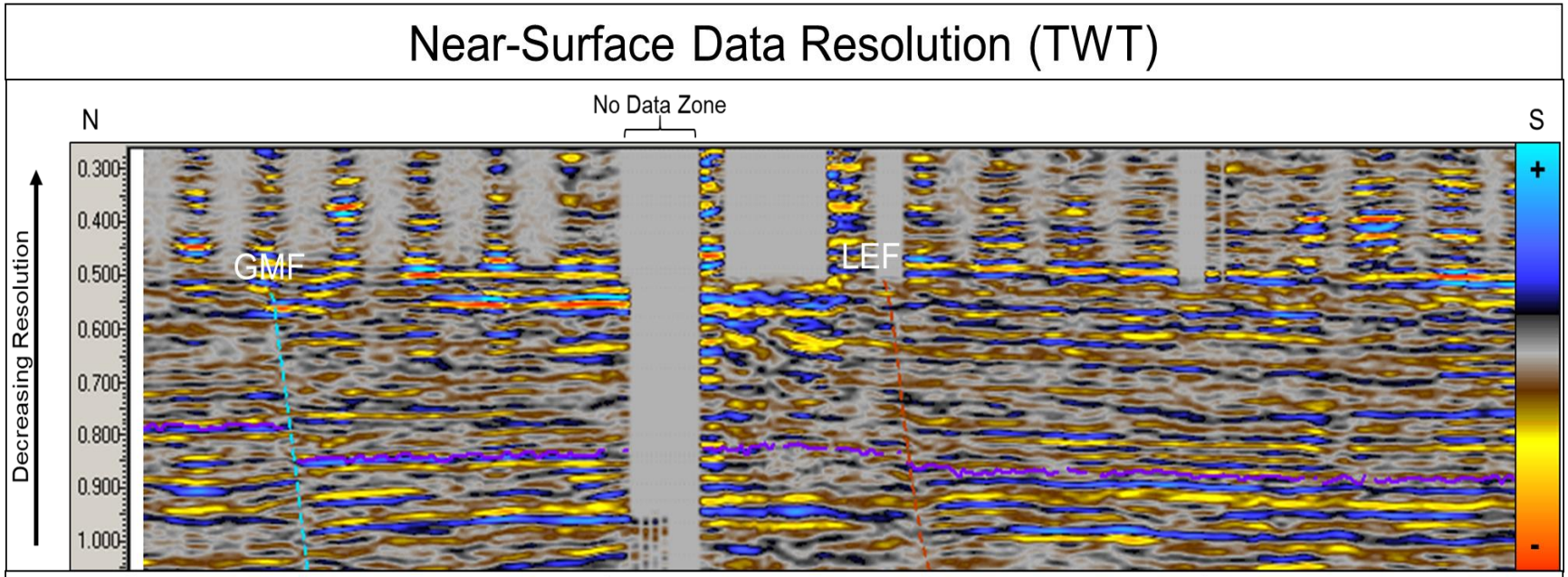

Figure 9. Illustrates near-surface seismic data within the seismic survey, the Leeville 3D Merge. The color bar, on the right, indicates the amplitudes of the seismic data. Positive amplitudes are colored blue, while the negative amplitudes are colored orange. From 1.000 s two-way travel time (TWT) up to 0.300 s TWT, resolution of the seismic data decreases and a no data zone is highlighted near the center. The Golden Meadow fault (GMF) is in blue, while the Lake Enfermer fault (LEF) is in brown.

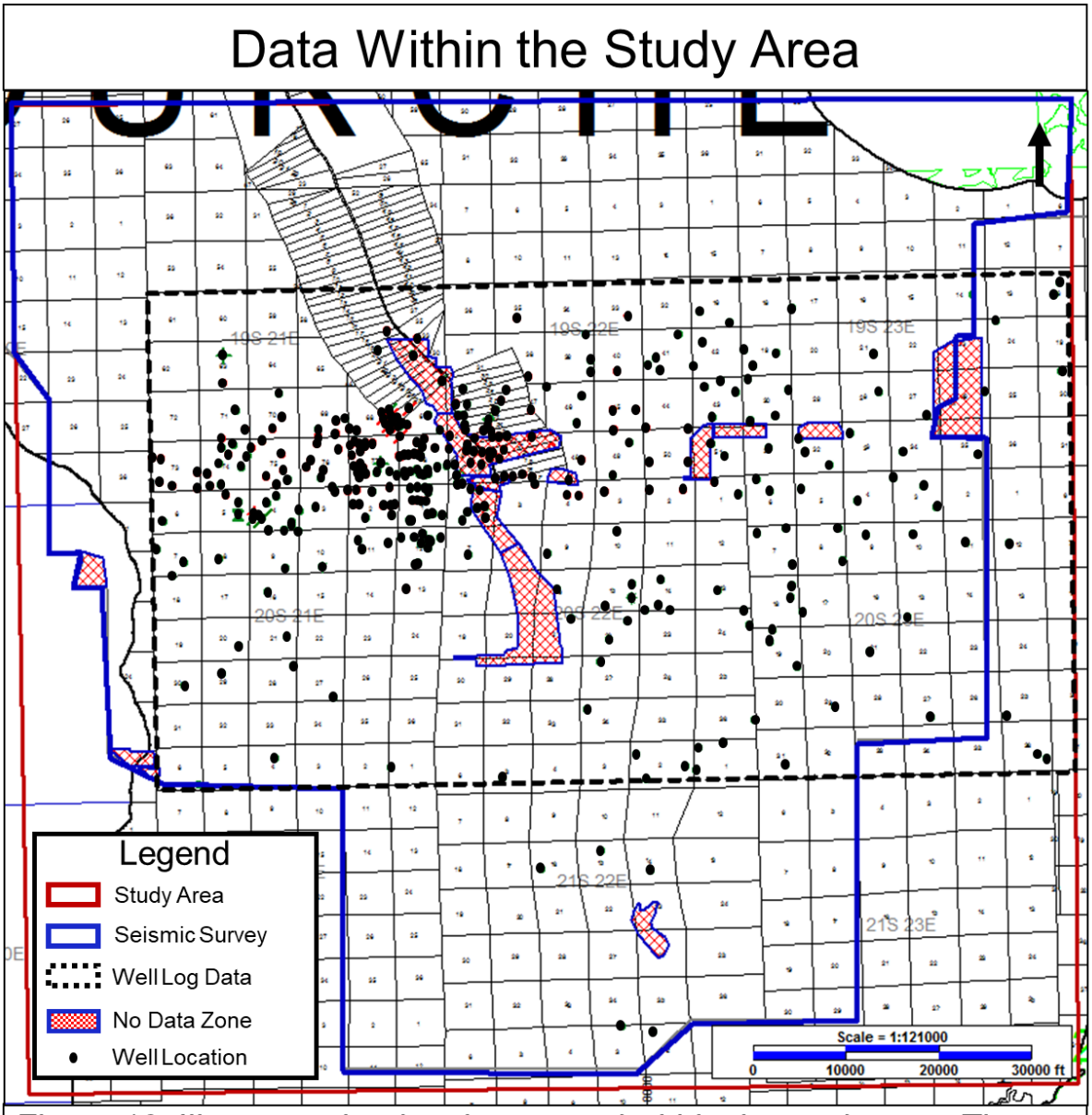

Figure 10. Illustrates the data interpreted within the study area. The red box outlines the extent of the study, the blue line outlines the extent of the seismic survey, the black-dotted box outlines the well log data coverage centered around the town of Golden Meadow, and the blue outlined polygons with red hachures indicate no data zones within the seismic survey.

Methods

I interpreted fault surfaces in the seismic data to map faults that displace shallow strata where shallow strata refer here to depths above 1 s TWT. Along these fault surfaces, multiple points are interpreted to map their geometries in the subsurface. Next, horizons were interpreted in order to produce regional structure maps (Figure 11). Following the seismic interpretation, I converted the fault surfaces into depth using a time versus depth chart, donated by Castex Energy. This made it easier to identify the exact location of faults at depth while correlating well logs. Well logs were correlated utilizing GR or SP logs with resistivity and conductivity signatures across the study area. This process was conducted by identifying similarities and recognizing patterns and interpreting those patterns to be within the same stratigraphic sections. These formation tops were first interpreted based on a type log of the 2700' sand from the Golden Meadow (Kolvoord, et al., 2008). The addition of two micropaleontological data points, Big A and Big B, were used to help correlate and date some of the strata back to the Late Miocene. Structure, isochore, and isochron maps were then produced from formation tops. Formation tops were then split into three epochs: Late Miocene, Pliocene, and Pleistocene. I determined these three divisions by using the correlation of Big A and Big B from the Late Miocene, a digitized map of the base of the Pleistocene (top of the Pliocene) (Sabate, 1968), and depositional thickness changes calculated from structure and isochore maps.

Then I calculated multiple expansion indices across major normal faults due to their laterally inequivalent growth patterns over time. These calculations are utilized to identify kinematic and non-kinematic sections to determine the history of fault movement for each growth fault.

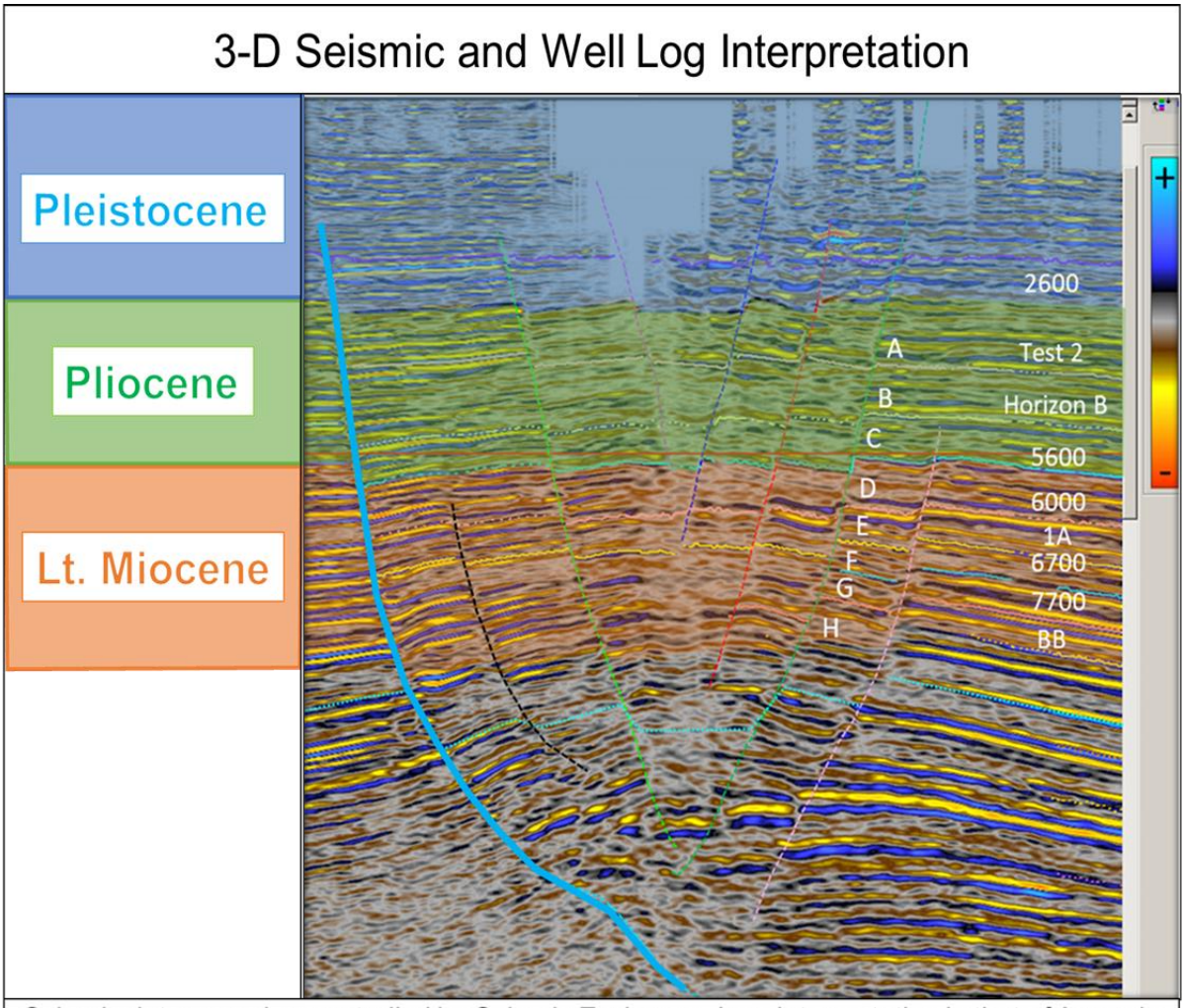

Seismic data owned or controlled by Seismic Exchange, Inc.; interpretation is that of Amanda Johnston

Figure 11. Illustrates 3D seismic data within the seismic survey, the Leeville 3D Merge, with interpreted horizon and well log data. The color bar, on the right, indicates the amplitudes of the seismic data. Positive amplitudes are colored blue, while the negative amplitudes are colored orange. The Golden Meadow fault (GMF) is in blue, while the multi-colored faults make up the graben.

Expansion indices (E.I.s) are the result of measurements of thickness changes or the ratio of stratigraphic growth across a fault. The ratio is the difference in thickness of sediments on the downthrown versus the difference in thickness of sediments on the upthrown sides of a fault (Cartwright et al., 1998). This ratio helps to define the timing of fault activity, or kinematic and non-kinematic zones. The interval of maximum expansion is the kinematic zone; if the age of the interval can be determined, then the age of the normal fault can be defined (Thorsen, 1963). Dating a fault is imperative while attempting to establish a geologic history of an area. Kinematic zones or intervals of maximum expansion are more accurate across listric normal faults. Calculated E.I.s over radial faults can be less accurate due to the decreased displacement off structure and dip, so expansion was only calculated across the LS to determine the timing of the cross-faults. There is a possible margin of error within these expansion indices in that a significant increase in expansion could be due to collecting data within a depositional feature, such as a channel. That margin of error is contingent upon that well's location within the channel, and how deep that channel is. More data would need to be obtained in the Miocene, Pliocene, and Pleistocene to identify these depositional features and better define an exact margin of error. In this study, E.I.s greater than one indicate growth along the fault surface.

Finally, I extrapolated the near-surface fault surfaces to the surface utilizing the Leeville 3D Merge seismic data. The faults were projected to the surface maintaining a constant dip angle. There is an error associated with these surface projections. If the actual dip of the fault surface does not remain constant, the dip may project more towards the hanging wall. I used a range of approximately 300 - 400 ft. These projections were overlain with the USGS Land

Area Change of Coastal Louisiana (1932 to 2016) map (Couvillion et al., 2017) in Google Earth to compare observed surface features, patterns of wetland loss, and the location of surface fault projections.

Results

Lake Enfermer Fault

Using the Leeville 3D Merge seismic survey, I interpreted fault surfaces within the study area. This interpretation allowed me to determine the shape and position of the LEF in geologic time. The LEF is an east-west striking listric normal fault and is downthrown to the south-southeast. Displacement occurs across the LEF in the shallow section of seismic data, and below the oldest correlated formation top, BB, in both of the seismic and well log data. I calculated the throw using seismic and well log data across the LEF. Displacement on this fault is up to 800 ft at depth in the Late Miocene interval on its eastward end (Figures 12-13). Additional structure maps are produced for the Late Miocene and are included in the appendix (A1-A6). Displacement up section is also observed in the Early Pliocene interval; these indicate throws up to 400 ft (Figures 14-15) (A7-A9), and displacement in the Early Pleistocene can reach up to 50 ft (Figures 16-17) (A10-A12).

The LEF penetrates through the Late Miocene. Isochore maps from the Late Miocene through the Pleistocene are analyzed to identify depositional trends throughout this interval over the study area. This analysis helps to understand the expansion indices of each fault in further detail. From these maps, a pattern of thickness variation is established during each epoch.

Structure Map of BB Formation Top

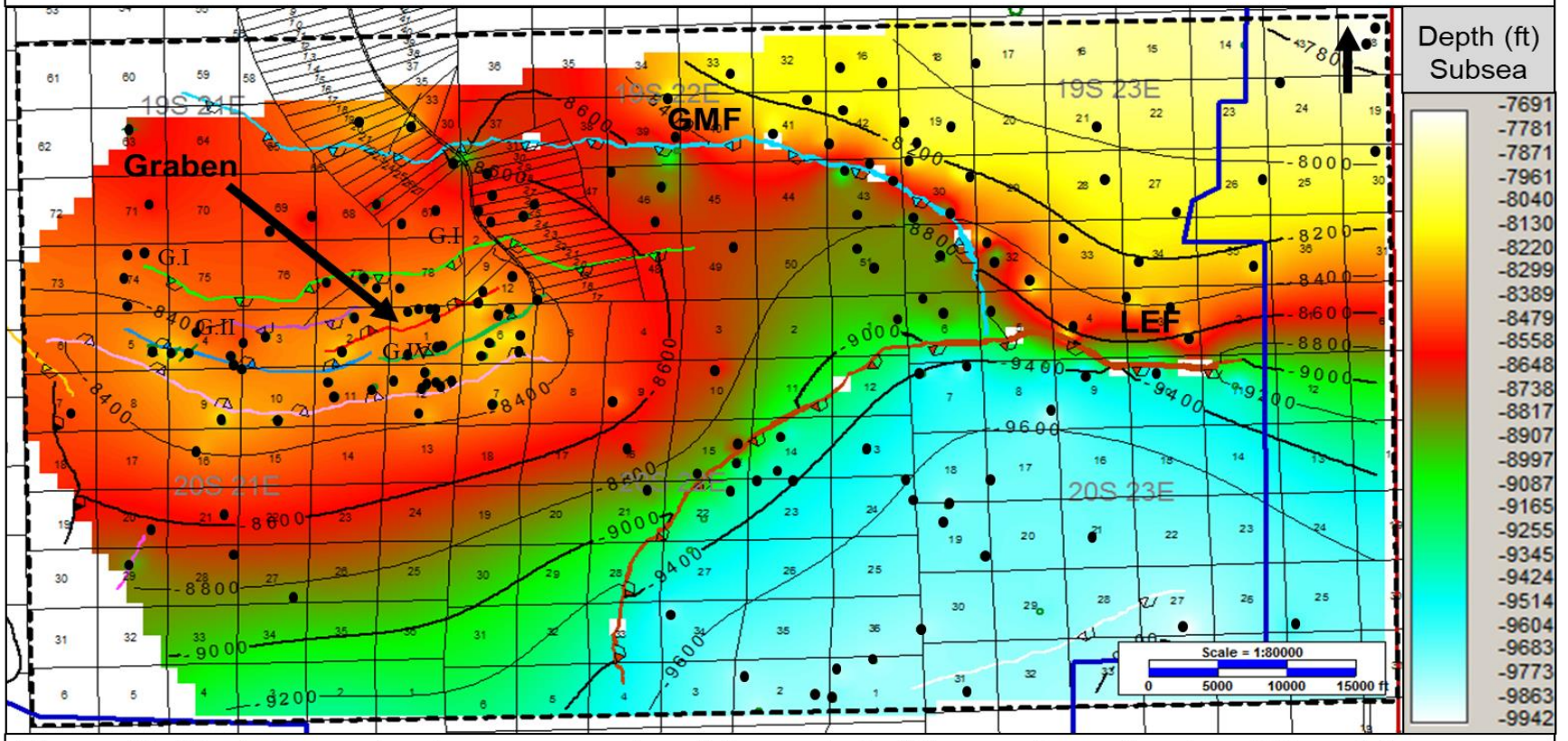

Figure 12. Illustrates a structure map produced from a Late Miocene formation top, BB, and the location of wells that were used within the study area. The blue line outlines the extent of the seismic survey, and the black-dotted box outlines the well log data coverage centered around the town of Golden Meadow. The Golden Meadow fault (GMF) is outlined in blue, the Lake Enfermer fault (LEF) is outlined in brown, and the black arrow is pointing to the graben. G I and II are two faults within the graben that are downthrown to the south. G IV is one of the six shallow faults within the graben that are downthrown to the north.

Structure Map of 8200 Formation Top

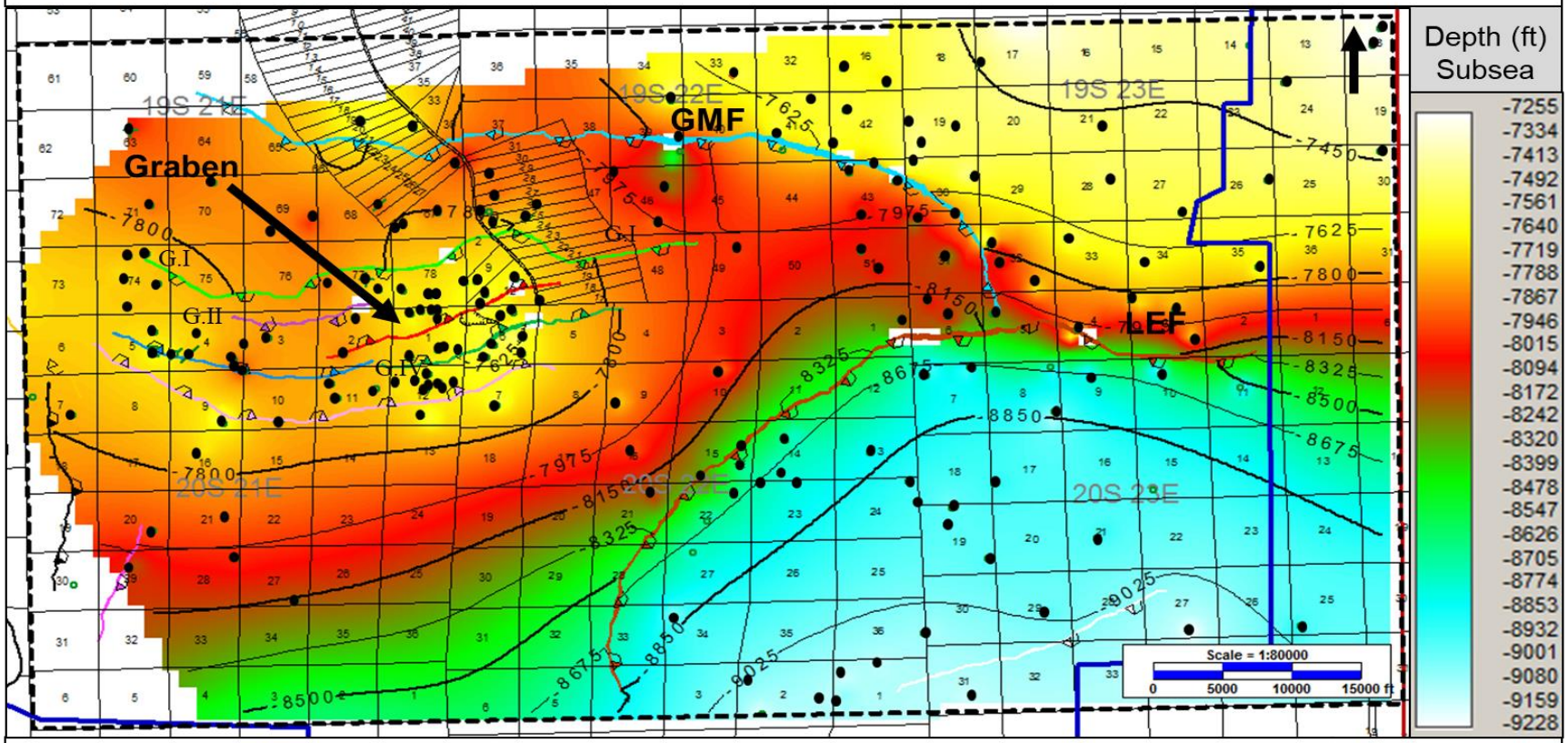

Figure 13. Illustrates a structure map produced from a Late Miocene formation top, 8200, and the location of wells that were used within the study area. The blue line outlines the extent of the seismic survey, and the black-dotted box outlines the well log data coverage centered around the town of Golden Meadow. The Golden Meadow fault (GMF) is outlined in blue, the Lake Enfermer fault (LEF) is outlined in brown, and the black arrow is pointing to the graben. G I and II are two faults within the graben that are downthrown to the south. G IV is one of the six shallow faults within the graben that are downthrown to the north.

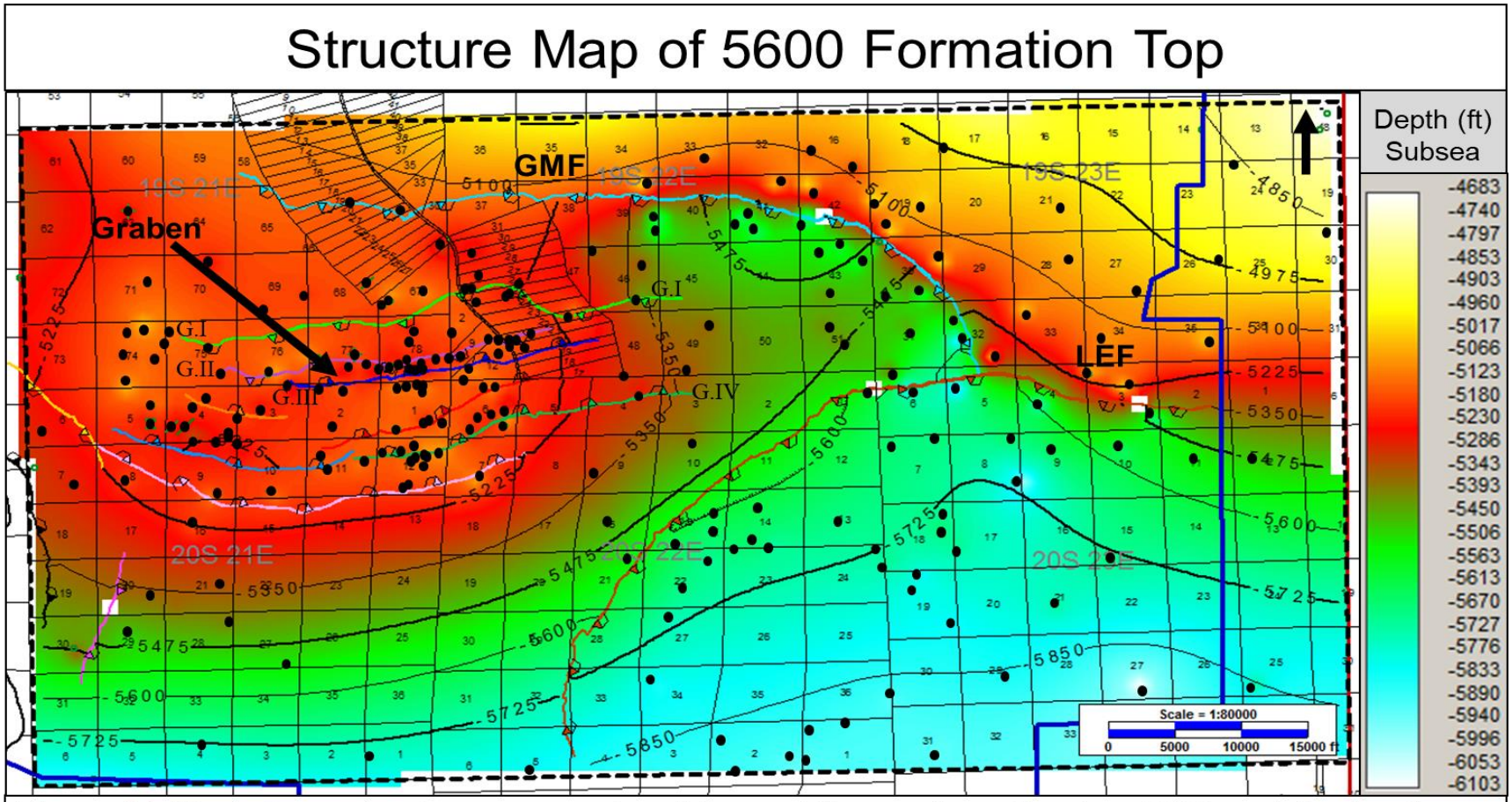

Figure 14. Illustrates a structure map produced from a Pliocene formation top, 5600, and the location of wells that were used within the study area. The blue line outlines the extent of the seismic survey, and the black-dotted box outlines the well log data coverage centered around the town of Golden Meadow. The Golden Meadow fault (GMF) is outlined in blue, the Lake Enfermer fault (LEF) is outlined in brown, and the black arrow is pointing to the graben. G I and II are two faults within the graben that are downthrown to the south. G III and IV are two of the six shallow faults within the graben that are downthrown to the north.

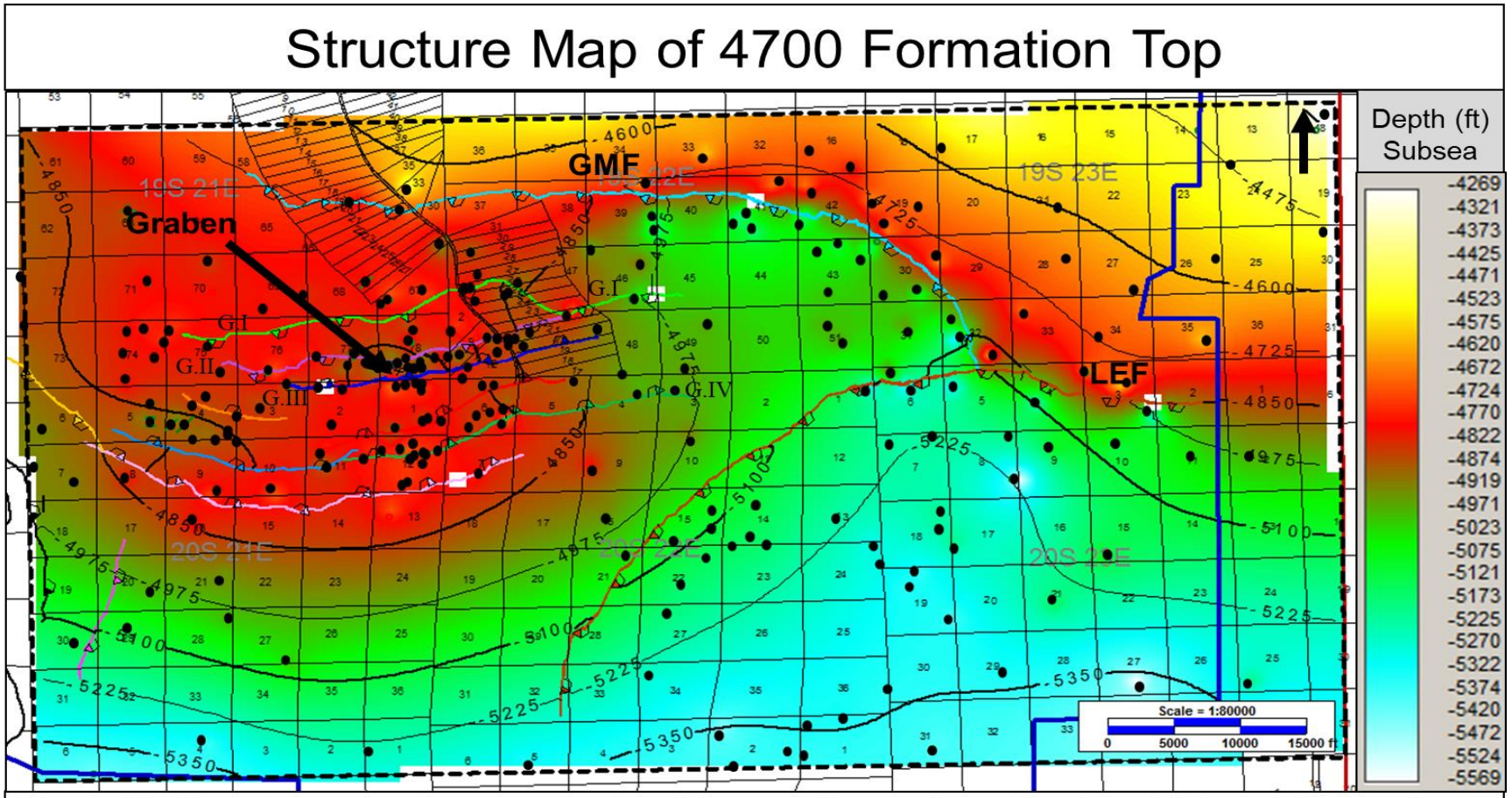

Figure 15. Illustrates a structure map produced from a Pliocene formation top, 4700, and the location of wells that were used within the study area. The blue line outlines the extent of the seismic survey, and the black-dotted box outlines the well log data coverage centered around the town of Golden Meadow. The Golden Meadow fault (GMF) is outlined in blue, the Lake Enfermer fault (LEF) is outlined in brown, and the black arrow is pointing to the graben. G I and II are two faults within the graben that are downthrown to the south. G III and IV are two of the six shallow faults within the graben that are downthrown to the north.

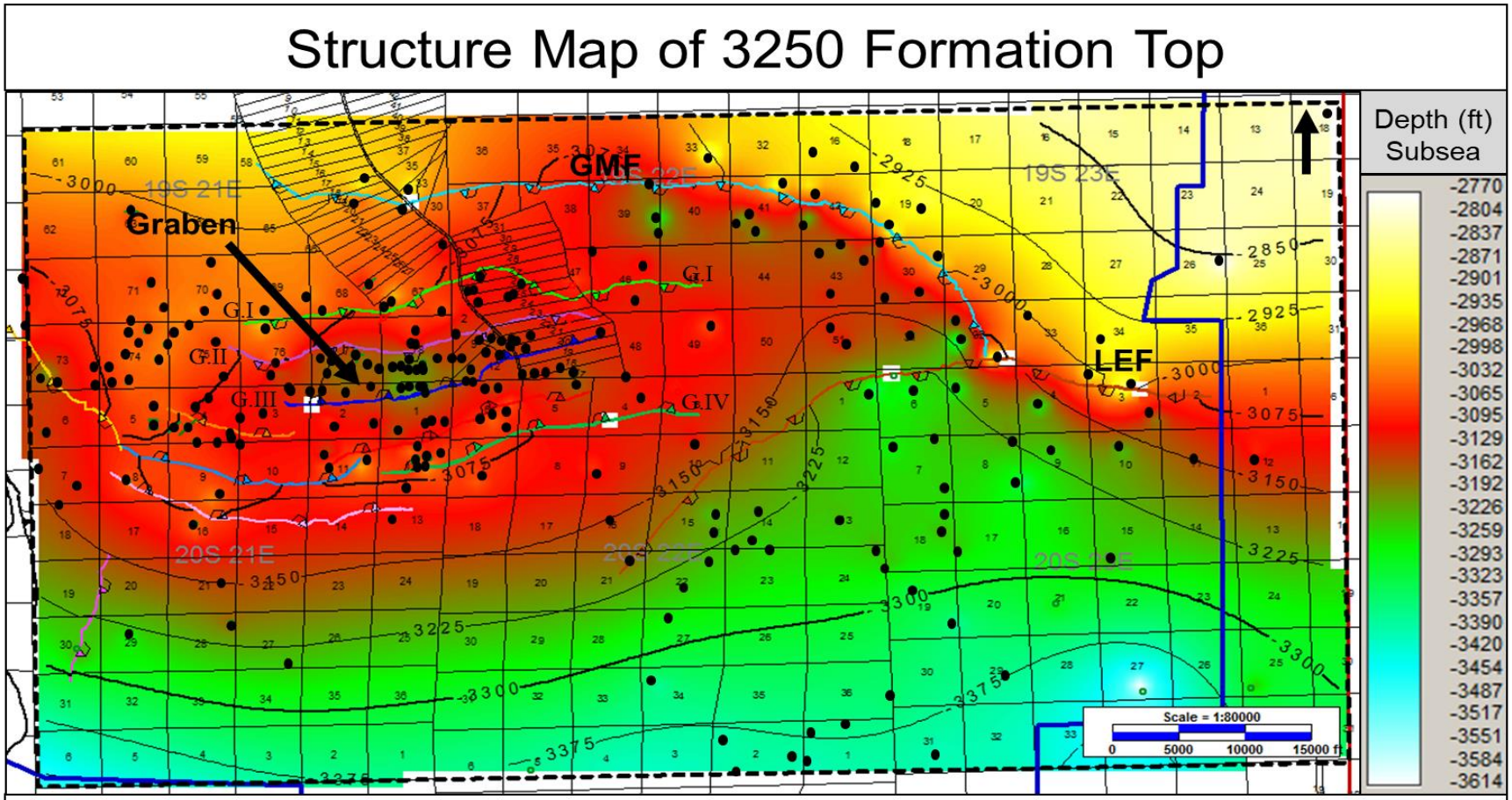

Figure 16. Illustrates a structure map produced from a Pleistocene formation top, 3250, and the location of wells that were used within the study area. The blue line outlines the extent of the seismic survey, and the black-dotted box outlines the well log data coverage centered around the town of Golden Meadow. The Golden Meadow fault (GMF) is outlined in blue, the Lake Enfermer fault (LEF) is outlined in brown, and the black arrow is pointing to the graben. G I and II are two faults within the graben that are downthrown to the south. G III and IV are two of the six shallow faults within the graben that are downthrown to the north.

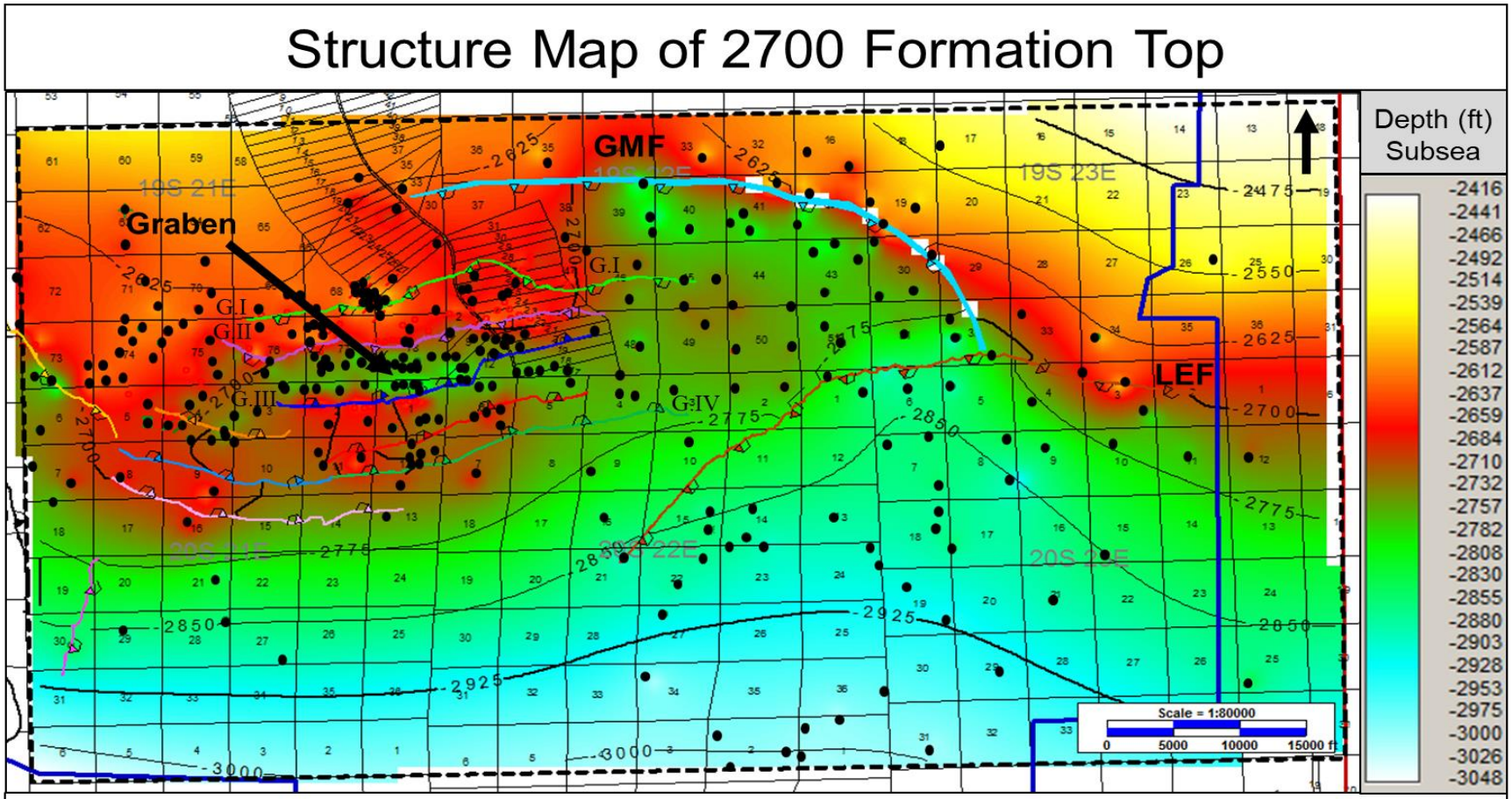

Figure 17. Illustrates a structure map produced from a Pleistocene formation top, 2700, and the location of wells that were used within the study area. The blue line outlines the extent of the seismic survey, and the black-dotted box outlines the well log data coverage centered around the town of Golden Meadow. The Golden Meadow fault (GMF) is outlined in blue, the Lake Enfermer fault (LEF) is outlined in brown, and the black arrow is pointing to the graben. G I and II are two faults within the graben that are downthrown to the south. G III and IV are two of the six shallow faults within the graben that are downthrown to the north.

Isochore Map of BB & 8200 Formation Tops

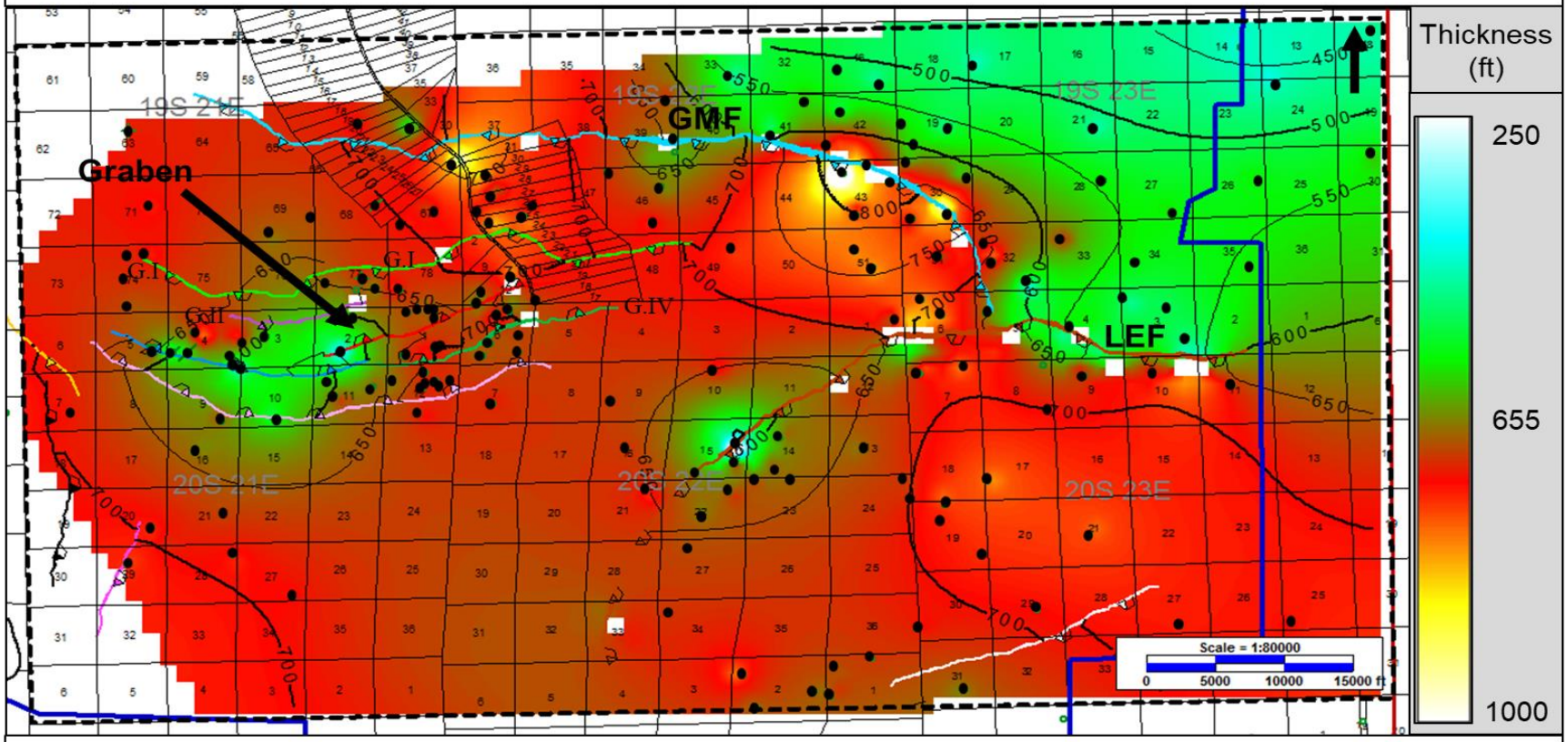

Figure 18. Illustrates an isochore map produced from Late Miocene formation tops, BB & 8200, and the location of wells that were used within the study area. The blue line outlines the extent of the seismic survey, and the black-dotted box outlines the well log data coverage centered around the town of Golden Meadow. The Golden Meadow fault (GMF) is outlined in blue, the Lake Enfermer fault (LEF) is outlined in brown, and the black arrow is pointing to the graben. G I and II are two faults within the graben that are downthrown to the south. G IV is one of the six shallow faults within the graben that are downthrown to the north.

The Miocene has the most distinct depositional trend, and while the Pliocene and Pleistocene are very similar, their patterns are lessened section. During the Miocene, the majority of the increase in thickness occurs along the downthrown fault block of LEF (Figure 18) (A13-A17). Within this time interval, thickness across the fault increases from the upthrown to the downthrown fault block between 50 and 100 ft. For example, the thickness on the upthrown block may be 550 ft in some areas, while thickness on the downthrown block may be increased to 650 ft total thickness. The thickness of strata increases to the east along the fault. In the Pliocene, the LEF continues to show evidence of expansion, along with other structures in the study area (Figure 19) (A18-A23). The calculated change in thickness from the upthrown to the downthrown fault block is about 25 to 75 ft. The thickness on the upthrown fault block is approximately 450 ft, whereas total thickness is about 500 ft on the adjacent part of the downthrown fault block. Overall stratal thickness continues to decrease throughout the Pleistocene. During this time, thickness on the downthrown side of the LEF is similar in the center of the graben, increasing from the upthrown block between 15 and 50 ft from 375 ft to 400 ft (Figure 20) (A24-A25).

Fault activity along the LEF is recorded by the expansion indices, E.I.s. Periods of maximum growth indicate times of fault activity. Four E.I.s were calculated across the LEF (Figure 21). In the west E.I. LE1 indicates a time of maximum growth between the 6700 and 7200 horizons which is in the Late Miocene. This E.I. LE1, is 1.65 (Figure 22a). Continuing northeast is E.I. of LE2, shows that the time of maximum growth shifts to horizons which is 1A to 6700 in the Late Miocene, which is 1.75 (Figure 22b). The E.I. of LE3, which indicates that the period of maximum growth is between 1B and 7700 horizons, is 1.96 (Figure 22c).

The last E.I. calculated for the LEF, LE4, is 2.53 (Figure 22d). The period of maximum growth also occurred between formation tops 1B and 7700 in the Late Miocene. Each E.I. is consistent with a period of maximum growth within the Late Miocene, and the interval with the highest average expansion also within the Late Miocene.

I projected the LEF to the surface of the Earth on Google Earth to compare the surface fault projections against satellite imagery. This fault is arcuate at the surface, and it is projected to be 5.81 miles long (Figure 23). As previously stated, this fault was projected to the surface by utilizing 3D seismic data keeping the constant dip of the fault. If there is an error with this projection, it will veer towards the hanging wall as it is unlikely that a fault would kink backwards towards the footwall.

Golden Meadow Fault

Along with the LEF, the GMF and its associated graben structure are interpreted within the seismic survey. The GMF is a normal growth fault, strikes east-west, is downthrown to the south and is listric with depth. The top of the Golden Meadow salt dome is at a depth of approximately -15344 ft. I utilized the seismic data to map the fault surface of the GMF; where it is adjacent to the salt body, there is a curvature or kink in the fault surface. With depth, other portions of the GMF surface continues to be consistent with the overall dip of the GMF. In the near surface, the eastern portion of this fault surface becomes very arcuate and abuts against the LEF at depth. Utilizing well log data, I calculated the throw across the GMF. Throw along the GMF is up to 400 ft in the Late Miocene (Figures 12-13) (Appendix 1-6). Up section, mapping within the Late Pliocene indicates throw of up to 200 ft (Figures

Isochore Map of 4700 & 5600 Formation Tops

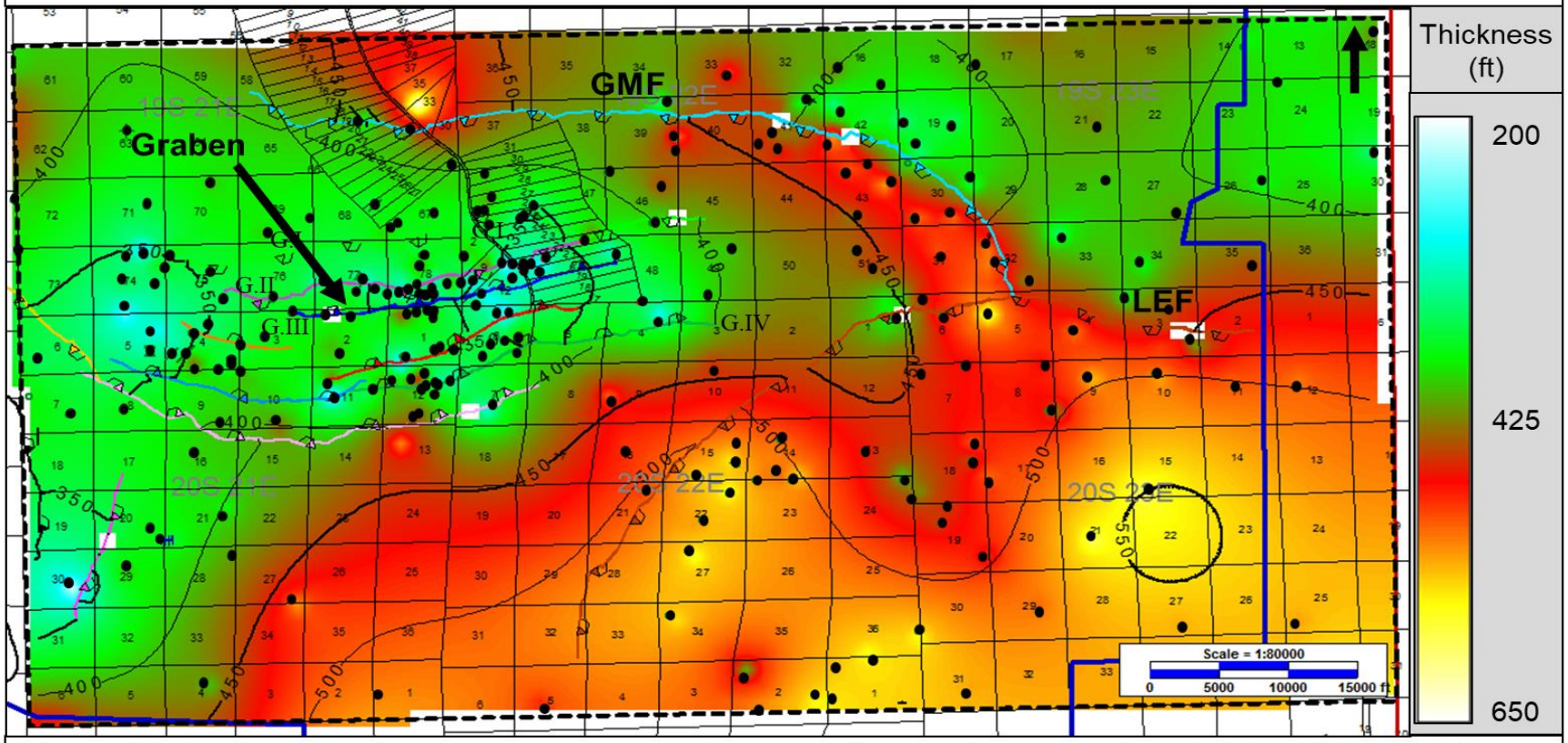

Figure 19. Illustrates a structure map produced from a Pliocene formation top, 4700 & 5600, and the location of wells that were used within the study area. The blue line outlines the extent of the seismic survey, and the black-dotted box outlines the well log data coverage centered around the town of Golden Meadow. The Golden Meadow fault (GMF) is outlined in blue, the Lake Enfermer fault (LEF) is outlined in brown, and the black arrow is pointing to the graben. G I and II are two faults within the graben that are downthrown to the south. G III and IV are two of the six shallow faults within the graben that are downthrown to the north.

Isochore Map of 2700 & 3250 Formation Tops

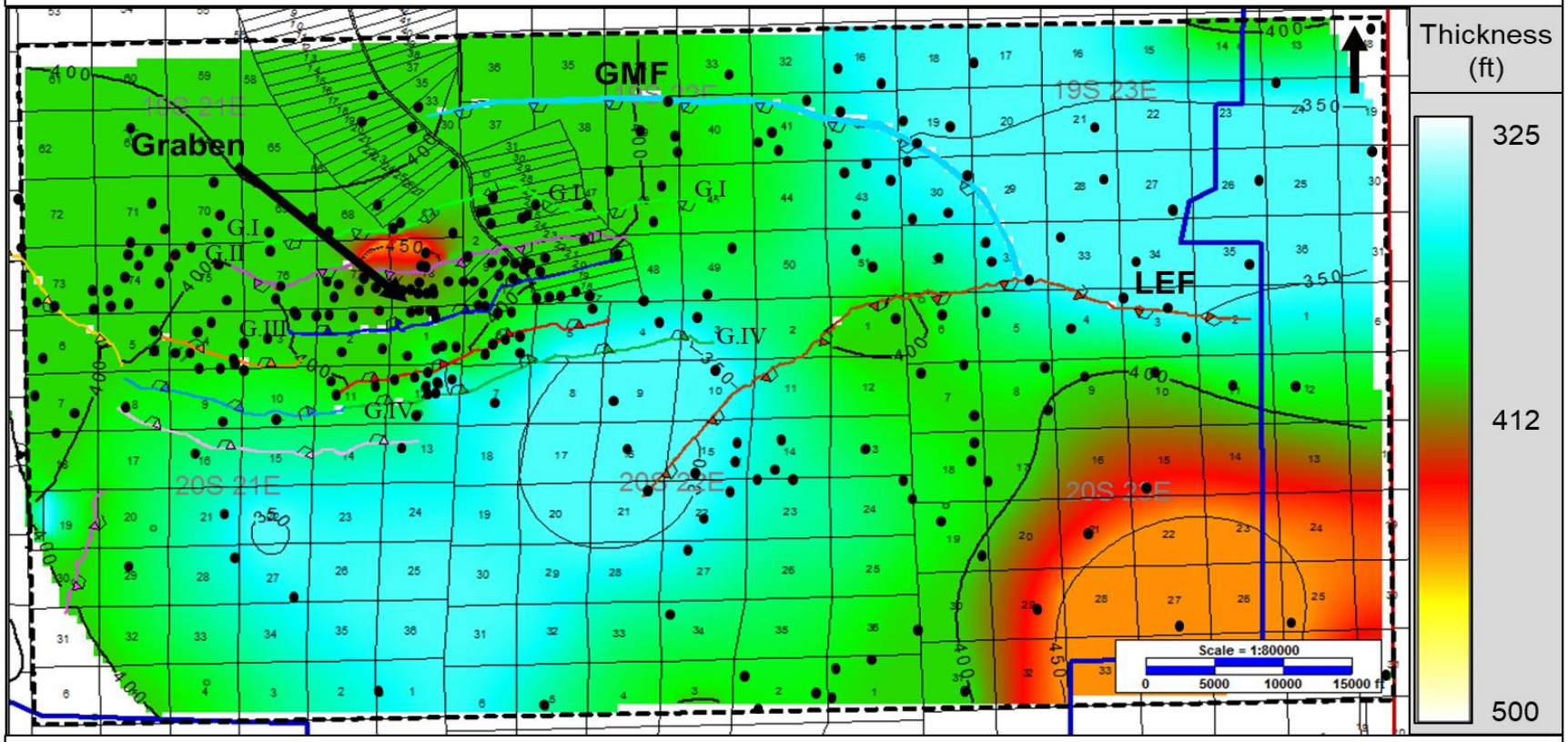

Figure 20. Illustrates a structure map produced from a Pleistocene formation top, 2700 & 3250, and the location of wells that were used within the study area. The blue line outlines the extent of the seismic survey, and the black-dotted box outlines the well log data coverage centered around the town of Golden Meadow. The Golden Meadow fault (GMF) is outlined in blue, the Lake Enfermer fault (LEF) is outlined in brown, and the black arrow is pointing to the graben. G I and II are two faults within the graben that are downthrown to the south. G III and IV are two of the six shallow faults within the graben that are downthrown to the north.

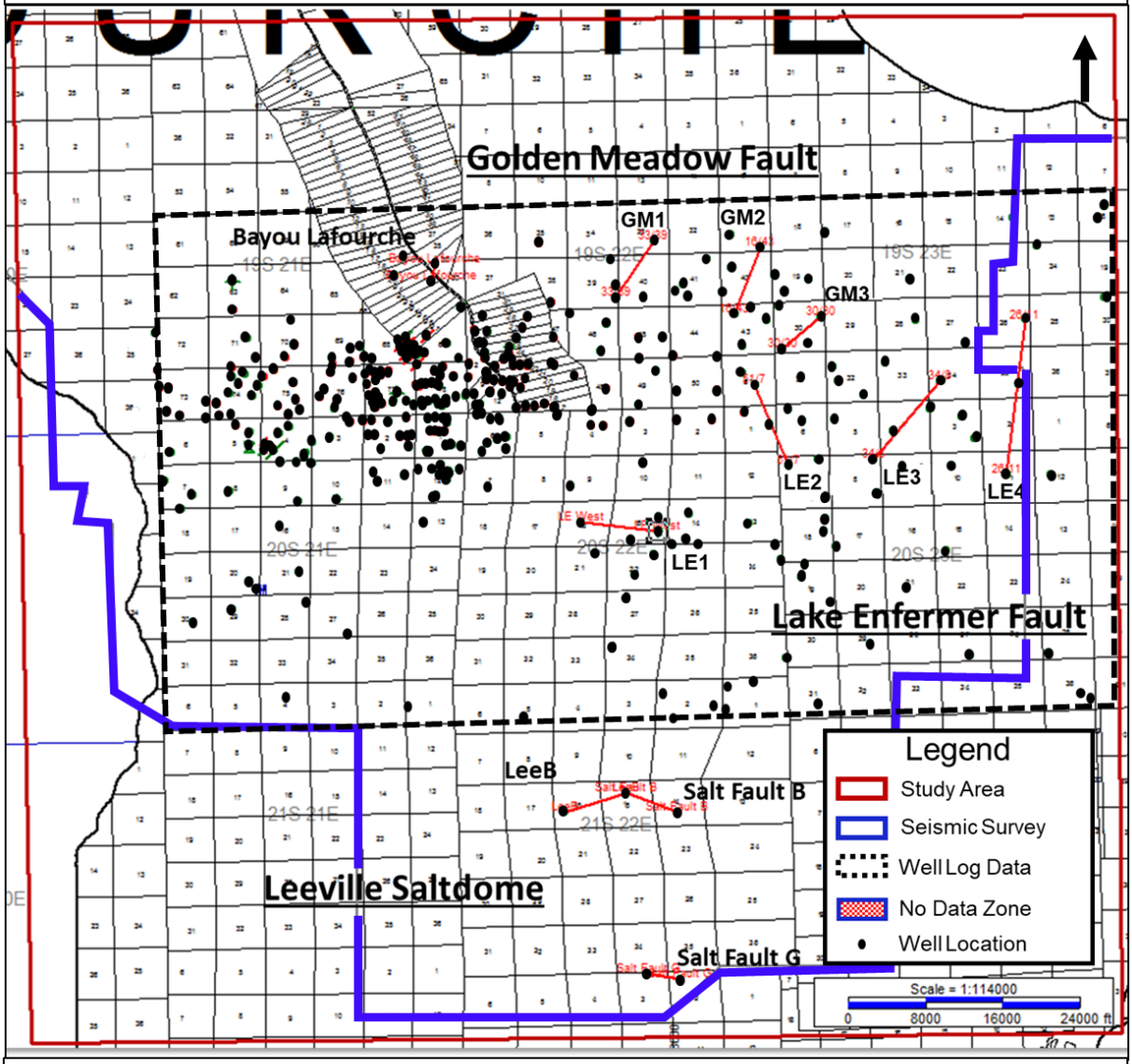

Figure 21. Illustrates the location of wells that were used to calculate expansion indexes within the study area. The red box outlines the extent of the study, the blue line outlines the extent of the seismic survey, and the black-dotted box outlines the well log data coverage centered around the town of Golden Meadow. Five additional wells were correlated to calculate expansion indexes around the Leeville Salt dome. Four expansion indexes were calculated for the Golden Meadow Fault: Bayou Lafourche, GM1, GM2, and GM3, listed from west to east respectively. Four expansion indexes were calculated for the Lake Enfermer Fault: LE1, LE2, LE3, and LE4, listed from west to east respectively. Lastly, three expansion indexes are calculated for the Leeville Saltdome: LeeB, Salt Fault B, and Salt Fault G, listed from west to east and north to south.

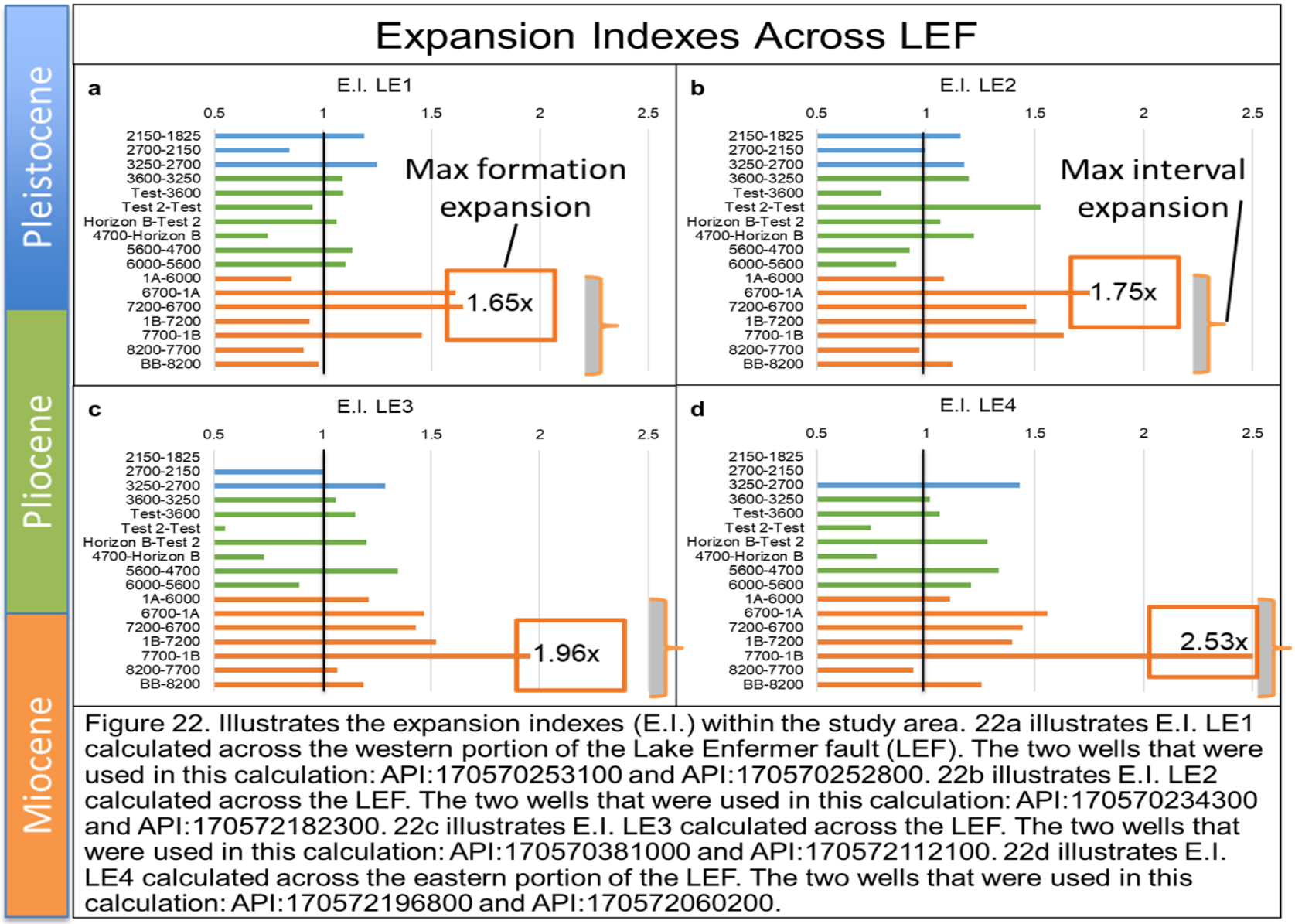

Figure 22. Illustrates the expansion indexes (E.I.) within the study area. 22a illustrates E.I. LE1 calculated across the western portion of the Lake Enfermer fault (LEF). The two wells that were used in this calculation: API:170570253100 and API:170570252800. 22b illustrates E.I. LE2 calculated across the LEF. The two wells that were used in this calculation: API:170570234300 and API:170572182300. 22c illustrates E.I. LE3 calculated across the LEF. The two wells that were used in this calculation: API:170570381000 and API:170572112100. 22d illustrates E.I. LE4 calculated across the eastern portion of the LEF. The two wells that were used in this calculation: API:170572196800 and API:170572060200.

Surface Fault Projections

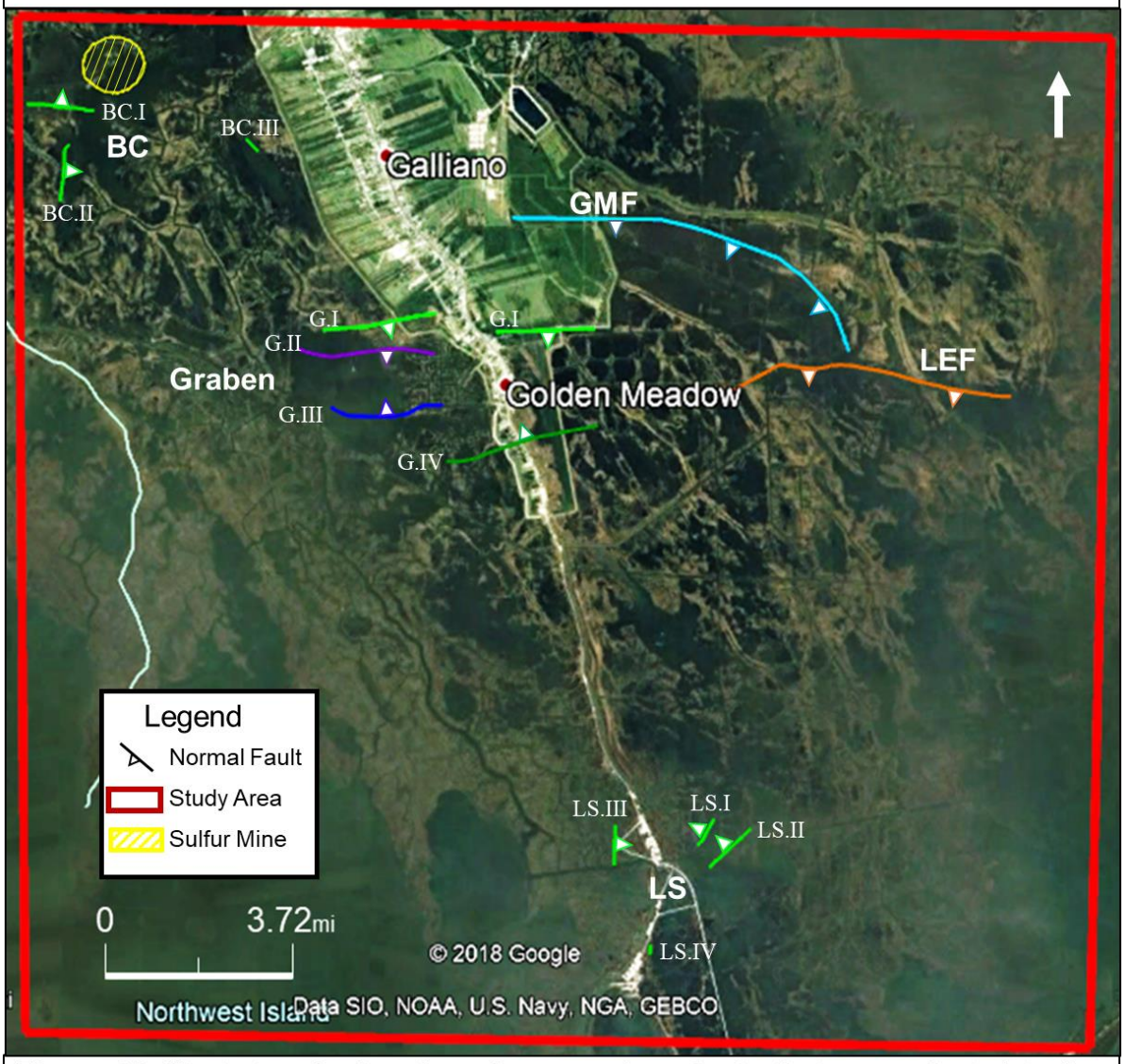

Figure 23. Illustrates the location of near-surface faults that are projected to the surface on Google Earth. The red box outlines the extent of the study and the yellow lined polygon identifies the approximate location of the Bully Camp Sulfur Mine (Gagliano et al., 2003). There are five structures labelled within the study area: Bully Camp salt dome (BC), Golden Meadow fault (GMF), Lake Enfermer fault (LEF), Graben, and the Leeville salt dome (LS). The GMF is projected to be 7.69mi long and the LEF is projected to be 5.81mi long. There are three surface faults projected near the BC: BC I (1.35mi), II (1.12mi), and III (0.34mi). Four faults are projected for the Graben: G I (4.25mi combined), G II (2.72mi), G III (2.26mi), and G IV (3.10mi). Four faults are also projected for the LS: LS I (0.60mi), LS II (1.09mi), LS III (0.75mi), and LS IV (0.18mi).

14-15) (Appendix 7-9), and the western portion of this fault is less active, dying towards the surface as illustrated by the difference between Figures 11 and 13. Along the more active eastern portion of the GMF, throw is as much as 50 ft in the Pleistocene interval (Figures 16-17) (A10-A12).

Similar to the LEF, the GMF shows displacement through deeper strata within the seismic data. Isochore maps are calculated utilizing well log data from throughout the Miocene to the Pleistocene. The Miocene isochore map illustrates local increases in thickness occurring along the GMF and its associated graben faults (Figure 18) (A13-A17). Displacement and sediment thickness increase along the downthrown fault block to the east, creating a roll-over anticline. Evidence of the rollover anticline can be seen in the western portion of the graben area where there is a localized thinning of sediments, indicating a possible paleo-high within the downthrown fault block. Figure 18 shows the calculated increase in thickness across the GMF; thicknesses increase in the downthrown block by 50 to 150 ft from west to east, respectively. The thickness in the upthrown block is approximately 650 ft, whereas thickness in the downthrown block is about 800 ft. In the Pliocene, as in the Miocene, increased growth along the GMF occurs predominantly along the eastern portion of the fault in comparison to the west. Growth within the associated graben faults occurs mostly in the center of the anticline downdip of the fault (Figure 19) (A18-A23). In the Pliocene, thickness across the GMF increases from 50 to 75 ft downthrown, from 400 ft thick to 475 ft thick. Throughout the Pleistocene, there is an increased sediment thickness measured across the eastern portion of the GMF of approximately 25 ft, e.g., the upthrown thickness is about 350 ft and the downthrown thickness is about 375 ft. Increased thicknesses occur locally in the graben

throughout the Pleistocene. Pleistocene thickness on the downthrown fault block are similar in the center of the graben to that of the LEF and are up to 450 ft (Figure 20) (A24-A25).

Fault activity is recorded along the GMF by calculating expansion indices. Four expansion indices illustrate growth along this fault (Figure 21). Starting in the west for the GMF is E.I. Bayou Lafourche, which is 5.10, and indicates a time of maximum growth is between the 4700 and Horizon B horizons in the Pliocene (Figure 24a). Continuing to the east, E.I. GM1 is 3.56, and the time of maximum growth shifts to horizons 4700 and Horizon B in the Pliocene (Figure 24b). Moving to the southeast, E.I. GM2 is 1.63, which indicates maximum growth or displacement between 8200 and BB horizons, the early Late Miocene (Figure 24c). The last E.I. calculated for the GMF is to the south-southeast of GM2, E.I. GM3. This calculation indicates a period of maximum growth between horizons 4700 and 5600, in the Early Pliocene equaling 1.41 (Figure 24d). Though the period of maximum growth for each E.I. is within the Pliocene interval, the interval with the largest average expansion is within the Late Miocene.

Synthetic and antithetic faults developed to the south of the GMF on the downthrown block, forming a graben. All shallow graben faults have an east-west strike, and there are eight in total. Four of these faults, along with the GMF, are projected to the surface by maintaining a constant fault dip. These synthetic and antithetic faults differ from the LEF and GMF because, despite increased displacement with depth, that displacement then decreases as they approach the GMF. At the surface the GMF is interpreted to be 7.69 miles long and penetrate past the Late Miocene at depth. The lime green synthetic fault shown in Figure 23 is

projected to be 4.25 miles in length at the surface. The purple synthetic fault is 2.72 miles at the surface. The blue antithetic fault is 2.26 miles at the surface. Lastly, the dark green antithetic fault is projected to be 3.10 miles at the surface (Figure 23).

Leeville Salt Dome

The LS is located in the south-central portion of the study area and is surrounded by many radial faults at depth. I interpreted the seismic data to map the shallow radial faults surrounding the shape of the LS. The geometry of the LS is that of an intrusive high amplitude diapiric salt stock that has a broad base and narrows up section, similar to a cone towards the surface (Jackson and Talbot, 1986). For the radial faults surrounding this salt stock, I calculated their displacement within the seismic data for the Pliocene epoch and found that the throw of these faults is approximately 75 ft on average, in the north-northeastern area around the LS (Figure 25). Displacement for this same interval is lower in the south-southwestern area around the LS at approximately 10 to 25 ft on average.

Radial faults strike close to perpendicular to salt domes, and displacement decreases away from the dome. I interpreted the seismic data to map these radial faults and to determine dip directions. Four faults are projected to the surface, and although the majority of these shallow faults are downthrown in a clockwise direction at depth, two faults that are projected to the surface are downthrown in the counter-clockwise direction. The two counter-clockwise (LS I and II) faults are located on the northeast corner of the LS (Figure 23). The shorter fault trace LS I cuts through Lake Jesse and is about 0.60 miles. The longer fault trace of LS II, cuts

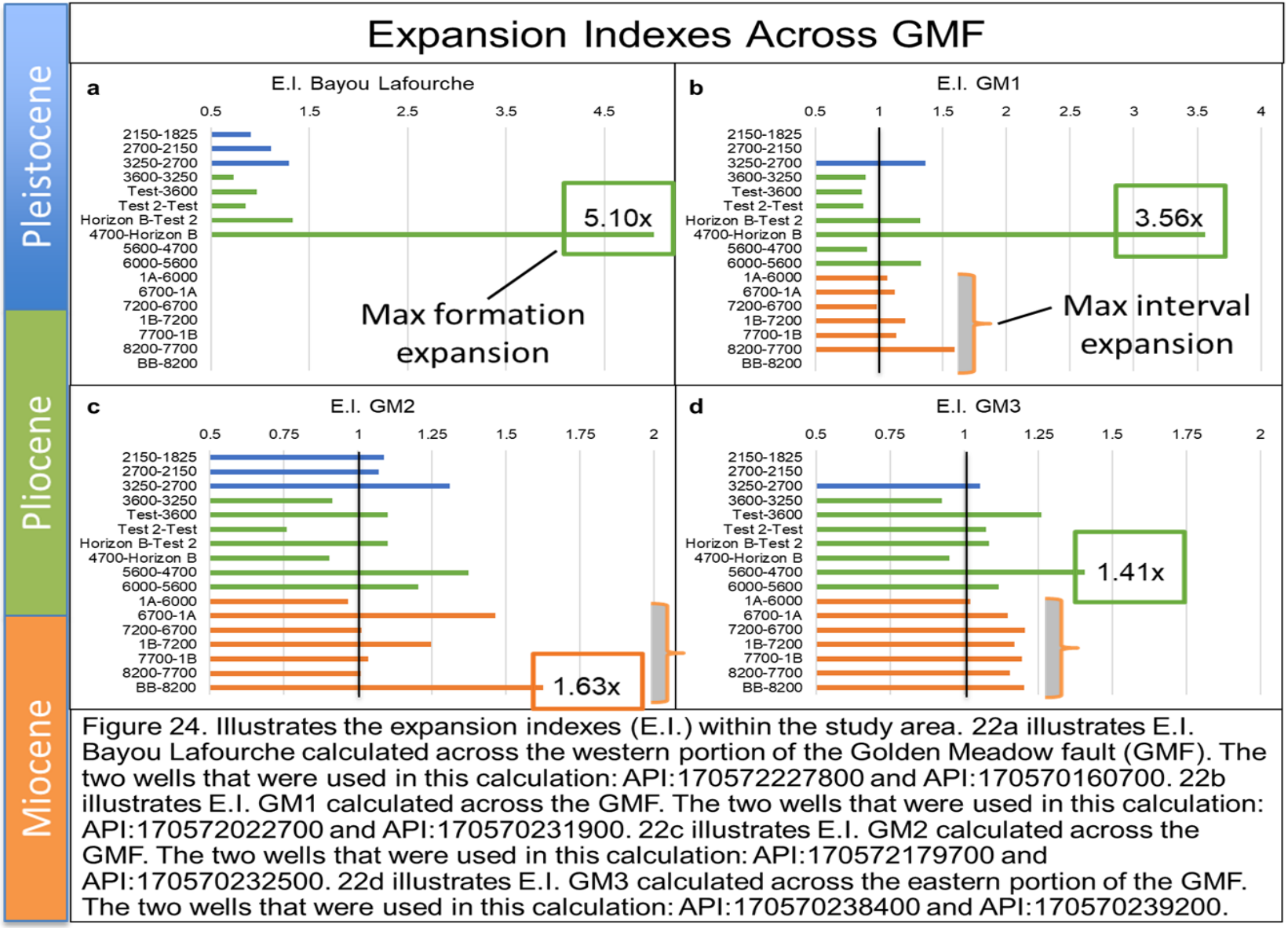

Figure 24. Illustrates the expansion indexes (E.I.) within the study area. 22a illustrates E.I. Bayou Lafourche calculated across the western portion of the Golden Meadow fault (GMF). The two wells that were used in this calculation: API:170572227800 and API:170570160700. 22b illustrates E.I. GM1 calculated across the GMF. The two wells that were used in this calculation: API:170572022700 and API:170570231900. 22c illustrates E.I. GM2 calculated across the GMF. The two wells that were used in this calculation: API:170572179700 and API:170570232500. 22d illustrates E.I. GM3 calculated across the eastern portion of the GMF. The two wells that were used in this calculation: API:170570238400 and API:170570239200.

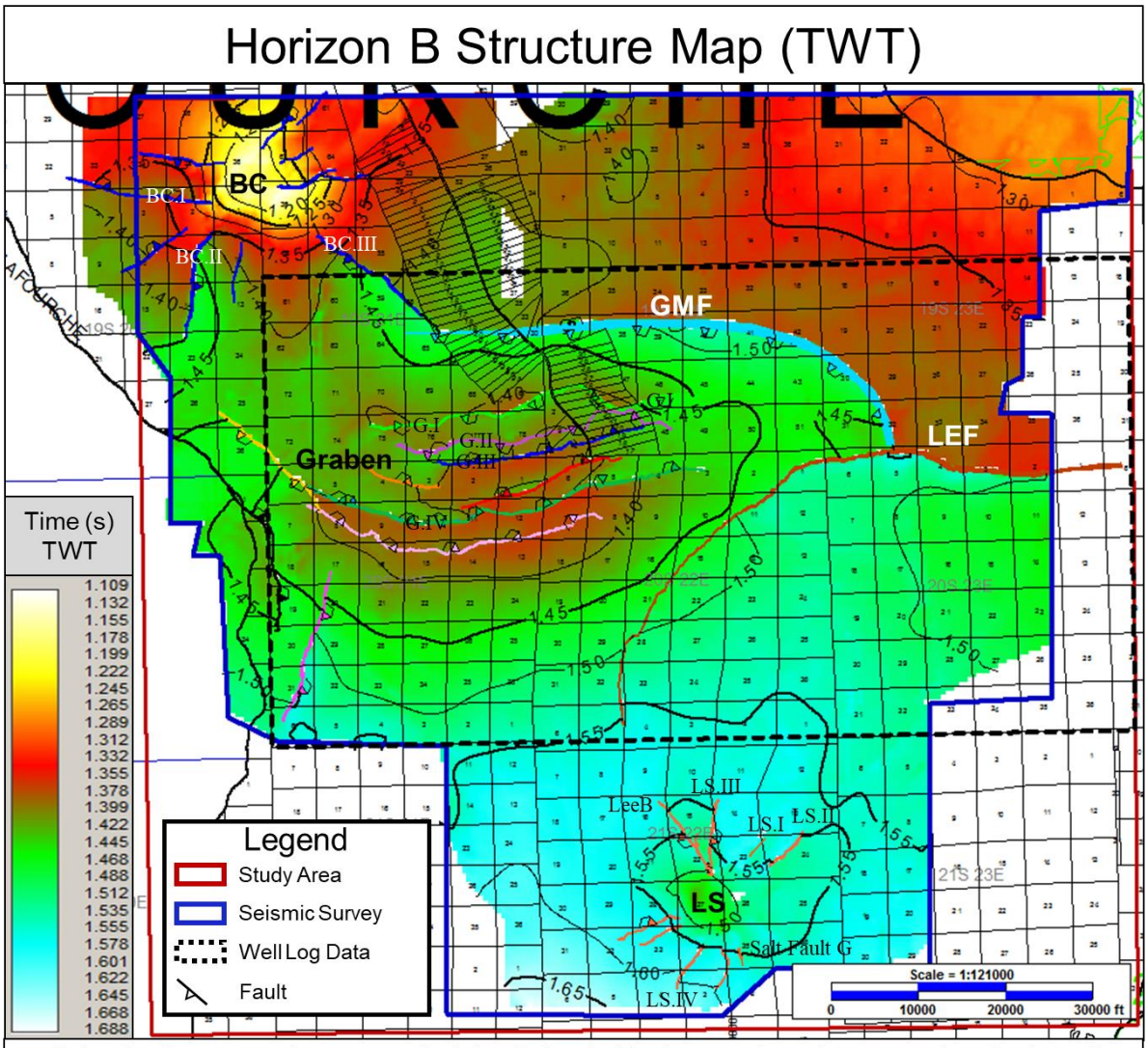

Seismic data owned or controlled by Seismic Exchange, Inc.; interpretation is that of Amanda Johnston

Figure 25. Illustrates the Horizon B structure map within the study area. The red box outlines the extent of the study, the blue line outlines the extent of the seismic survey, and the black-dotted box outlines the well log data coverage centered around the town of Golden Meadow. This map is a structure map in two-way travel time (TWT). Within the seismic data and according to the time v. depth chart, 1s is approximately 3000 ft. Five structures labelled within the study area: Bully Camp salt dome (BC), Golden Meadow fault (GMF), Lake Enfermer fault (LEF), Graben, and the Leeville salt dome (LS). There are three surface faults projected near the BC: BC I, II, and III. There are seven faults within the graben, four faults are projected to the surface for the Graben: G I, II, III, and G IV. There are many shallow faults surrounding the LS, four faults are projected to the surface: LS I, II, III, and LS IV. LeeB and Salt Fault G are also labelled around the LS, expansion indexes are calculated for these faults.

through the Southwestern Louisiana Canal and is projected to be 1.09 miles long. The other fault that is downthrown in a counter-clockwise direction is LeeB which is downthrown to the west and does not penetrate the surface. This shallow fault is offset by LS III, downthrown to the east, creating an ‘X' pattern north-northwest of the salt dome (Figure 25). Expansion indices are calculated to determine if these faults became active contemporaneously or if there is a cross-cutting relationship that would make one fault likely to be the more dominant fault today. LeeB is downthrown to the west whenever LS III is downthrown to the east. It does not appear that LeeB displaces the surface, but LS III has a projected length of 0.75 miles at the surface. LeeB is interpreted to have initiated in the Pliocene, and LS III became active in the Pleistocene (Figure 23). The last radial fault that may extend to the surface is LS IV which is projected to be 0.18 miles.

Three expansion indices are calculated around the Leeville salt dome (Figure 21). Starting in the northwest, E.I. LeeB is 1.13; this indicates a period of maximum growth between horizons Test and Test 2, i.e. during the Middle Pliocene (Figure 26a). Moving to the east, E.I. LS III is 1.33 and indicates maximum growth between the 2150 and 2500 (Figure 26b). Lastly to the southeast is E.I. Salt Fault G equaling 1.34; this fault appears to penetrate near-surface sediments but not the surface. The time of maximum growth of Salt Fault G shifts to horizons 4700 and Horizon B in the Pliocene (Figure 26c).

Bully Camp Salt Dome

The BC is located in the northwest portion of the study area and surrounded by many shallow radial faults (Figure 25). Utilizing the seismic data, I determined the shape of the BC and

calculated the throw of the shallow faults around the dome. The allochthonous Louann Salt that forms the BC is closer to the surface than that of LS by approximately 1600 ft. The shape of the stalk is more columnar than conical like the LS. Many shallow faults surround the dome, and the throw of these faults was calculated within the Pliocene interval (Figure 25). The radial faults located to the south of the dome have the highest throws, increasing from about 150 to 300 ft from the eastern and western regions to the southwest respectively. Faults located in the east and western areas around the BC have a throw of approximately 150 ft, throw is less on the faults to the north, i.e. about 50 or 60 ft on average.

Only three of these shallow faults are projected to the surface (Figure 26). There does not appear to be a directionality of throw for these radial faults, but they share the characteristics of all radial faults (Ocamb, 1961). The northernmost radial fault, BC I, strikes east-west and is downthrown to the north. This fault is projected to be 1.35 miles long. To the south is BC II, a north-south striking fault that appears to penetrate the top of the seismic volume. It is downthrown to the east and is projected to be about 1.12 miles long, cutting through Lake Bully Camp. While most faults are independent of other structures within the study area, there is one radial fault to the southeast of the dome, BC III, striking northwest-southeast that dies out against the GMF at depth (Figures 23 and 25). On the surface, this fault trace is approximately 0.34 miles long and downthrown to the southwest.

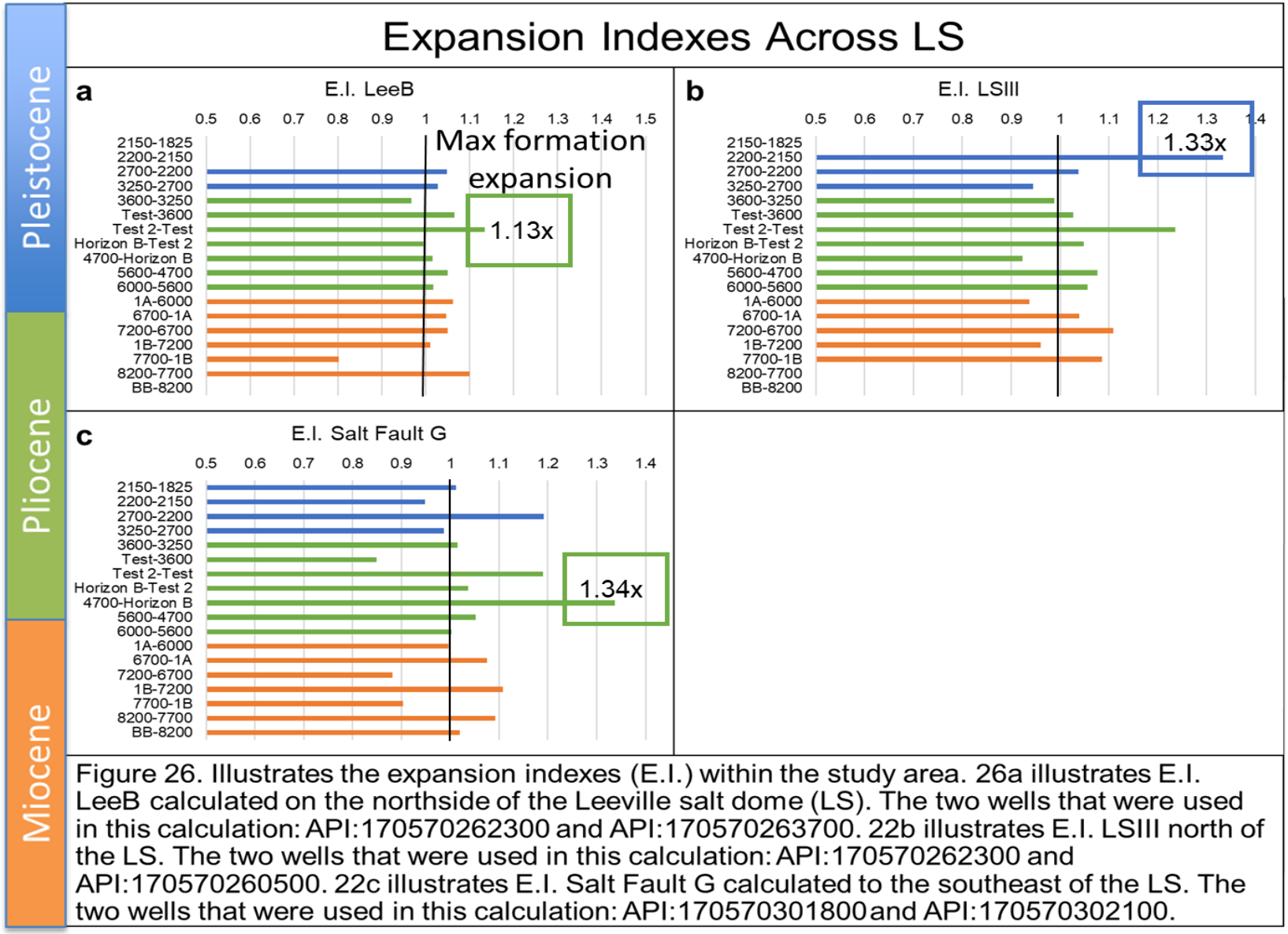

Figure 26. Illustrates the expansion indexes (E.I.) within the study area. 26a illustrates E.I. LeeB calculated on the northside of the Leeville salt dome (LS). The two wells that were used in this calculation: API:170570262300 and API:170570263700. 22b illustrates E.I. LSIII north of the LS. The two wells that were used in this calculation: API:170570262300 and API:170570260500. 22c illustrates E.I. Salt Fault G calculated to the southeast of the LS. The two wells that were used in this calculation: API:170570301800 and API:170570302100.

Discussion

Faults that extend to the surface may influence surface geomorphology and wetland loss. Characterizing fault displacement over time, i.e. determining its history, may help predict if fault movement can be expected today. The oil and gas industry have been mapping subsurface faults and salt domes in coastal Louisiana since before the 1930s and that knowledge has been underutilized in studying subsidence (Wallace et al., 1966 and Sabate, 1968). In the past, subsidence was measured with tide gauge data, and aerial imagery was used to identify potential areas of subsidence from wetland loss patterns at the surface (Gagliano et al., 1981, Turner, 1987, Gagliano et al., 2003, and Couvillion et al., 2017). Since that time some of Louisiana's oil and gas well log data, and in rare cases 3D seismic data, became available to those outside of the industry as a primary tool for identifying potential surface-penetrating faults (Armstrong et al., 2013). High-resolution seismic data in the near surface have also led to new perspectives on subsurface contributors of subsidence (Lopez et al., 1997 and Roberts et al., 2008).

Below the Late Miocene, stratigraphic correlations can become complicated, making it difficult to estimate stratigraphic expansion utilizing well log data alone (Kolvoord et al., 2008). Additional challenges include the potential for increased lateral displacement with depth, alongside increased vertical movement and the possibility that some strata may only be found on one side of the fault blocks. Younger strata are interpreted within the 3D seismic data; however, additional paleontological data are needed to provide a reliable method to age-date these horizons, more specifically to differentiate between the Early and Middle Miocene, within the seismic data (Kolvoord et al., 2008). My results are interpreted to

determine the growth history of the LEF, GMF, and several of the radial faults surrounding the LS to examine if fault activity, or subsurface geology, may have influenced wetland loss near Golden Meadow, Louisiana.

Growth Faults

The Middle Miocene began with a period of marine transgressions (Curtis, 1970). A marine regression developed later in the Middle Miocene that allowed for the progradation of many shelf-edge deltas to develop to the south towards the GOM (Curtis, 1970). The delta fronts appear to form two negative lineaments, ‘a' and ‘b,' that align closely with the GMFZ (Figure 27). The spatial coincidence of Middle Miocene deltas with the GMFZ strongly suggests that fault activity along this zone began during or soon after this period. The eastern lineament, the toe of Delta IXb, stops to the north of the city of present-day Golden Meadow (Curtis, 1970) and four marsh breaks, interpreted in 1966, have also been highlighted within the study area (Figure 27). Two of the highlighted marsh breaks lay closely to projections of the GMF and LEF, indicating that wetland loss over this area may have been occurring before the 1960’s. The continuing the fall of Miocene sea level allowed for the progradation of this delta over southern Louisiana to develop and due to continued sedimentation and sediment loading, the GMF first became active sometime in the Middle Miocene due to a shelf-edge failure with an east-west strike (Kolvord et al., 2008) (Figure 28). This agrees with my structure and isochore maps (Figures 12 and 18). E.I.s determined in the present study over the GMF provide evidence that fault activity was already occurring during the deepest interval of investigation, i.e. formation tops 8200 and BB (Figure 28). Isochore data shown in

Trend of Middle Miocene Regressive Deltas in South Louisiana

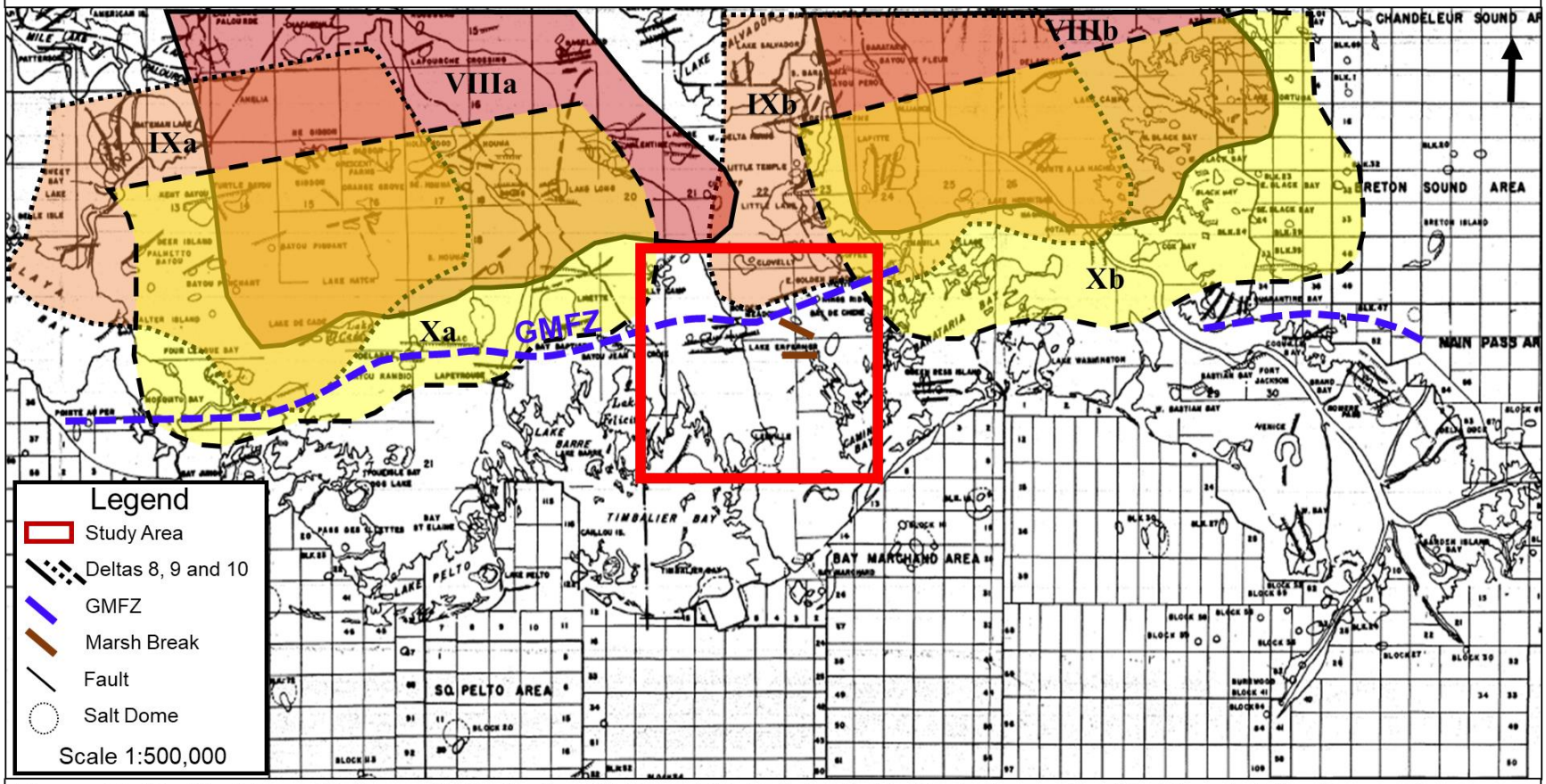

Figure 27. Modified from Wallace, 1966, Curtis, 1970, and McCulloh, 2001. Illustrates a simplified trend of the Regressive Middle Miocene deltas in comparison to the study area and the Golden Meadow Fault Zone (GMFZ). Portions of the GMFZ are adjacent to the Miocene delta fronts in the dotted blue line. The red box outlines the extent of the study, the red polygons with solid outlines identify Deltas VIIIa-b (8), orange polygons with round dot outlines identify Deltas IXa-b (9), and yellow polygons with dashed outlines identify Deltas Xa-b (10). Marsh breaks, or dieback, is identified with brown lines in the study area. Throughout the map, faults are drawn as solids lines and salt domes are illustrated as dotted polygons.

Figure 18, from this interval also indicates thickening on the upthrown fault block of the GMF, implying that deposition occurred first then continued growth across the fault increased with displacement. This also indicates that as accommodation space decreased, the GMF then became a pathway for sedimentation of the distal portion of Delta IXb during its progradation to the south-southeast over the present-day location of the LEF (Figure 29) (Curtis, 1970). Depositional loading then caused the plastic flow of salt (or possibly slip along a shale body) during the Late Miocene. The LEF initiated during this continuation of sediment deposition.

Due to earlier indications of fault activity over the GMF, the absolute time that the GMF was initially displaced cannot be interpreted but can provide evidence of the fault geometry during the Late Miocene (Figure 18). The GMF is arcuate laterally to the east and terminates to the west. The strike of GMF appears to conform to the shape of a local embayment following the line of increased sediment deposition or change in thickness (Ocamb, 1961). There is no change in thickness that points toward fault activity within the graben in Figure 18. Decreased displacement to the west along the GMF may have been due to the GMF's growth towards a radial fault associated with the BC. It is possible that radial faults are connecting or linking the GMF with other segments of the GMFZ in Terrebonne Parish.

The LEF is laterally arcuate, similar to the GMF. Curvature to the west may be related to the local depocenter that it appears to be outlining, potentially the continuation of Delta IXb (Figure 29). I infer that the LEF initially became active in the early Late Miocene, after the GMF and during the continued deposition of Delta IXb from this increase in thickness. The

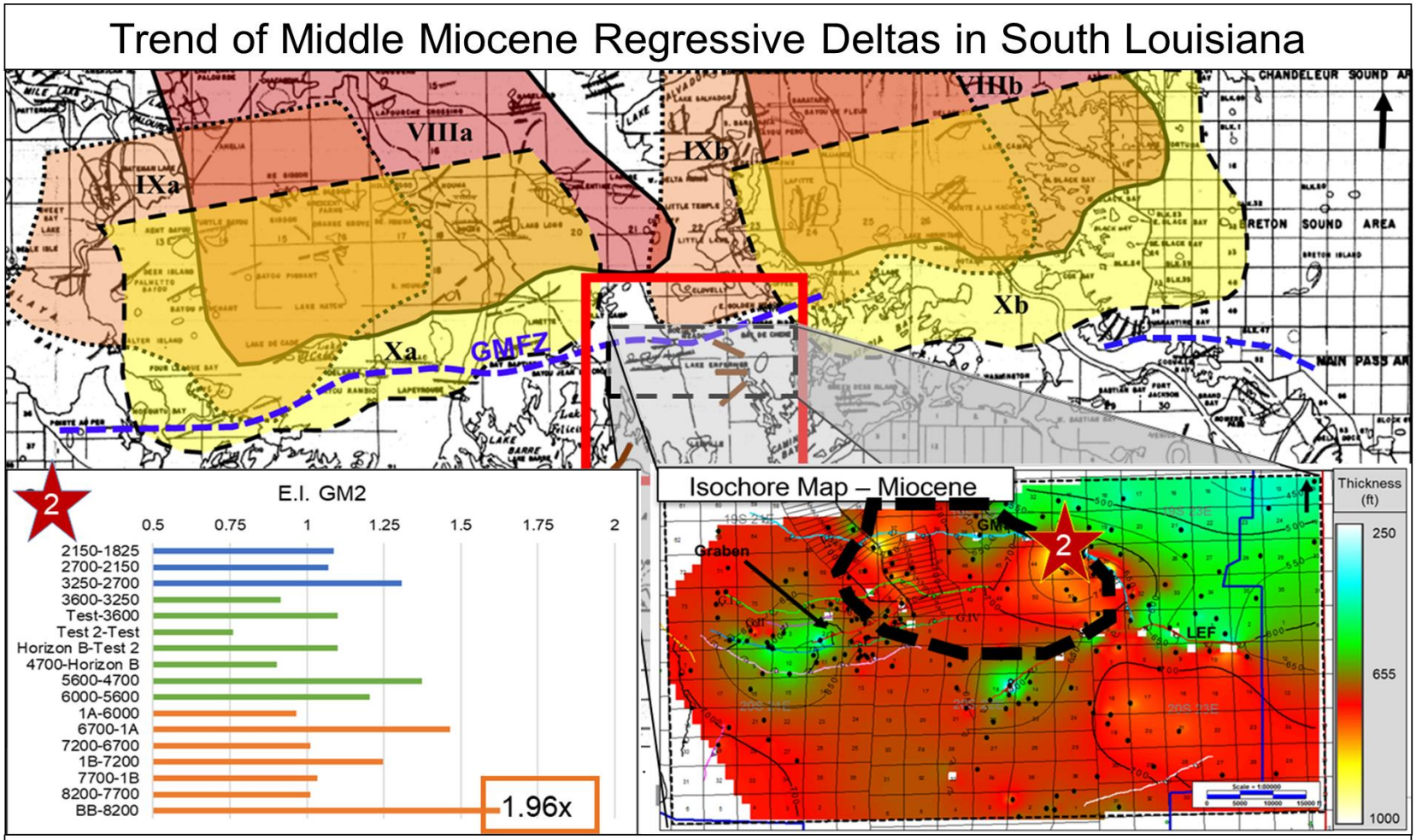

Figure 28. Modified from Wallace, 1966, Curtis, 1970, and McCulloh, 2001. Illustrates a simplified trend of the Regressive Middle Miocene deltas in comparison to the study area and the Golden Meadow Fault Zone (GMFZ). Portions of the GMFZ are adjacent to the Miocene delta fronts in the dotted blue line. The red box outlines the extent of the study, the red polygons with solid outlines identify Deltas VIIIa-b (8), orange polygons with round dot outlines identify Deltas IXa-b (9), and yellow polygons with dashed outlines identify Deltas Xa-b (10). Marsh breaks, or dieback, is identified with brown lines in the study area. Throughout the map, faults are drawn as solids lines and salt domes are illustrated as dotted polygons. E.I (Expansion Index) GM2's surface location is located at the red star on the isochore map on the bottom right. The black dotted outline within the isochore map represents an outline of an interpreted delta.

area with the most accommodation space and with the most significant increase in thickness is likely where the delta would have crossed the fault along the central-eastern portion of the LEF. The isochore may also indicate that the LEF could have been activated by the gradual displacement of one fault that conforms to Delta IXb as the amount of displacement is not equivalent laterally, and there is no expansion calculated at E.I. LE1. As the LEF was displaced, my results indicate an increasing amount of throw to the east-northeast, on the north side of the paleo-embayment in the Late Miocene.

To provide more evidence of how this fault was initially displaced, expansion indices are calculated across the fault. It is essential to determine the expansion history because it potentially predicts current wetland loss trends. Calculations of formation tops from this interval in the Late Miocene (8200 and BB) demonstrate no expansion at E.I. LE1 and increasing expansion from E.I. LE1-4 (Figure 22a-d), which implies that the LEF may have been initiated as one fault with increasing displacement from LE1 to LE4. Throughout the rest of the Late Miocene, displacement across both the GMF and LEF continues to increase to the east (Appendix 1-6). However, while there is consistent expansion across the LEF down dip, expansion across the GMF is sporadic during the Late Miocene (A13-A17). These results correlate well with the calculated E.I. values in the Miocene. The E.I.s show a general decreasing trend in expansion up section across both the LEF and GMF, which is expected of a growth fault (Figures 22 and 24) (Ocamb, 1961). Like the isochores, the E.I.s over the GMF illustrate erratic growth trends with expansion in some areas while there is no change across the fault in others (Figure 24). Across the LEF, there is a correlation between displacement and expansion. Late Miocene E.I.s show relatively consistent expansion in the

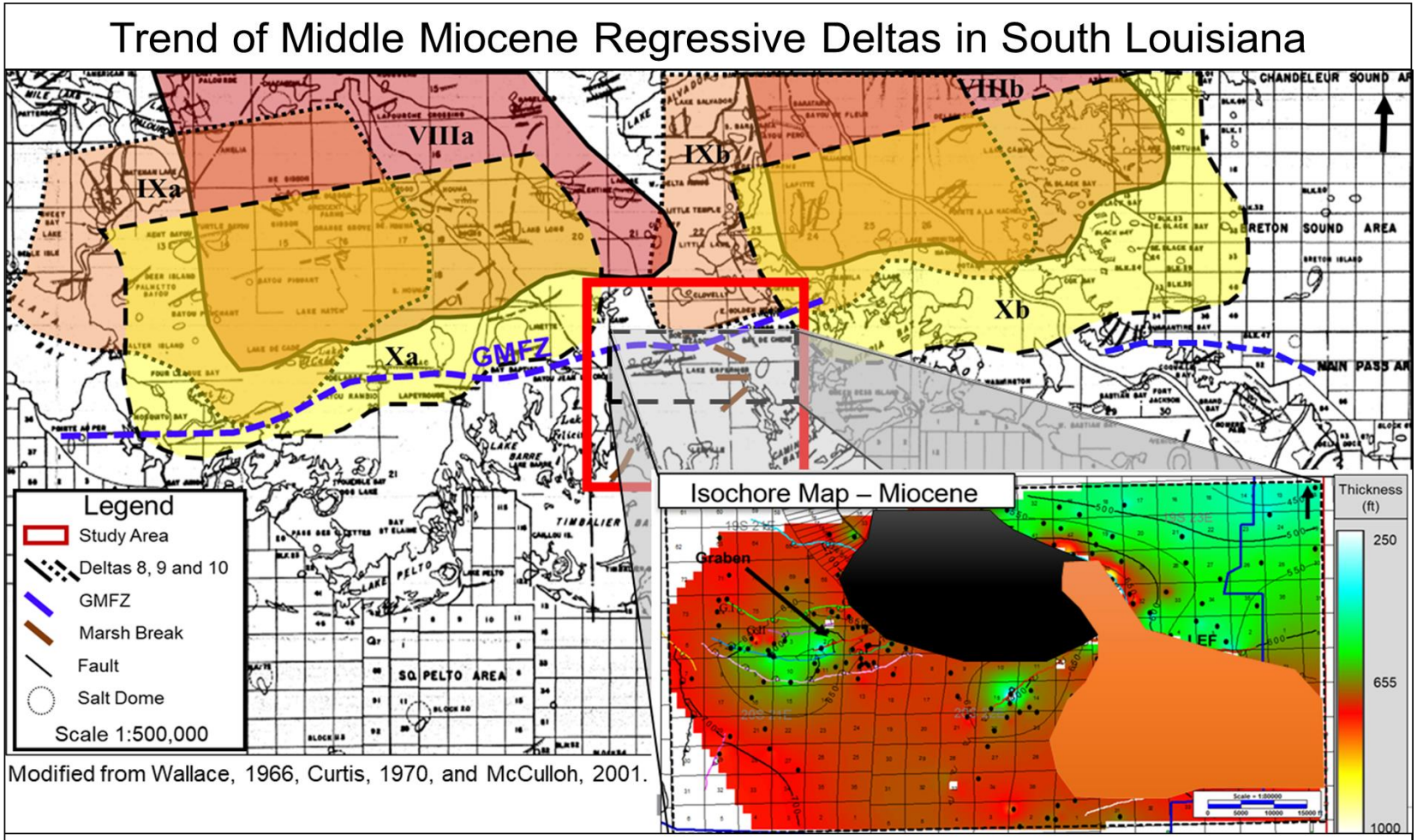

Figure 29. Modified from Wallace, 1966, Curtis, 1970, and McCulloh, 2001. Illustrates a simplified trend of the Regressive Middle Miocene deltas in comparison to the study area and the Golden Meadow Fault Zone (GMFZ). Portions of the GMFZ are adjacent to the Miocene delta fronts in the dotted blue line. The red box outlines the extent of the study, the red polygons with solid outlines identify Deltas VIIIa-b (8), orange polygons with round dot outlines identify Deltas IXa-b (9), and yellow polygons with dashed outlines identify Deltas Xa-b (10). Marsh breaks, or dieback, is identified with brown lines in the study area. Throughout the map, faults are drawn as solids lines and salt domes are illustrated as dotted polygons. The black and orange filled in polygons within the isochore map represent interpreted deltas. Black representing a Middle Miocene delta, and orange representing a Late Miocene delta.

Miocene over the LEF, except over E.I. LE 1, where expansion becomes sporadic up section (Figure 22a).

Moving into the Early Pliocene, structure maps show that the continuing trend of lower displacement rates along the western portions of both the GMF and LEF (Figures 14-15) (A7-A10); the increased rates of displacement along the eastern curvatures are described previously in the Results section. Isochores from the Pliocene indicate continued expansion on the eastward portion of the downthrown fault block over the GMF. As in the Miocene, Pliocene expansion is sporadic across the GMF, however, expansion across the LEF can also become sporadic during this interval unlike the Miocene (A18-A23).

Isochores illustrate that the graben south of the GMF develops in association with a roll-over anticline, initiating between the 4700 and Horizon B formation tops (Figure 30). The axis of this anticlinal feature is east-west, and the faults that developed along this feature also strike east-west. The amount of the expansion occurring on the downthrown fault block of the GMF starts to shift from the hanging wall toward the fault surface to over the graben area down dip. E.I.s are not calculated along the faults within the graben, only across the GMF, LEF, and three radial faults. E.I.s across the GMF and LEF within the Pliocene show anomalously increasing expansion over the GMF, between the 4700 ft and Horizon B formation tops, where E.I. is 5.10 (Figure 24). The cause of this is most likely a channel or another localized depositional feature. This would explain the initiation and expansion within the graben. E.I.s up section exhibit a general decrease in expansion across both the GMF and LEF. Across the LEF, E.I.s range between 1.0 and 1.3. The eastern portion of the LEF has

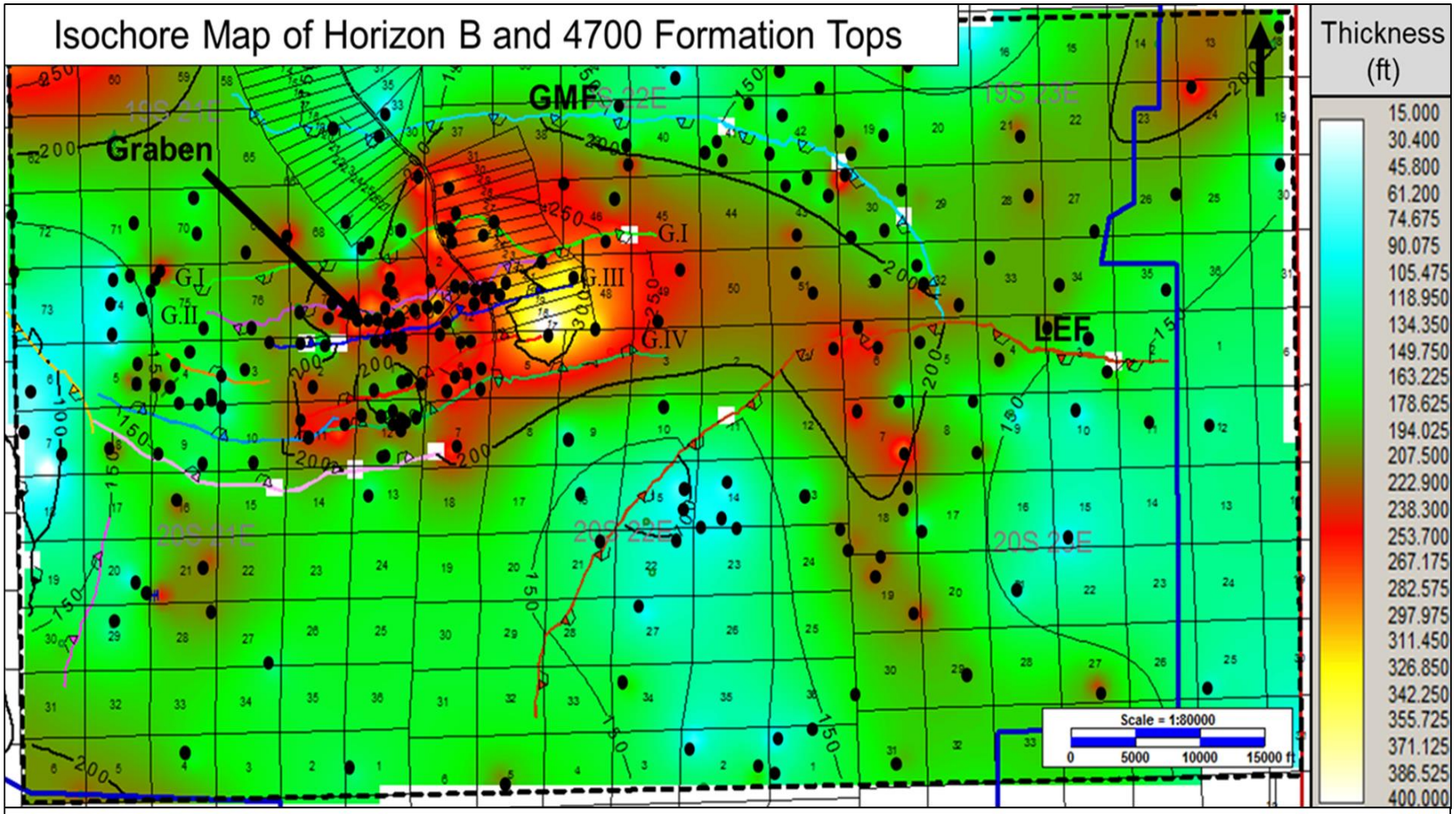

Figure 30. Illustrates an isochore map from a portion of the study area indicating increased thickness within the study area.

the greatest amount of throw in the Miocene and has a gradual decrease in displacement up section to the Late Pliocene (Figure 22). In contrast, the western portion of this fault had lower displacement and shows more sporadic and increasing displacement up section. These sporadic values mean that the E. I. on the eastern portion of the fault may be more predictable than the western portion because they follow the trend of increasing growth and displacement with depth, excluding increases in E.I. due to depositional features. Meaning that with more detailed calculations across the fault, it may be possible to predict expansion values in areas of low data, like the Holocene strata.

Because of decreased well control along the growth faults within the Pleistocene interval, my interpretation and its level of confidence is less constrained for this time interval (Figures 16-17) (A11-A12). During this period, growth not only decreases and dies out over the western portion of the GMF but also along the western portion of the LEF. When comparing structure maps from the Late Miocene to the Pleistocene, we observe that structural features are affecting the deposition of sediments up to 2000 ft above section, even when a fault is dying out (Figures 12 and 17). We observe this by noticing the pull-down of a contour towards the main fault on the downthrown fault block of the LEF. For example, in Figure 28 the -1950 ft contour curves north, to the south of the remaining LEF. Displacement along the LEF decreases, and dies out, on the western portion of the fault throughout the Pleistocene to the present day. E.I.s calculated across the LEF that show expansion within the Pleistocene, but data are sparse (Figure 22). E.I.s illustrate that most of the growth that occurs along the GMF, shifts to the central part of the fault between (Figure 20) (A24-A25). Rates of expansion are between 0.80 and 0.95, providing evidence that the GMF near Bayou

Lafourche dies out towards the surface (Figure 24). Over time, the total amount of expansion and displacement across the GMF and LEF have decreased since these normal faults were initially activated. This decreasing trend of expansion is in part due to factors like sea level fluctuation, amount of sediment deposition, and salt movement at depth. Due to less available well control and Pleistocene and Holocene expansion cannot be made. However, these results do indicate that current rates of expansion have significantly decreased. The placement of Catfish Lake corresponds well with displacements calculated on the western portion of this feature within Pleistocene structure maps over this area (Figure 31). However, this graben structure appears to affect land loss rates as well. For example, Catfish Lake seems to sit within the western portion of the graben and is bound by synthetic and antithetic faults (Figure 32).

Wetland loss mapped by the USGS from 1932 to 2016 is compared with projected surface faults (Couvillion et al., 2017). It illustrates significant land loss on the downthrown fault block in the eastern portions of both the GMF and LEF. These results in figures 22, 24, and 32, show that there is a direct relationship between the amount of displacement at depth during the Miocene and Pleistocene epochs and wetland loss at the surface for the growth faults located within the study area. Across both growth faults, more displacement was measured to the east at depth, and there is more land loss measured to the east at the surface. This trend does not relate to the faults within the graben. Gagliano and others (2003) projected the GMF onto the surface based on the visible marsh break from aerial imagery (Figure 33). Figure 33a compares Gagliano's (2003) fault surface with the fault projection made utilizing seismic data in this study; the two are approximately 1300 ft apart. Figure

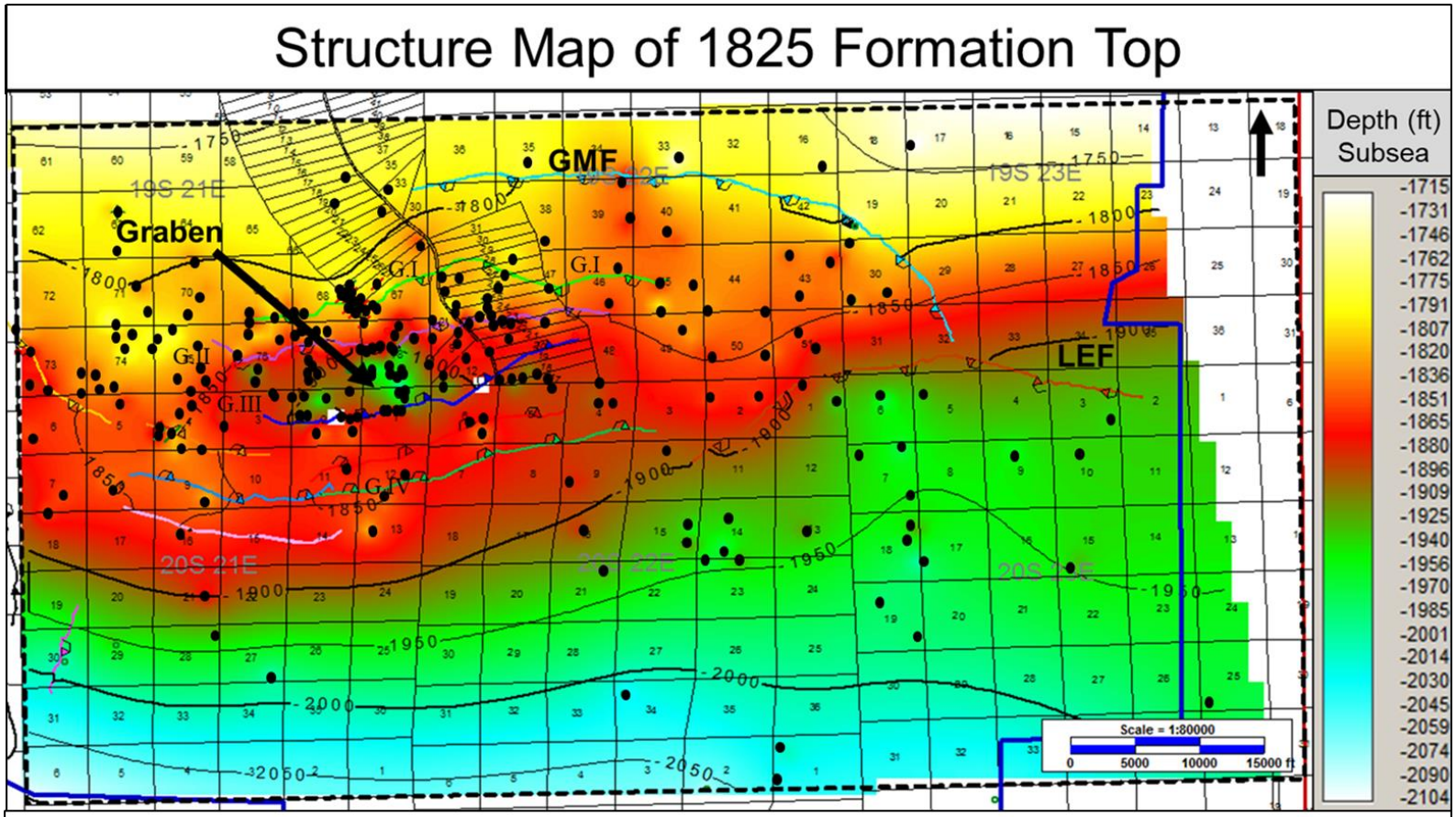

Figure 31. Illustrates a structure map produced from a Pleistocene formation top, 1825, and the location of wells that were used within the study area. The blue line outlines the extent of the seismic survey, and the black-dotted box outlines the well log data coverage centered around the town of Golden Meadow. The Golden Meadow fault (GMF) is outlined in blue, the Lake Enfermer fault (LEF) is outlined in brown, and the black arrow is pointing to the graben. G I and II are two faults within the graben that are downthrown to the south. G III and IV are two of the six shallow faults within the graben that are downthrown to the north.

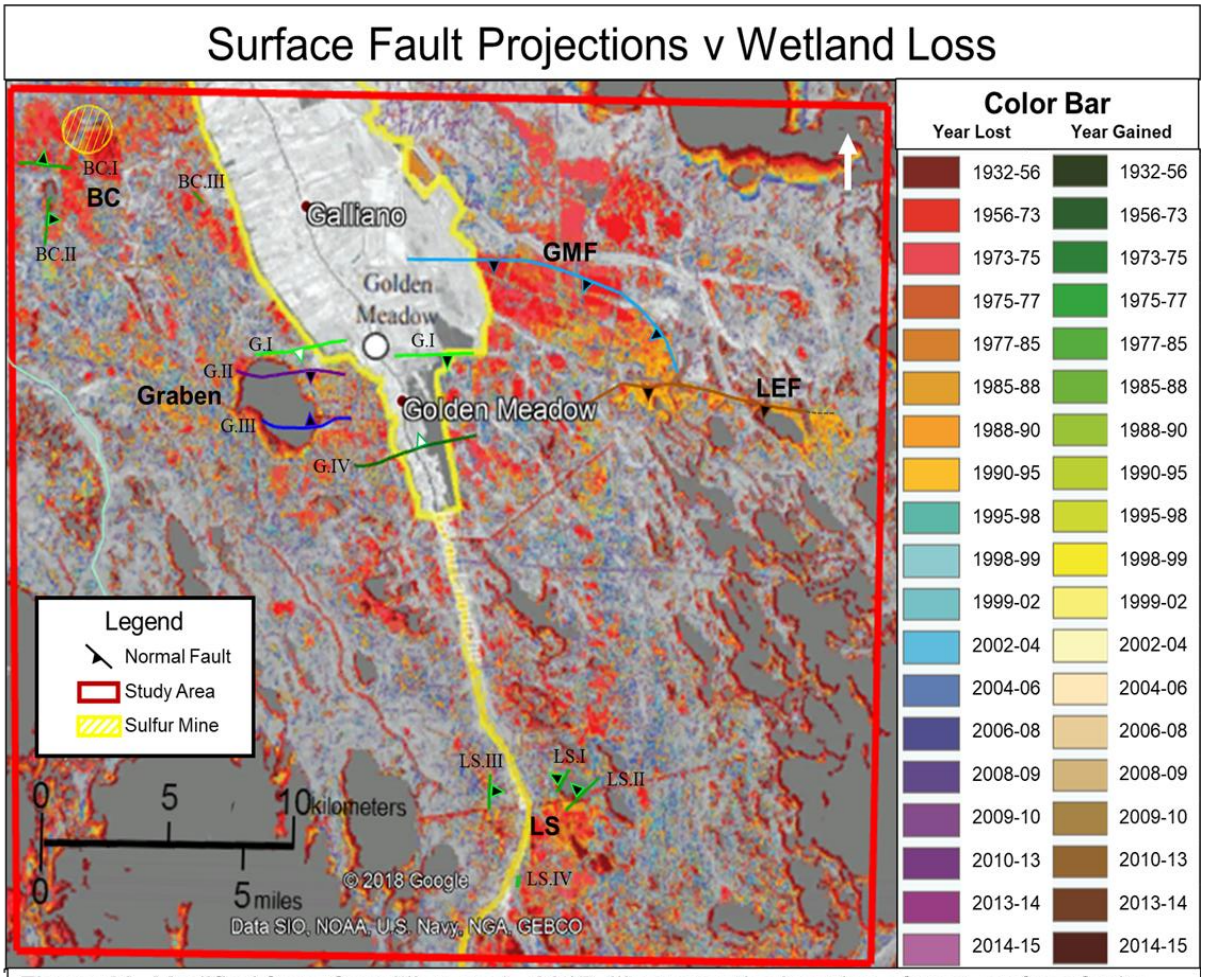

Figure 32. Modified from Couvillion et al., 2017. Illustrates the location of near-surface faults that are projected to the surface on Google Earth. The red box outlines the extent of the study and the yellow lined polygon identifies the approximate location of the Bully Camp Sulfur Mine (Gagliano et al., 2003). The color bar denotes the mapped time period in which land change occurred. Within the study area, there was increased land loss between 1956-1975, but high land loss also occurred through 1995 at least. There are five structures labelled within the study area: Bully Camp salt dome (BC), Golden Meadow fault (GMF), Lake Enfermer fault (LEF), Graben, and the Leeville salt dome (LS). The GMF is projected to be 7.69mi and the LEF is projected to be 5.81mi. There are three surface faults projected near the BC: BC I (1.35mi), II (1.12mi), and III (0.34mi). Four faults are projected for the Graben: G I (4.25mi combined), G II (2.72mi), G III (2.26mi), and G IV (3.10mi). Four faults are also projected for the LS: LS I (0.60mi), LS II (1.09mi), LS III (0.75mi), and LS IV (0.18mi).

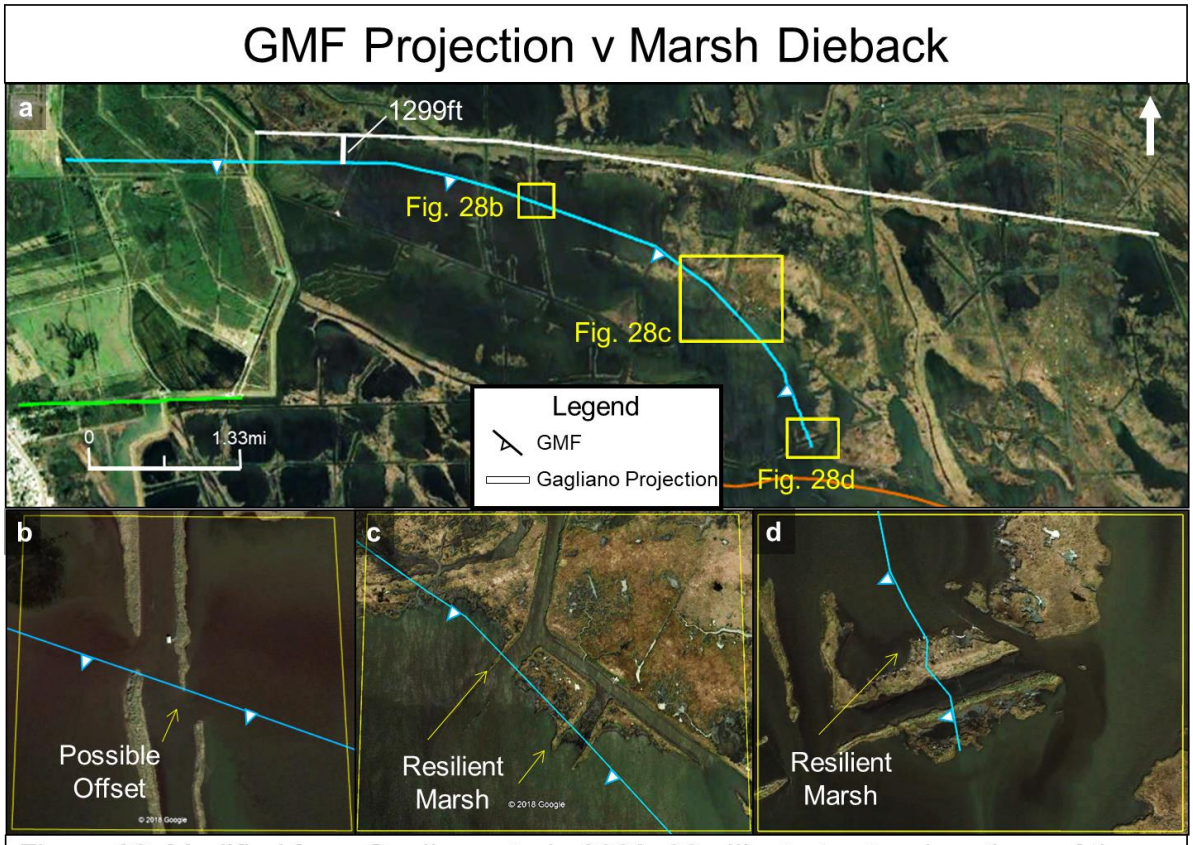

Figure 33. Modified from Gagliano et al., 2003. 33a Illustrates two locations of the Golden Meadow fault (GMF) projected to the surface on Google Earth. The white line represents the GMF interpreted from the surface utilizing the placement of marsh dieback (Gagliano et al., 2003). The light blue line represents the GMF projected from the subsurface utilizing seismic data. The two interpretations are about 1299ft apart from one another. The light blue GMF is projected to be 7.69mi. 33b illustrates a portion of the projected GMF onto the marsh. Gagliano and others' (2003) projection is to the north. 33c illustrates the GMF to the south lies adjacent to what might be a more resilient part of the marsh. 33d illustrates another portion of the GMF, the yellow arrow is pointing towards a possible resilient part of the marsh.

33b, 33c, and 33d pictures some evidence that the fault surface location of the GMF maybe south of the marsh dieback, e.g., areas tangent to open water on resilient marshes and areas of possible displacement.

Figure 32 also illustrates that one of the most distinct areas of wetland loss occurs on the downthrown fault block of the eastern portion of the LEF, which is outlined in brown. Breaks in the marsh might indicate the extent of the LEF at the surface; however, I project the fault surface to cut through the marsh to the south of the predominant marsh cut. Due to continuing marsh deterioration to the east, this fault is thought to extend beyond the border of the seismic survey (Gagliano et al., 2003). In comparison, the western portion of the fault does not appear to be significantly impacting land loss rates. Gagliano and others (2003) projected the LEF onto the surface based on the visible marsh break from aerial imagery (Figure 34). Figure 34a compares Gagliano's (2003) fault surface with the fault projection made utilizing seismic data in this study; the two are approximately 880 ft apart. Figure 34b and 34c show similar evidence as the GMF of areas that might indicate that the surface location of the LEF is to the south of the marsh dieback. So, while compaction and marsh-edge erosion may be on-going throughout the area, the predominant factor of land change in this localized section is subsidence along the LEF.

Leeville Salt Dome

The LS was deposited as the Louann Salt in the Jurassic Period. With continuing sediment loading, this portion of the Louann Salt became allochthonous, eventually forming the present-day LS. Based on seismic observations of thinning strata against the dome, the LS

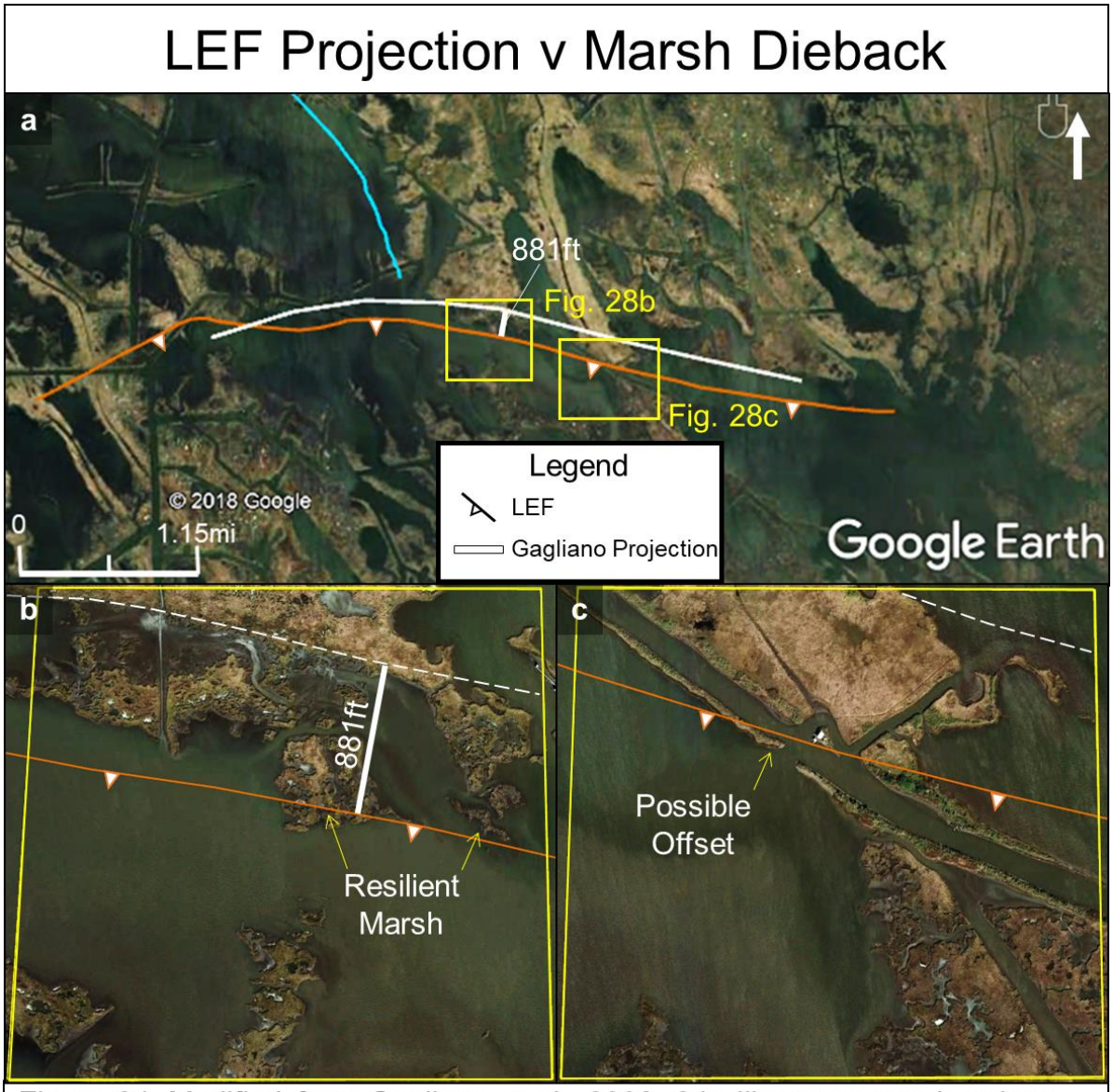

Figure 34. Modified from Gagliano et al., 2003. 34a Illustrates two locations of the Lake Enfermer fault (LEF) projected to the surface on Google Earth. The white line represents the LEF interpreted from the surface utilizing the placement of marsh dieback (Gagliano et al., 2003). The brown line represents the LEF projected from the subsurface utilizing seismic data. The two interpretations are 881ft apart from one another. The brown LEF is projected to be 5.81mi. 34b illustrates a portion of the projected LEF onto the marsh. Gagliano and others' (2003) projection to the north is on the marsh break. The LEF to the south lies adjacent to what might be a more resilient part of the marsh. 34c illustrates a possible offset perpendicular to a dredged portion of Lake Enfermer.

appears to have begun forming before the Late Miocene, possibly within the Paleocene period. Because of the LS's long history of the movement and the geometry of salt piercing overlying sediments, it creates a more complex network of radial faults and more faults form with continuous movement of salt. I measured fault displacement on shallow radial faults utilizing structure maps and E.I.s (Figure 25). Calculated E.I.s based on well log data may have higher margins of error, due to the decreased dip of radial faults in comparison to listric growth faults like the LEF and GMF. Because of this, only three calculations are completed over three faults to create a record of activity.

Two radial faults appear to have influenced the path of Bayou Lafourche and it crosses the LS. The Bayou shifts east to the north of the salt dome and turns west to the south of the salt dome (Figure 32). In the north, LS III and LeeB radial faults form a cross-cutting relationship. E.I.s indicate that while LeeB formed in the Pliocene, LS III formed in the Pleistocene offsetting LeeB. LeeB is downthrown to the west, while LE III is downthrown to the east. Because LE III became the dominant fault in the Pleistocene, it created an area of lower relief to the east of the fault. The areas of low relief within the paleo-bathymetry of the Pleistocene, likely due to radial fault activity. This provided accommodation and allowed space for the formation of lakes and Bayou Lafourche to develop with continuing deposition of the Lafourche Lobe of the Mississippi River Delta Complex. Locating these lows created in the Pleistocene due to fault movement may point to areas of greater wetland loss today. The last radial fault that may have controlled the trajectory of Bayou Lafourche is Salt Fault G, to the southeast of the LS (Figure 21). The calculated E.I. illustrates that this fault initiated in the Late Pliocene with continued activity into the Pleistocene, allowing the Bayou to shift

back to the west. If these radial faults continue to be active today as suggested by the calculated expansion indices, it may allow for continued displacement and land loss surrounding the growth faults in the future. Not only did these radial faults impact the pathway of the Bayou, but they also led to many marsh breaks and small bodies of water that have the potential to delineate faults that reach the surface. For example, smaller bodies of water appear to be adjacent to the radial faults of the LS on its northeastern corner, specifically LS I and II (Figure 32).

Growth faults, salt tectonics and radial faults were creating lows on the downthrown fault blocks and smaller anticlinal features as a result of this faulting, affecting the surface geomorphology. Defining that both growth faults became active in the Middle-Late Miocene helped to determine that the formation of salt domes initiated this activity based on expansion indices and literature (McBride, 1998 and Stover et al., 2001). This deformation created the paleo-bathymetry of the study area. A positive correlation appears when this relationship, between the paleo-bathymetry of the Pleistocene and total measured land loss today, is tested with an overlay of the USGS Land Area Change of Coastal Louisiana (1932 to 2016) map on Google Earth with an overlay of potential surface faults (Figure 32) (Couvillion et al., 2017).

Conclusion

These results and observations illustrate that there is a relationship between surface geomorphology, wetland loss, and subsurface structures, suggesting that active deformation exerts control on wetland loss within this study area in southern Louisiana. Changes in the land surface indicate that even if no fault scarp exists at the surface, subsidence and possibly land loss may still occur due to activity today and later compaction. In the past, the

progression of Miocene deltas initiated growth faults within the study area, and this process continued through the Pleistocene with continued sedimentation and progradation of the Mississippi Delta Complex. This activity affected the geomorphology of the area and sediment routing, especially in the case of Bayou Lafourche. These results indicate that there is a strong spatial correlation to the total amount of land loss and the downthrown blocks of the growth faults and radial faults examined. Areas measuring lower total land loss that are separate from these structural features are more likely the consequence of other factors such as compaction of Holocene sediments and low sediment supply. However, other factors may also contribute to land loss, e.g., saltwater intrusion into freshwater marshes, glacial isostatic adjustment, and fluid withdrawal, particularly groundwater withdrawal (Yuill et al., 2009 and Dokka, 2011). Thus, many different factors work together to create the land change that is seen today. These findings have implications that may change the outlook on how to protect the Louisiana coastline and lead to new, or apply different, engineering techniques to infrastructure surrounding many coastal communities, e.g., changing bridge designs. Making these changes will better protect both the communities that are impacted by land loss and the investment being made to implement these projects.

This project can be built on by interpreting well log data closer to the surface and acquiring near-surface data to extend these interpretations. A continuum of this project will be completed in the future, funded by The Water Institute of the Gulf, to gather CHIRP and core data throughout parts of southern Louisiana, including transects along Bayou Lafourche. These data will test whether the fault projections discussed here may reach the surface. I

anticipate finding a depression of sediments, like the results found within Adams Bay (Roberts et al., 2008), over the graben structure near the city of Golden Meadow.

Reference List

Adams, R. D., B. B. Barrett, J. H. Blackmon, B. W. Gane, and W. G. McIntire, 1976, Barataria Basin: Geologic and Framework: Center for Wetland Loss Research, Sea Grant Publication no. LSU-T-76-008, p.1-103, https://repository.library.noaa.gov/view/noaa/11666

Armstrong, C., D. Mohrig, T. Hess, T. George, and K. M. Straub, 2013, Influence of Growth Faults on Coastal Systems: Examples from the Late Miocene to Recent Mississippi River Delta, Sedimentary Geology, p.1-13.

Atwater, G. I., and M. Forman, 1959, Nature of Growth of Southern Louisiana Salt Domes and its Effect on Petroleum Accumulation: AAPG Bulletin, v. 43, No. 11, p.2592-2595.

Ayrer, J., 2013, Subsurface Stratigraphic Architecture of Pleistocene Sediments in the Greater New Orleans Area: LSU Master's Thesis, no. 1710. https://digitalcommons.lsu.edu/gradschool_theses/1710

Bader Jr, L. R., and McWilliams, P. T., 1983, Lake Enfermer Field: Lafourche Parish, Louisiana: New Orleans Geological Society, Oil and Gas Fields of Southeast Louisiana, v. 3, p.22-22G

Barton, D., 1933, Mechanics of Formation of Salt domes with Special Reference to Gulf Coast Salt Domes of Texas and Louisiana: AAPG Bulletin, v. 17, No. 9, p.1025-1035.

Beckman, J.D. and A.K. Williamson, 1990, Salt-dome locations in the Gulf Coastal Plain, south-central United States (pp. 3-4). Austin, TX: US Geological Survey.

Blum, M. D., J. H. Tomkin, A. Purcell, and R. R. Lancaster, 2008, Ups and Downs of the Mississippi Delta: The Geological Society of America, v. 36, no. 9, p.675–678. https://doi.org/10.1130/G24728A.1

Blum, M. D., and H. H. Roberts, 2009, Drowning of the Mississippi Delta due to insufficient sediment supply and global sea-level rise: NATURE GEOSCIENCE, v. 2, p.488-491

Cartwright, J., R. Bouroullec, D. James, and H. Johnson, 1998, Polycyclic Motion History of Some Gulf Coast Growth Faults from High-Resolution Displacement Analysis: Geology, v. 26, no. 9, p. 819–822.

Chamberlain, E. L., T. E. Törnqvist, Z. Shen, B. Mauz, and J. Wallinga, 2018, Anatomy of Mississippi Delta growth and its implications for coastal restoration: Science Advances, v.4, n.4, DOI: 10.1126/sciadv.aar4740

Couvillion, B. R., H. Beck, D. Schoolmaster, and M. Fischer, 2017, Land area change in coastal Louisiana (1932 to 2016): U.S. Geological Survey, Scientific Investigations Map 3381, 1.

Couvillion, B. R., J. A. Barras, G. D. Steyer, W. Sleavin, M. Fischer, H. Beck, and N. Trahan, 2011, Land Area Change in Coastal Louisiana (1932 to 2010): U.S. Geological Survey, Scientific Investigations Map 3164, 1.

Curtis, D. M., 1970, Miocene Deltaic Sedimentation, Louisiana Gulf Coast: S.E.P.M. Special Publication, v. 15, p. 293-308.

Dokka, R. K., 2011, The Role of Deep Processes in Late 20th Century Subsidence of New Orleans and Coastal Areas of Southern Louisiana and Mississippi: Journal of Geophysical Research: Solid Earth, v. 116, no. 6, p. 1–25. https://doi.org/10.1029/2010JB008008.

Foote. R.Q., L. M. Massingill, R. H. Wells, G. L. Dolton, and M. M. Ball, 1992, Geologic Framework for Petroleum Assessment of the Western Gulf Basin, Province 112: Department of the Interior U.S. Geological Survey, Open-File Report 89-450B.

Gagliano, S. M., 1994, An Environmental-Economic Blueprint for Restoring the Louisiana Coastal Zone: Report of the Governor's Office of Coastal Activities Sciences Advisory Panel Workshop. http://www.lacoastpost.com/BLUEPRINT%20PLAN-1994.pdf

Gagliano, S., E. B. Kemp III, K. M. Wicker, and K. S. Wiltenmuth, 2003, Active Geological Faults and Land Change in southeastern Louisiana: A Study of the Contribution of Faulting to Relative Subsidence Rates, Land Loss, and Resulting Effects on Flood Control, Navigation, Hurricane Protection and Coastal Restoration Projects: U.S. Army Corps of Engineers, Contract No. DACW 29-00-C-0034

Gagliano, S. M., K. J. Meyer-Arendt, and K. M. Wicker, 1981, Land Loss in the Mississippi River Deltaic Plain: Gulf Coast Association of Geological Societies Transactions, v. 31, p. 295–300.

Gould, H. R., 1970, The Mississippi Delta Complex: The Society of Economic Paleontologists and Mineralogists (SEPM) Deltaic Sedimentation, Modern and Ancient, v. 15, p. 3–30.

Heinrich, P. V., 2000, De Quincy Fault-Line Scarp, Beauregard and Calcasieu Parishes, Louisiana: Basin Research Institute Bulletin, v. 9, p. 38–50.

Jackson, M.P. and C.J. Talbot, 1986, External shapes, strain rates, and dynamics of salt structures. Geological Society of America Bulletin, 97(3), pp.305-323.

Kolvoord, K. S., A. R. Peterson, R. C. Laforge, and R. W. Block, 2008, Rejuvenation of a Shallow Reservoir in The Seventy-year-old Golden Meadow Field, Lafourche Parish, Louisiana: Gulf Coast Association of Geological Societies Transactions, v. 58, p. 543–60.

Kuecher, G. J., H. H. Roberts, M. D. Thompson and I. Matthews, 2001, Evidence for Active Faulting in the Terrebonne Delta Plain, South Louisiana: Implications for Wetland Loss and the Vertical Migration of Petroleum: AAPG/DEG, Environmental Geosciences, v. 8, no. 2, p. 77-94.

Little, R. E., 2003, An Investigation of a Salt-Dome Environment at South Timbalier 54, Gulf of Mexico: LSU Master's Thesis, 3354. https://digitalcommons.lsu.edu/gradschool_theses/3354

Lopez, J. A., S. Penland, and J. Williams, 1997, Confirmation of Active Geologic Faults in Lake Pontchartrain in Southeast Louisiana: Gulf Coast Association of Geological Societies Transactions, v. 47, p. 299–303.

Martin, E., 2006, Fault Induced Subsidence Near Empire and Bastian Bay, Louisiana: Tulane University Master's Thesis.

McBride, B. C., 1998, The Evolution of Allochthonous Salt along a Megaregional Profile across the Northern Gulf of Mexico Basin: AAPG Bulletin, v. 82, no. 5B, p. 1037–1054.

McCulloh, R.P., 2001, Active Faults in East Baton Rouge Parish, Louisiana: Louisiana Geological Survey.

McLindon, C., K. Haggar, and A. Johnson, 2015, Oil and Gas Industry Infrastructure in Coastal Louisiana: The New Orleans Geological Society (NOGS).

Morton, R.A., N.A. Buster, and M.D. Krohn, 2002, Subsurface controls on historical subsidence rates and associated wetland loss in southcentral Louisiana: Gulf Coast Association of Geological Societies Transactions, v. 52, p. 767-778.

NOGS, 1983, Leeville: Lafourche Area: New Orleans Geological Society, Book/Publication Salt Domes of South Louisiana, v.3, p.44-45.

Ocamb, R. D., 1961, Growth Faults of South Louisiana: Gulf Coast Association of Geological Societies Transactions, v. 11, p. 139-175.

Roberts, H. H., R. A. Morton, and A. M. Freeman, 2008, A High-Resolution Seismic Assessment of Faulting in the Louisiana Coastal Plain: Gulf Coast Association of Geological Societies Transactions, v. 58, p. 733–46.

Rowan M. G., K. F. Inman, 2005, Counterregional-Style Deformation in the Deep Shelf of the Northern Gulf of Mexico: Gulf Coast Association of Geological Societies Transactions, v.55, p.716-724

Rowan, M. G., M. P. A. Jackson, and B. D. Trudgill, 1999, Salt Related Fault Families and Fault Welds in the Northern Gulf of Mexico: AAPG Bulletin, v. 83, no. 9, p.1454–84. https://doi.org/10.1306/E4FD41E3-1732-11D7-8645000102C1865D.

Sabate, R.W, 1968, Pleistocene Oil and Gas in Coastal Louisiana: Gulf Coast Association of Geological Societies Transactions, v. 10, Figure 3.

Schuster, D. C., 1995, Deformation of Allochthonous Salt and Evolution of Related Salt – Structural Systems, Eastern Louisiana Gulf Coast: AAPG Memoir, no. 65, p. 177–198.

Shen, Zhixiong, N. H. Dawers, T. E. Tornqvist, N. M. Gasparini, M. P. Hijma, and B. Mauz, 2016, Mechanisms of Late Quaternary Fault Throw-rate Variability along the North Central Gulf of Mexico Coast: Implications for Coastal Subsidence: Basin Research, p. 1-14.

Stover, S. C., S. Ge, P. Weimer, and B. C. McBride, 2001, The Effects of Salt Evolution, Structural Development, and Fault Propagation on Late Mesozoic-Cenozoic Oil Migration: A Two-Dimensional Fluid-Flow Study along a Megaregional Profile in the Northern Gulf of Mexico Basin: AAPG Bulletin, v. 85, no. 11, p. 1945–1966.

The Diggings, 2019, "Bully Camp Dome Mine" in Lafourche, LA, Sulfur Past Producer: https://thediggings.com/mines/usgs10105164

Thorsen, C.E, 1963, Age of Growth Faulting in Southeast Louisiana: Gulf Coast Association of Geological Societies Transactions, v. 13, p. 103-110.

Wallace, V E, B. H. Dehart, J. E. LeBlanc, R. E. Bonar, J. C. Koffskey, M. G. Rossi, et al., 1966, Fault and Salt Map of South Louisiana: Gulf Coast Association of Geological Societies, p. 1-2, Scale 1:245,000.

Weimer, P. and R. T. Buffler, 1992, Structural Geology and Evolution of the Mississippi Fan Fold Belt, Deep Gulf of Mexico: AAPG Bulletin, v. 76, no. 2, p. 225-251.

Winker, C. D., 1982, Cenozoic Shelf Margins, Northwestern Gulf of Mexico: Gulf Coast Association of Geological Societies, v. 32, p. 427-448.

Yeager, K. M., C. A. Brunner, M. A. Kulp, D. Fischer, R. A. Feagin, K. J. Schindler, J. Prouhet, and G. Bera, 2012, Significance of Active Growth Faulting on Marsh Accretion Processes in the Lower Pearl River, Louisiana: Geomorphology, 153–154, p. 127–143.

Yuill, B., D. Lavoie, and D. J. Reed, 2009, Understanding Subsidence in Coastal Louisiana: Journal of Coastal Research: Special Issue 54, p. 23 – 36.

Appendix

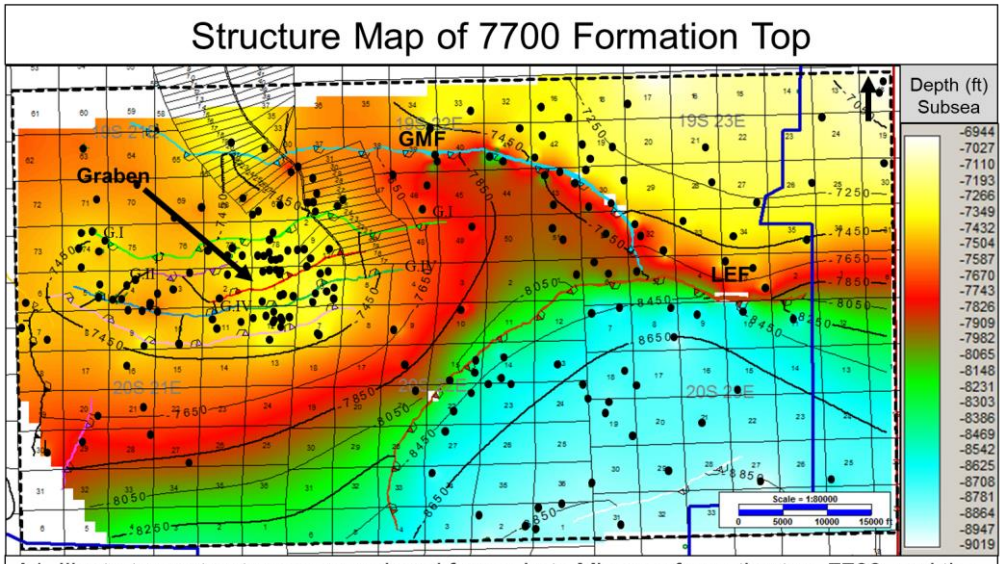

A1. Illustrates a structure map produced from a Late Miocene formation top, 7700, and the location of wells that were used within the study area. The blue line outlines the extent of the seismic survey, and the black-dotted box outlines the well log data coverage centered around the city of Golden Meadow. The Golden Meadow fault (GMF) is outlined in blue, the Lake Enfermer fault (LEF) is outlined in brown, and the black arrow is pointing to the graben. G I and II are two faults within the graben that are downthrown to the south. G IV is one of the six shallow faults within the graben that are downthrown to the north.

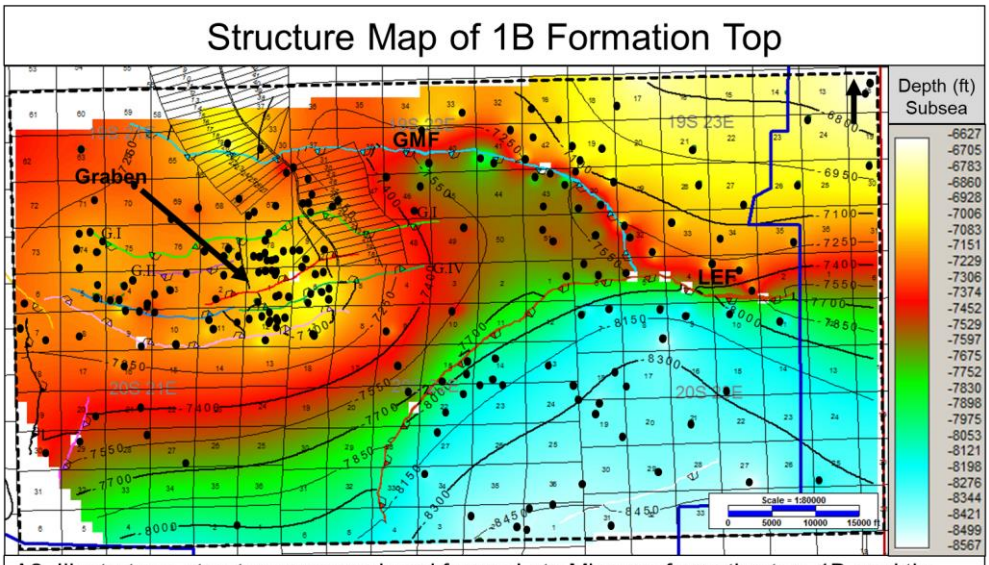

A2. Illustrates a structure map produced from a Late Miocene formation top, 1B, and the location of wells that were used within the study area. The blue line outlines the extent of the seismic survey, and the black-dotted box outlines the well log data coverage centered around the city of Golden Meadow. The Golden Meadow fault (GMF) is outlined in blue, the Lake Enfermer fault (LEF) is outlined in brown, and the black arrow is pointing to the graben. G I and II are two faults within the graben that are downthrown to the south. G IV is one of the six shallow faults within the graben that are downthrown to the north.

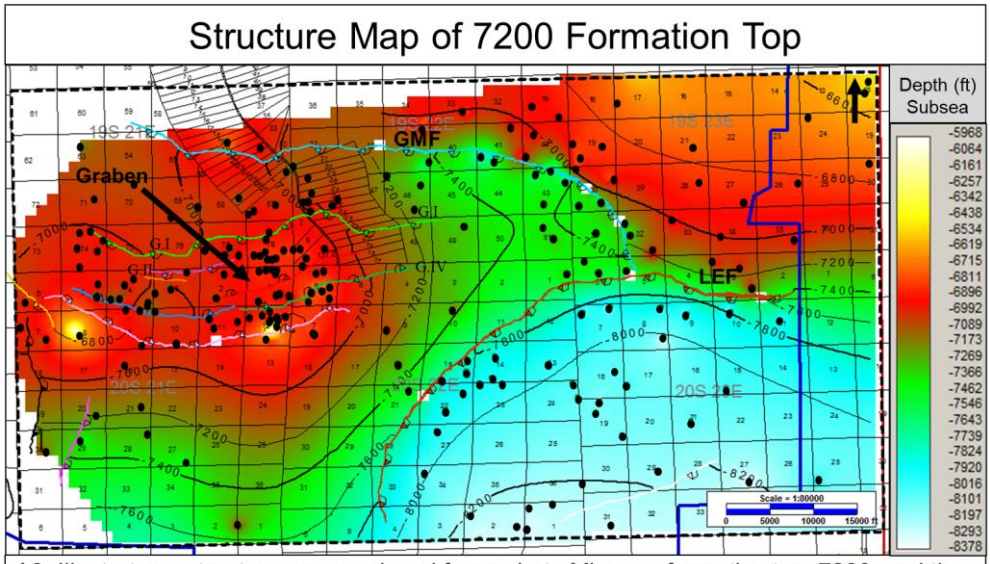

A3. Illustrates a structure map produced from a Late Miocene formation top, 7200, and the location of wells that were used within the study area. The blue line outlines the extent of the seismic survey, and the black-dotted box outlines the well log data coverage centered around the city of Golden Meadow. The Golden Meadow fault (GMF) is outlined in blue, the Lake Enfermer fault (LEF) is outlined in brown, and the black arrow is pointing to the graben. G I and II are two faults within the graben that are downthrown to the south. G IV is one of the six shallow faults within the graben that are downthrown to the north.

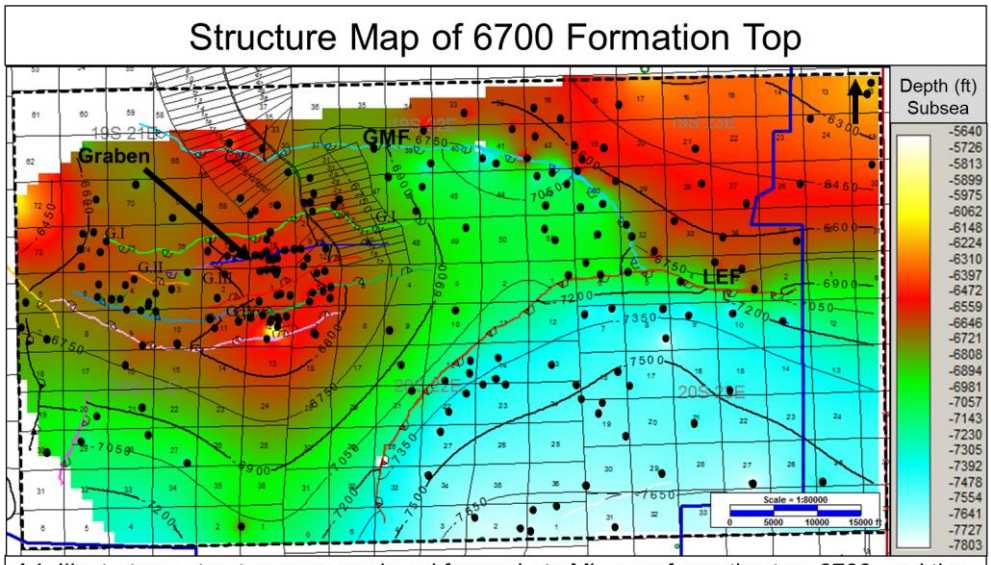

A4. Illustrates a structure map produced from a Late Miocene formation top, 6700, and the location of wells that were used within the study area. The blue line outlines the extent of the seismic survey, and the black-dotted box outlines the well log data coverage centered around the city of Golden Meadow. The Golden Meadow fault (GMF) is outlined in blue, the Lake Enfermer fault (LEF) is outlined in brown, and the black arrow is pointing to the graben. G I and II are two faults within the graben that are downthrown to the south. G III and IV are two of the six shallow faults within the graben that are downthrown to the north.

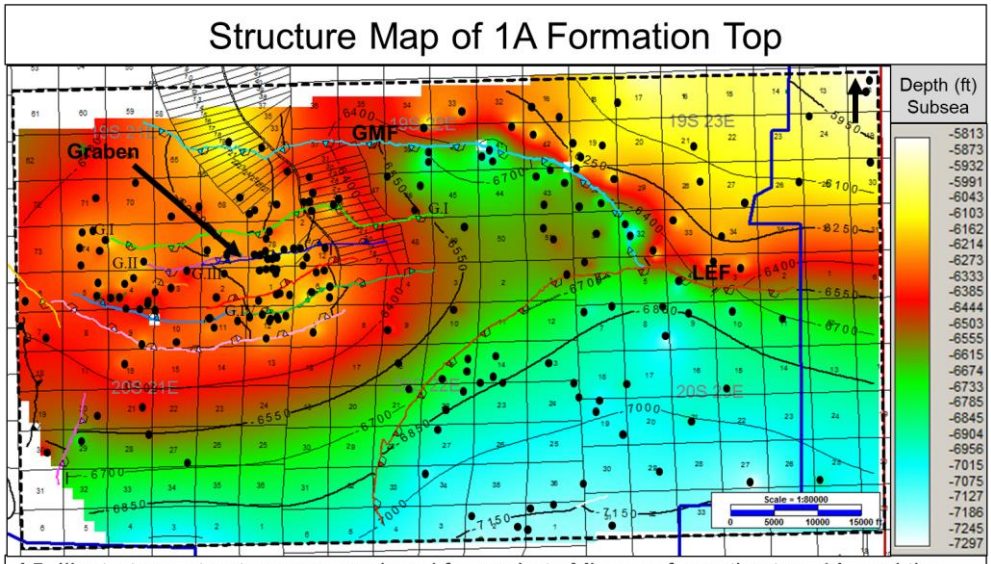

A5. Illustrates a structure map produced from a Late Miocene formation top, 1A, and the location of wells that were used within the study area. The blue line outlines the extent of the seismic survey, and the black-dotted box outlines the well log data coverage centered around the city of Golden Meadow. The Golden Meadow fault (GMF) is outlined in blue, the Lake Enfermer fault (LEF) is outlined in brown, and the black arrow is pointing to the graben. G I and II are two faults within the graben that are downthrown to the south. G III and IV are two of the six shallow faults within the graben that are downthrown to the north.

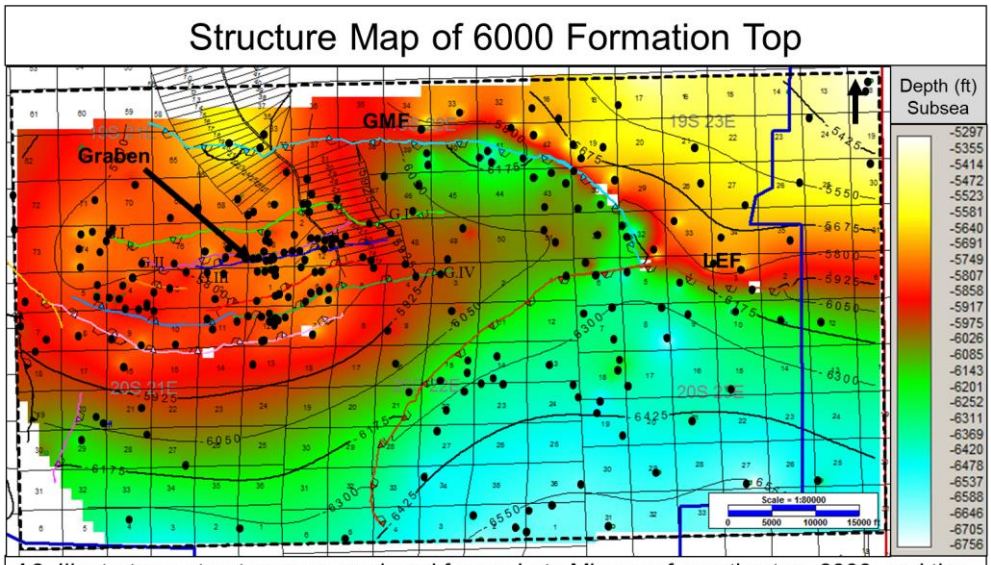

A6. Illustrates a structure map produced from a Late Miocene formation top, 6000, and the location of wells that were used within the study area. The blue line outlines the extent of the seismic survey, and the black-dotted box outlines the well log data coverage centered around the city of Golden Meadow. The Golden Meadow fault (GMF) is outlined in blue, the Lake Enfermer fault (LEF) is outlined in brown, and the black arrow is pointing to the graben. G I and II are two faults within the graben that are downthrown to the south. G III and IV are two of the six shallow faults within the graben that are downthrown to the north.

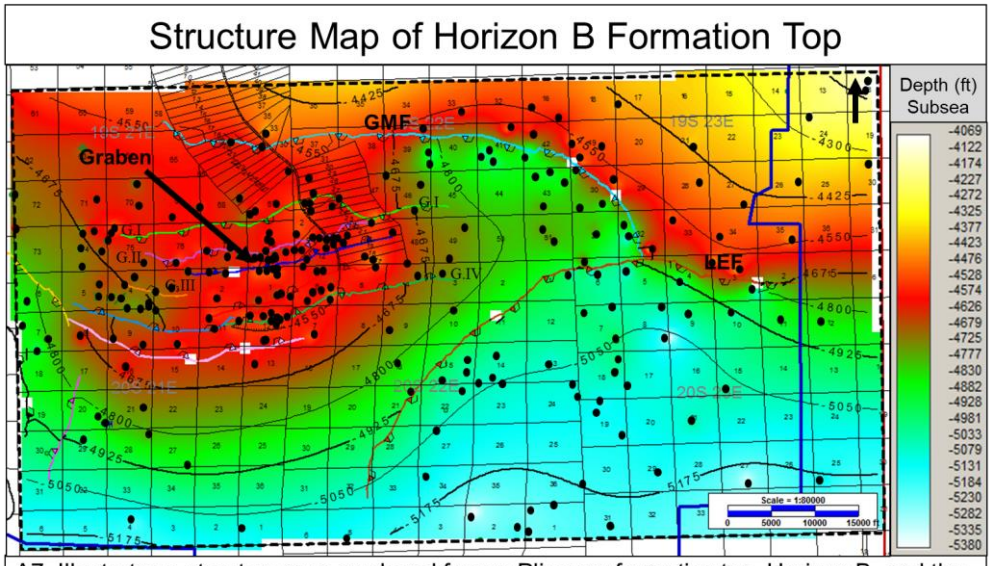

A7. Illustrates a structure map produced from a Pliocene formation top, Horizon B, and the location of wells that were used within the study area. The blue line outlines the extent of the seismic survey, and the black-dotted box outlines the well log data coverage centered around the city of Golden Meadow. The Golden Meadow fault (GMF) is outlined in blue, the Lake Enfermer fault (LEF) is outlined in brown, and the black arrow is pointing to the graben. G I and II are two faults within the graben that are downthrown to the south. G III and IV are two of the six shallow faults within the graben that are downthrown to the north.

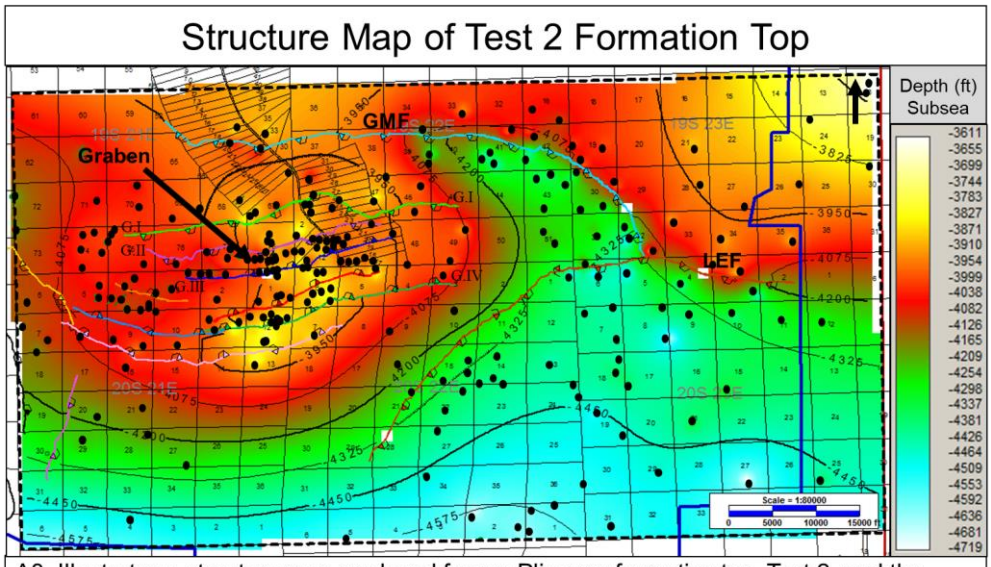

A8. Illustrates a structure map produced from a Pliocene formation top, Test 2, and the location of wells that were used within the study area. The blue line outlines the extent of the seismic survey, and the black-dotted box outlines the well log data coverage centered around the city of Golden Meadow. The Golden Meadow fault (GMF) is outlined in blue, the Lake Enfermer fault (LEF) is outlined in brown, and the black arrow is pointing to the graben. G I and II are two faults within the graben that are downthrown to the south. G III and IV are two of the six shallow faults within the graben that are downthrown to the north.

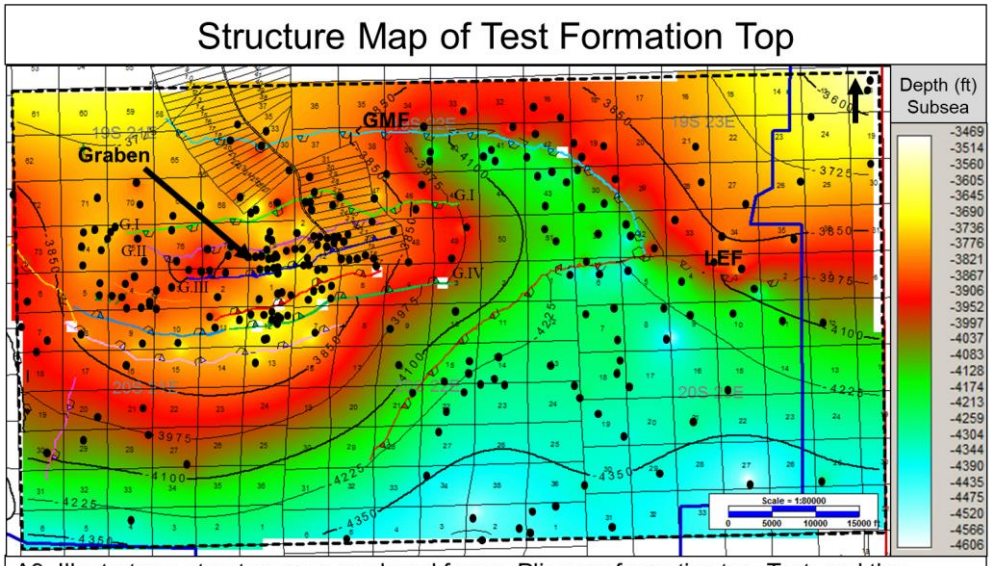

A9. Illustrates a structure map produced from a Pliocene formation top, Test, and the location of wells that were used within the study area. The blue line outlines the extent of the seismic survey, and the black-dotted box outlines the well log data coverage centered around the city of Golden Meadow. The Golden Meadow fault (GMF) is outlined in blue, the Lake Enfermer fault (LEF) is outlined in brown, and the black arrow is pointing to the graben. G I and II are two faults within the graben that are downthrown to the south. G III and IV are two of the six shallow faults within the graben that are downthrown to the north.

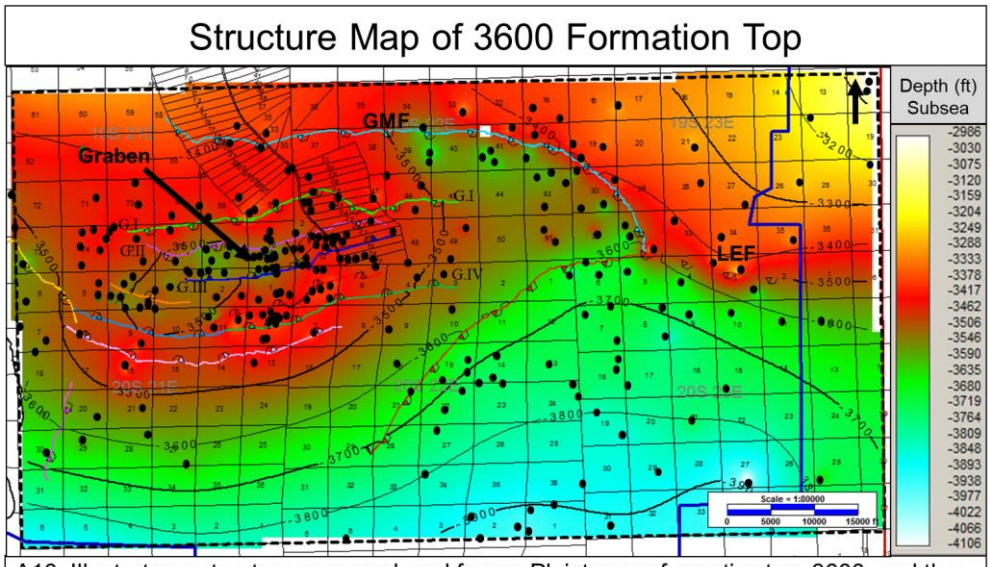

A10. Illustrates a structure map produced from a Pleistocene formation top, 3600, and the location of wells that were used within the study area. The blue line outlines the extent of the seismic survey, and the black-dotted box outlines the well log data coverage centered around the city of Golden Meadow. The Golden Meadow fault (GMF) is outlined in blue, the Lake Enfermer fault (LEF) is outlined in brown, and the black arrow is pointing to the graben. G I and II are two faults within the graben that are downthrown to the south. G III and IV are two of the six shallow faults within the graben that are downthrown to the north.

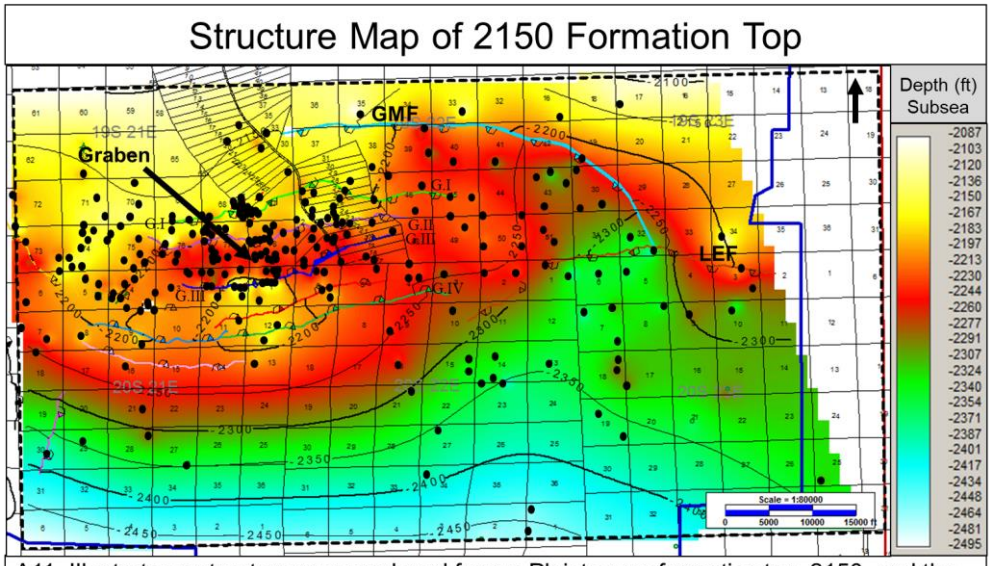

A11. Illustrates a structure map produced from a Pleistocene formation top, 2150, and the location of wells that were used within the study area. The blue line outlines the extent of the seismic survey, and the black-dotted box outlines the well log data coverage centered around the city of Golden Meadow. The Golden Meadow fault (GMF) is outlined in blue, the Lake Enfermer fault (LEF) is outlined in brown, and the black arrow is pointing to the graben. G I and II are two faults within the graben that are downthrown to the south. G III and IV are two of the six shallow faults within the graben that are downthrown to the north.

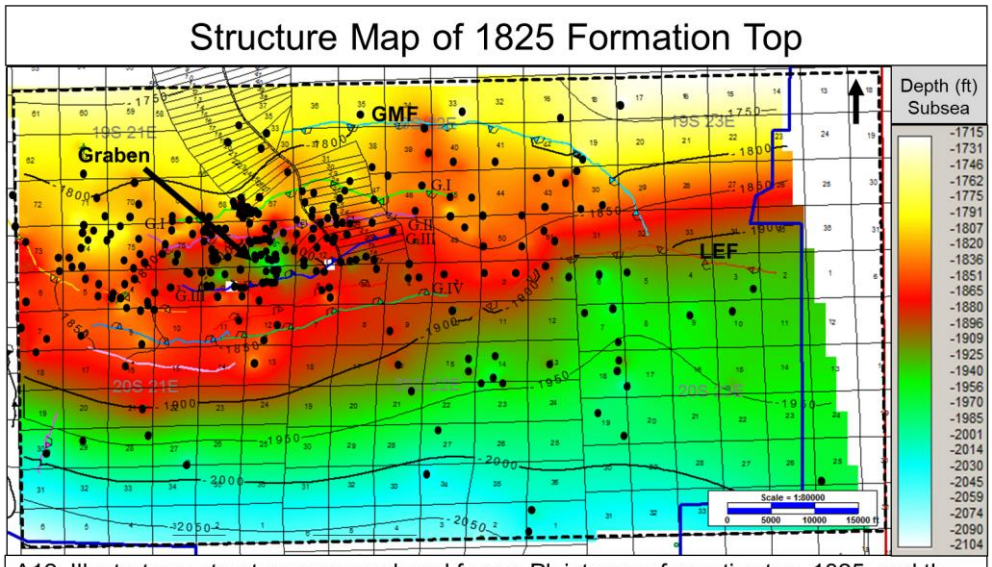

A12. Illustrates a structure map produced from a Pleistocene formation top, 1825, and the location of wells that were used within the study area. The blue line outlines the extent of the seismic survey, and the black-dotted box outlines the well log data coverage centered around the city of Golden Meadow. The Golden Meadow fault (GMF) is outlined in blue, the Lake Enfermer fault (LEF) is outlined in brown, and the black arrow is pointing to the graben. G I and II are two faults within the graben that are downthrown to the south. G III and IV are two of the six shallow faults within the graben that are downthrown to the north.

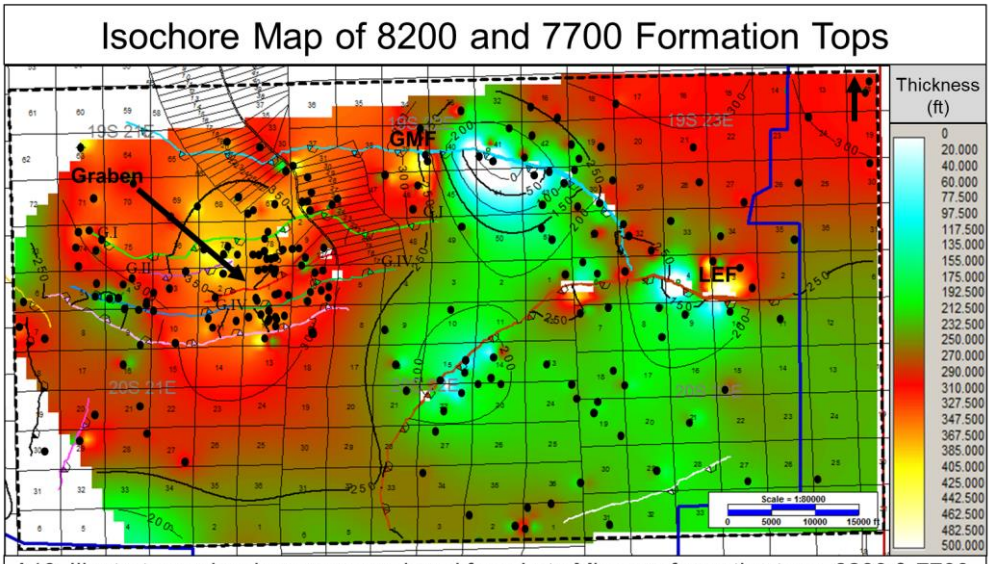

A13. Illustrates an isochore map produced from Late Miocene formation tops, 8200 & 7700, and the location of wells that were used within the study area. The blue line outlines the extent of the seismic survey, and the black-dotted box outlines the well log data coverage centered around the city of Golden Meadow. The Golden Meadow fault (GMF) is outlined in blue, the Lake Enfermer fault (LEF) is outlined in brown, and the black arrow is pointing to the graben. G I and II are two faults within the graben that are downthrown to the south. G IV is one of the six shallow faults within the graben that are downthrown to the north.

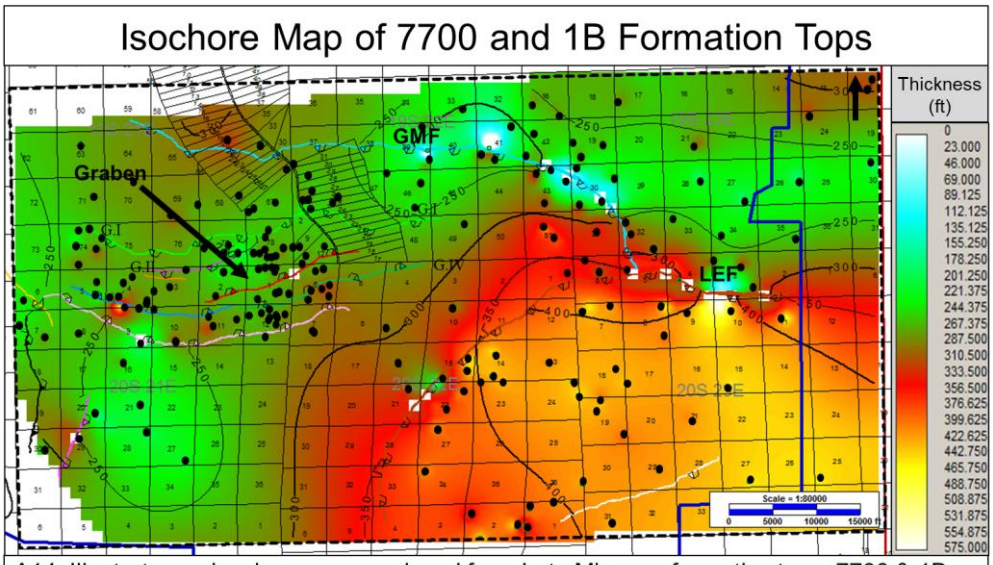

A14. Illustrates an isochore map produced from Late Miocene formation tops, 7700 & 1B, and the location of wells that were used within the study area. The blue line outlines the extent of the seismic survey, and the black-dotted box outlines the well log data coverage centered around the city of Golden Meadow. The Golden Meadow fault (GMF) is outlined in blue, the Lake Enfermer fault (LEF) is outlined in brown, and the black arrow is pointing to the graben. G I and II are two faults within the graben that are downthrown to the south. G IV is one of the six shallow faults within the graben that are downthrown to the north.

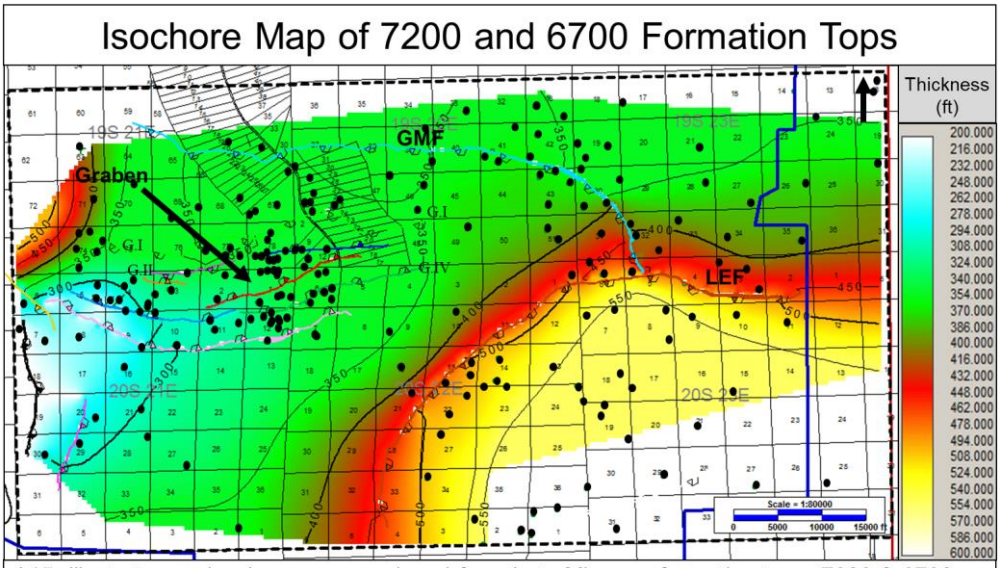

A15. Illustrates an isochore map produced from Late Miocene formation tops, 7200 & 6700, and the location of wells that were used within the study area. The blue line outlines the extent of the seismic survey, and the black-dotted box outlines the well log data coverage centered around the city of Golden Meadow. The Golden Meadow fault (GMF) is outlined in blue, the Lake Enfermer fault (LEF) is outlined in brown, and the black arrow is pointing to the graben. G I and II are two faults within the graben that are downthrown to the south. G III and IV are two of the six shallow faults within the graben that are downthrown to the north.

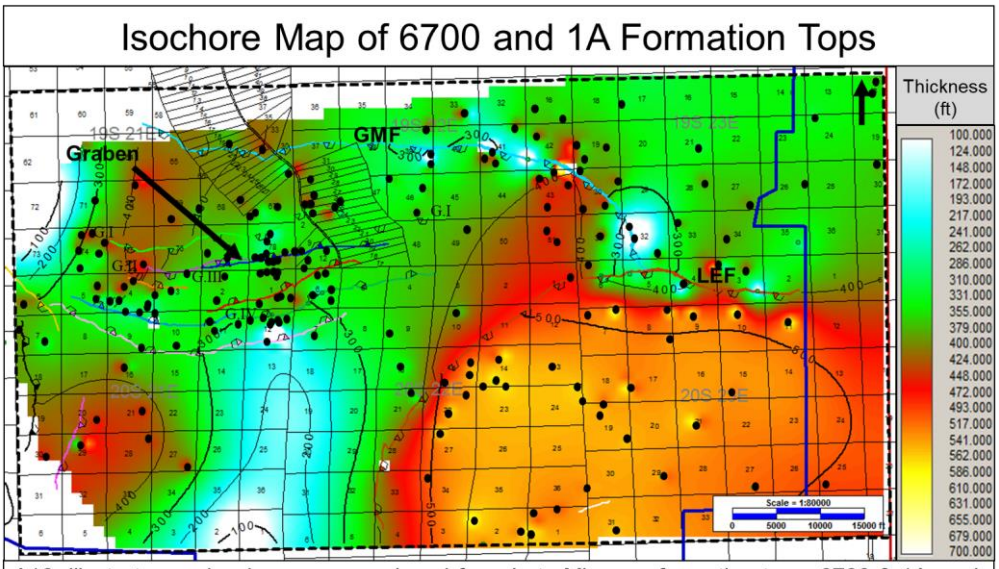

A16. Illustrates an isochore map produced from Late Miocene formation tops, 6700 & 1A, and the location of wells that were used within the study area. The blue line outlines the extent of the seismic survey, and the black-dotted box outlines the well log data coverage centered around the city of Golden Meadow. The Golden Meadow fault (GMF) is outlined in blue, the Lake Enfermer fault (LEF) is outlined in brown, and the black arrow is pointing to the graben. G I and II are two faults within the graben that are downthrown to the south. G III and IV are two of the six shallow faults within the graben that are downthrown to the north.

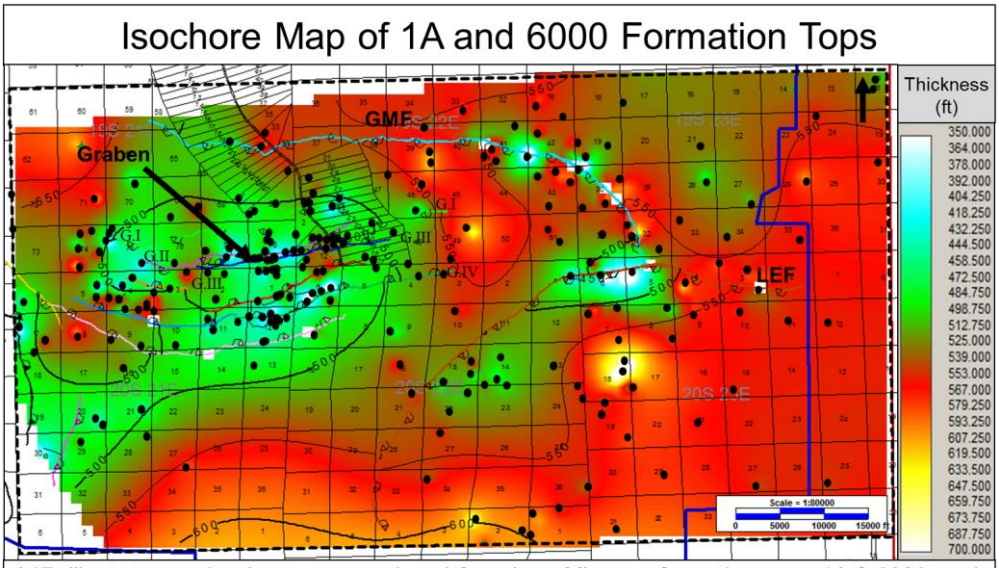

A17. Illustrates an isochore map produced from Late Miocene formation tops, 1A & 6000, and the location of wells that were used within the study area. The blue line outlines the extent of the seismic survey, and the black-dotted box outlines the well log data coverage centered around the city of Golden Meadow. The Golden Meadow fault (GMF) is outlined in blue, the Lake Enfermer fault (LEF) is outlined in brown, and the black arrow is pointing to the graben. G I and II are two faults within the graben that are downthrown to the south. G III and IV are two of the six shallow faults within the graben that are downthrown to the north.

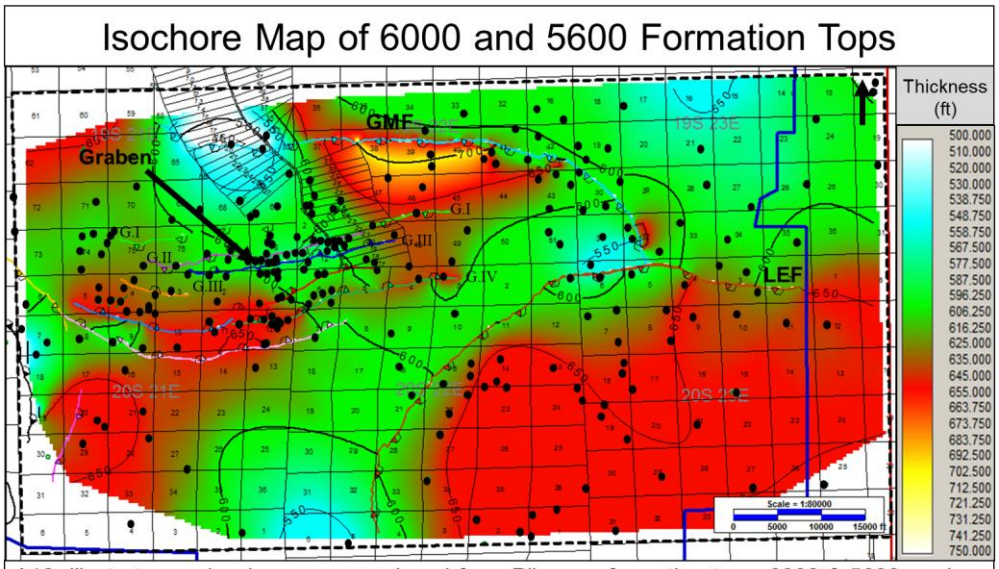

A18. Illustrates an isochore map produced from Pliocene formation tops, 6000 & 5600, and the location of wells that were used within the study area. The blue line outlines the extent of the seismic survey, and the black-dotted box outlines the well log data coverage centered around the city of Golden Meadow. The Golden Meadow fault (GMF) is outlined in blue, the Lake Enfermer fault (LEF) is outlined in brown, and the black arrow is pointing to the graben. G I and II are two faults within the graben that are downthrown to the south. G III and IV are two of the six shallow faults within the graben that are downthrown to the north.

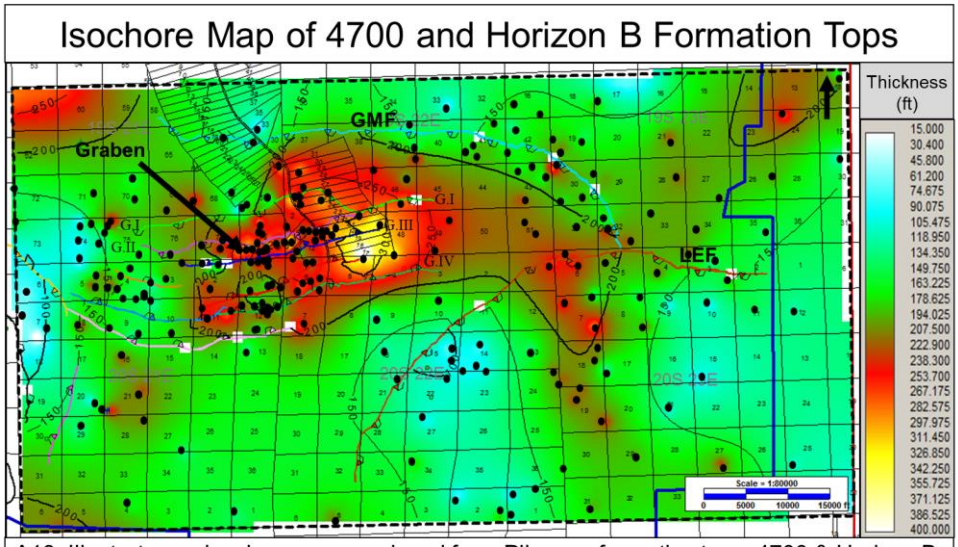

A19. Illustrates an isochore map produced from Pliocene formation tops, 4700 & Horizon B, and the location of wells that were used within the study area. The blue line outlines the extent of the seismic survey, and the black-dotted box outlines the well log data coverage centered around the city of Golden Meadow. The Golden Meadow fault (GMF) is outlined in blue, the Lake Enfermer fault (LEF) is outlined in brown, and the black arrow is pointing to the graben. G I and II are two faults within the graben that are downthrown to the south. G III and IV are two of the six shallow faults within the graben that are downthrown to the north.

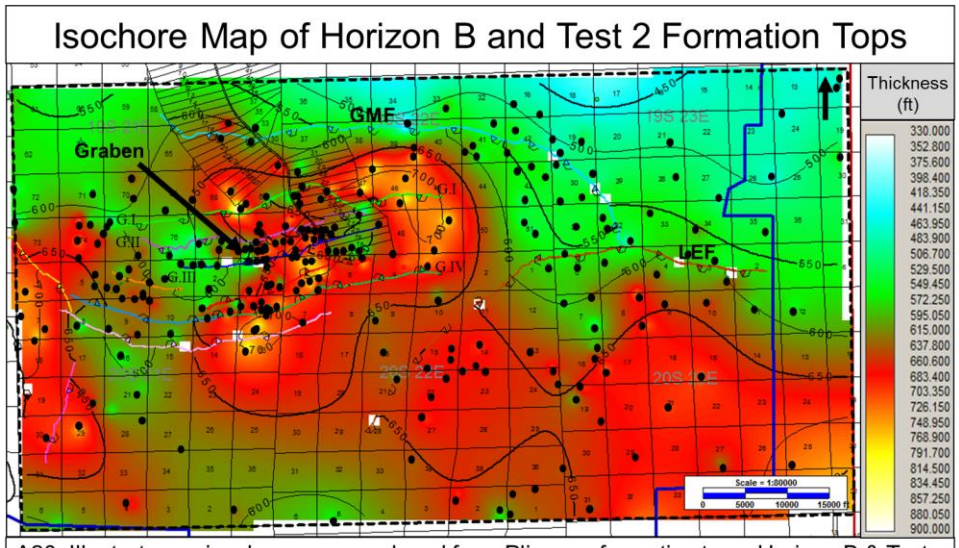

A20. Illustrates an isochore map produced from Pliocene formation tops, Horizon B & Test 2, and the location of wells that were used within the study area. The blue line outlines the extent of the seismic survey, and the black-dotted box outlines the well log data coverage centered around the city of Golden Meadow. The Golden Meadow fault (GMF) is outlined in blue, the Lake Enfermer fault (LEF) is outlined in brown, and the black arrow is pointing to the graben. G I and II are two faults within the graben that are downthrown to the south. G III and IV are two of the six shallow faults within the graben that are downthrown to the north.

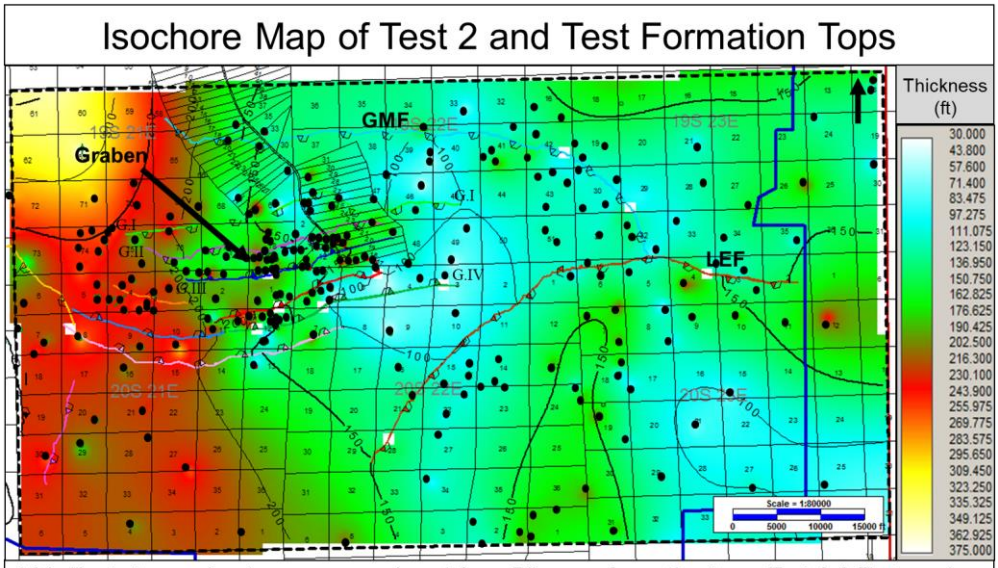

A21. Illustrates an isochore map produced from Pliocene formation tops, Test 2 & Test, and the location of wells that were used within the study area. The blue line outlines the extent of the seismic survey, and the black-dotted box outlines the well log data coverage centered around the city of Golden Meadow. The Golden Meadow fault (GMF) is outlined in blue, the Lake Enfermer fault (LEF) is outlined in brown, and the black arrow is pointing to the graben. G I and II are two faults within the graben that are downthrown to the south. G III and IV are two of the six shallow faults within the graben that are downthrown to the north.

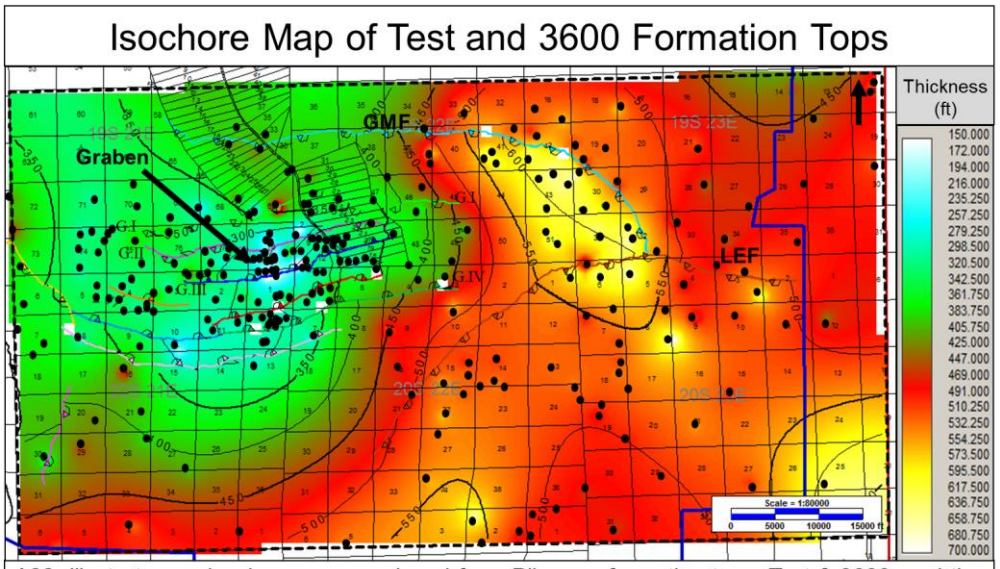

A22. Illustrates an isochore map produced from Pliocene formation tops, Test & 3600, and the location of wells that were used within the study area. The blue line outlines the extent of the seismic survey, and the black-dotted box outlines the well log data coverage centered around the city of Golden Meadow. The Golden Meadow fault (GMF) is outlined in blue, the Lake Enfermer fault (LEF) is outlined in brown, and the black arrow is pointing to the graben. G I and II are two faults within the graben that are downthrown to the south. G III and IV are two of the six shallow faults within the graben that are downthrown to the north.

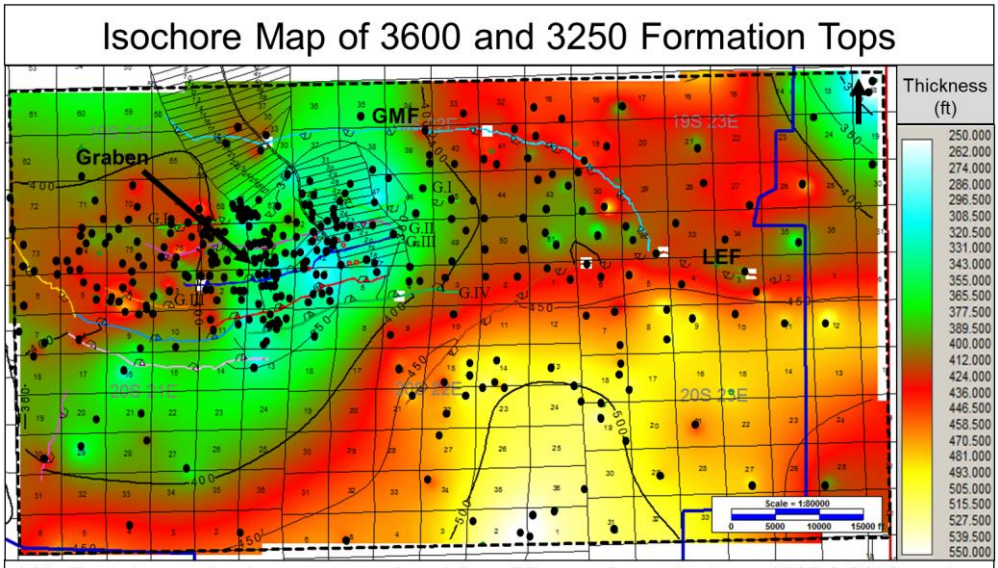

A23. Illustrates an isochore map produced from Pliocene formation tops, 3600 & 3250, and the location of wells that were used within the study area. The blue line outlines the extent of the seismic survey, and the black-dotted box outlines the well log data coverage centered around the city of Golden Meadow. The Golden Meadow fault (GMF) is outlined in blue, the Lake Enfermer fault (LEF) is outlined in brown, and the black arrow is pointing to the graben. G I and II are two faults within the graben that are downthrown to the south. G III and IV are two of the six shallow faults within the graben that are downthrown to the north.

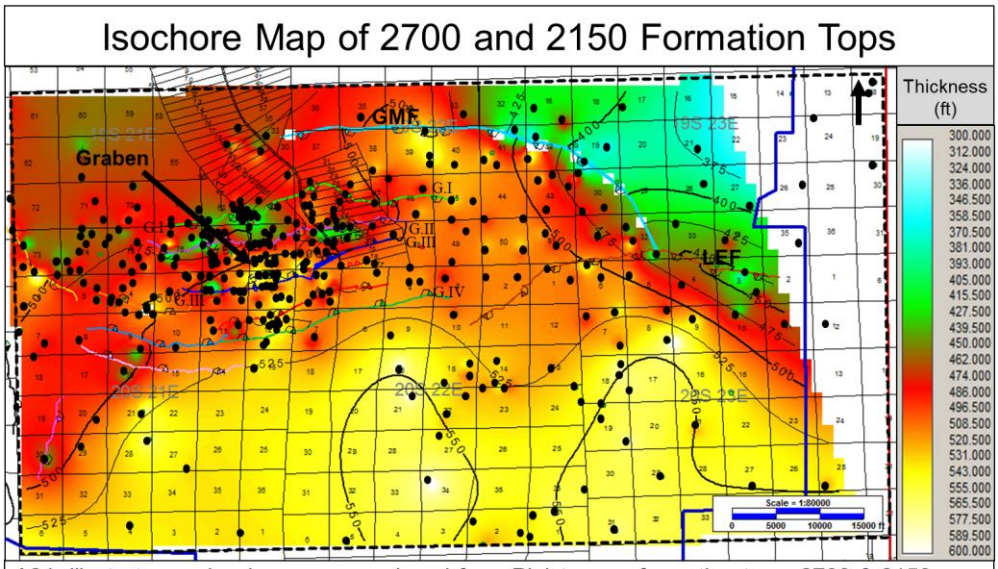

A24. Illustrates an isochore map produced from Pleistocene formation tops, 2700 & 2150, and the location of wells that were used within the study area. The blue line outlines the extent of the seismic survey, and the black-dotted box outlines the well log data coverage centered around the city of Golden Meadow. The Golden Meadow fault (GMF) is outlined in blue, the Lake Enfermer fault (LEF) is outlined in brown, and the black arrow is pointing to the graben. G I and II are two faults within the graben that are downthrown to the south. G III and IV are two of the six shallow faults within the graben that are downthrown to the north.

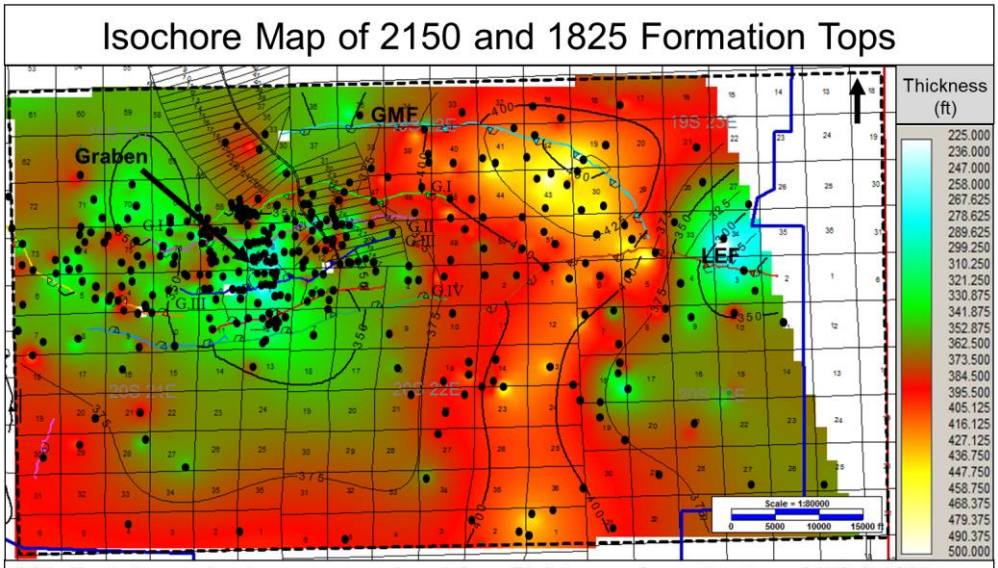

A25. Illustrates an isochore map produced from Pleistocene formation tops, 2150 & 1825, and the location of wells that were used within the study area. The blue line outlines the extent of the seismic survey, and the black-dotted box outlines the well log data coverage centered around the city of Golden Meadow. The Golden Meadow fault (GMF) is outlined in blue, the Lake Enfermer fault (LEF) is outlined in brown, and the black arrow is pointing to the graben. G I and II are two faults within the graben that are downthrown to the south. G III and IV are two of the six shallow faults within the graben that are downthrown to the north.

Biographical Sketch

Amanda Johnston grew up in The Woodlands, Texas and attended Stephen F. Austin State University and the University of Louisiana at Lafayette, where she earned a Bachelor of Science in Geology and a Master of Science in Geology respectively. The daughter of Brian and Jean Johnston, she was the recipient of the Matthew Martin Field Camp Scholarship at Stephen F. Austin State University. During her time with the University of Louisiana at Lafayette's Masters Program, she served as the student chapter's AAPG President from 2016-2017 and sat on the Lafayette Geological Society's Board as a Student Liaison during that same year. Through 2017 and 2018, Amanda served as a Girls on the Run volunteer at Woodvale Elementary mentoring third and fourth-grade girls through an experience-based curriculum which creatively integrates running.